Vacuum Steam Desuperheating and Condensation: An Experimental Investigation

A thesis
submitted in fulfilment
of the requirements for the degree
of

Master of Engineering

at

The University of Waikato

by

AKASH LAXMAN LOKHANDE

THE UNIVERSITY OF
WAIKATO
Te Whare Wānanga o Waikato

2015

Abstract

Steam condensation plays an essential role in supplying and removing heat in many industrial applications, including the energy sector. It therefore is a phenomena of significance that requires deep understanding. This thesis presents effective vacuum steam condensation on the shell-side of vertical shell and tube condenser (VSTC) accompanying steam desuperheating. It describes a fundamental study of heat transfer in VSTC with considerations of several factors; explicitly degree of superheat related with each vacuum steam pressure, temperature waviness in desuperheating section, and steam condensation in absence of non-condensable gas (NCG). Experiments performed on the VSTC are:

Steam desuperheating and condensation in the shell-side VSTC at a variety of vacuum steam pressures and respective steam flowrates, vacuum steam desuperheating and condensation in the shell-side of VSTC at reduced steam flowrates, and vacuum steam desuperheating and condensation at tube wall temperatures up to steam saturation temperature ($T_2 \geq T_{sat}$) to analyse dry heat transfer in the desuperheating section. To examine the stated aim, test facility was built in the laboratory of the University of Waikato.

By generating desuperheating and condensation models for each test pressure, this investigation proves that vacuum steam condensation best occurs without involvement of superheat. About 60% of the VSTC occupied with desuperheating, and the heat transfer involved in desuperheating is minor approximately 1 kW, whereas, the condensation section of VSTC has heat transfer about 10 kW. By reducing the steam flow-rate, 10% reduction in the desuperheating section and 20% to 50% reduction in the Reynolds number was observed. After raising the tube wall temperature up to the steam saturation temperature, a smooth temperature profile across the desuperheating the section was seen with significant sensible heat transfer. Obstruction linked with superheated steam condensation in the dairy industrial leads to poor heat transfer area utilization by the desuperheating section and therefore, reduction of the evaporator rating or oversizing of the heat exchangers to attain appropriate duty.

Acknowledgements

I am ever grateful to GOD ALMIGHTY for his graces and blessings upon me. I could never have stand where I am today without the faith in you, the ALMIGHTY. This thesis owes its existence to confidence and inspiration of my parents, sisters, supervisors, and my dearest friends.

This is my first time to live and study in an overseas country, and New Zealand does not give me any chance of gloom. I would like to recognise and pay my respect to the society, University of Waikato and the landscape of New Zealand. This thesis upgraded my engineering knowledge, which created confidence in me to deal with actual problems incurred in the engineering field and located interest to move into postgraduate study. I would like to express my deepest gratitude to my chief supervisor Dr Martin J. Atkins, and my other supervisor Dr Timothy G. Walmsley. I would like to recognise the notable support given by Dr Martin and Dr Timothy, without your supervision, I could never complete my research. Dr Martin was an outstanding supervisor and Dr Timothy was a great mentor. The conversations with Dr Martin always upgraded my knowledge about research and practice. The industrial site visits, Hamilton social cricket league and visit to Fieldays 2015 with him were memorable. I appreciate Dr Timothy for his friendly assistance, sharing thoughts and compassion to teach me new concepts.

I have enjoyed the opportunity to be a part of the Energy Research Group, University of Waikato directed by Prof. Peter Kamp, Associate Prof. Michael Walmsley, and Senior Researcher Dr James Neale. I would like to thank Energy Research Group for granting a study research award, and express my heartfelt wish to work ahead with Energy Research Group. I would also like to thank research officer Lance Wong and friends Amir, and James for their guidance and support who were part of Energy Research Group. I wish to thank faculty members, Associate Dean Dr Janis Swan & senior lecturer Dr James Carson of science & engineering, for providing me fortune to enrol as ME student in the University of Waikato. I would also like to recognise Science and Engineering librarian Cheryl Ward, for assisting me throughout the research finding journal articles and word formatting. Finally yet importantly, thank you Mom and Dad for everything. There are not enough words in the world to express my appreciation, but I think this is a good start. I owe you one.

Contents

List of Figures

List of Tables

Nomenclature

Acronyms

DP transmitter	Differential pressure transmitter
HEX	Heat Exchanger
bar_g/kPa_g	Gauge pressure
LMTD	Log-mean temperature difference Method
MVR	Mechanical Vapour Recompression
NCG	Non-condensable gas
PID	Proportional-integral-derivative feedback
PRV	Pressure reducer Valve
TEMA	Tubular Exchanger Manufacturers Association
TVR	Thermal Vapour Recompression
VSD	Variable speed drive
VSTC	Vertical Shell and Tube condenser

Symbolization

c_p	Specific heat (kJ/kg˚C)
$\dot{m}$	Mass flow rate (kg/s)
h	coefficient (W/m² ˚C)
P	pressure (kPa)
A	Area (m²)
T	Temperature (°C)
U”	Averaged heat transfer coefficient (w/m²˚C)
dh	Change in enthalpy (kJ/kg)
dQ	Quantity of heat flow, (W)
dT	Change in temperature (°c)
e	Emissivity
k	Thermal conductivity, (W/m ˚C)
r	Radius of tube (m)
σ	Stefan-Boltzmann constant (W/m²K^4)
A_c	Cross-sectional area (m²)
C^*	Heat capacity ratio

$D_{hydraulic}$	Shell hydraulic diameter (m)
D_{is}	Inner shell diameter (m)
L_c	Characteristic length of heat exchanger
N_t	Number of tubes
Q_{max}	Maximum heat transfer (W)
$\Delta T_{superheat}$	Degree of superheat (˚C)
ε	Effectiveness
l	Length of vertical shell and tube condenser (m)
L_{crit}	Critical length of desuperheating section (m)
Nu	Nusselt number for turbulent film condensation
P_{system}	System pressure (kPa)
q''	Heat flux (kW/m²)
h''	Local heat transfer coefficient
T_1 - T_{15}	Various Temperatures by thermocouple (˚C)
ΣR	Overall resistance
NTU	number of transfer units
P	Pressure of tank (kPa)
Pr	Prandtl number
Q	Actual heat transfer (W)
Re	Reynolds number
V	Velocity of fluid(m/s)
d	Diameter (m)
t	Thickness of tube (m)
ΔT_{LMTD}	Log mean temperature difference (°C)
Δh	Enthalpy difference (kJ/kg)
ΔT	Temperature difference (°C)
μ	Viscosity of fluid
ρ	Density (kg/m³)

Subscripts/superscripts

h_1	Hot inlet	i	Inside of tube
h_2	Hot outlet	in	inlet
c_1	Cold inlet	is	Inside of shell
c_2	Cold outlet	max	maximum
$1-15$	Thermocouple numbers	min	minimum
		o	Outside of tube
g	Gas phase	out	drain
h	Hot side	s	steam
T	Turbulent	sat	saturation
c	Cold side	t	tubes
$cond$	condensation	tr	Transition
$crit$	Critical	w	water
$desup$	desuperheat		

Chapter One

Introduction

1.1 Context

Several process and power generation industries require vacuum pressure condensers. Condensation occurs when a superheated fluid such as steam cools to and then below its saturation temperature. Condensation can occur by direct contact with subcooled medium or indirect contact, which is surface condensation. Surface condensation in heat exchangers is the most common condensation phenomena seen in industrial applications. Steam is a common heating medium in the industries. A wide range of industries in New Zealand use steam as a heating medium and driving force, usually manufacturing industries, such as pulp and paper, wood products, food, beverage and tobacco, petroleum, coal, chemical and related product manufacturing. About 16.5% of New Zealand's Gross Domestic Product (GDP) is derived from these industries (Statistics New Zealand, 2014). Furnaces, steam driven equipment such as dryers, evaporators, and condensers are major unit operations in these industries that boost the production and ultimately the economy of the country. Temperature and pressure should be high enough to make steam dry saturated to improve rate of heat transfer, however not superheated.

Processes in the food and beverage industries are heat sensitive and have a particular requirement of vapour saturation temperatures at vacuum pressures for precise heat exchange to maintain product quality. For example, in the dairy industry, multi-effect evaporators produce concentrated milk using vacuum-pressure steam on the shell-side. The shell-side acts as a condenser. The application of Mechanical Vapour Recompression (MVR) and Thermal Vapour Recompression (TVR) helps to improve an evaporator's energy efficiency. Nevertheless, both recompression techniques invariably produce superheated vacuum-pressure steam, which affects the heat transfer coefficients and therefore the performance of the evaporators. The pulp and paper industry has similar vacuum steam condensation requirements. Vacuum steam has its application in the cooking stage (removal of lignin) and secondary processes such as recovery of dissolved inorganic and organic solids. Wastewater with dissolved organics (e.g. lignin), and inorganic chemicals (e.g. sodium sulphide) i.e. black liquor pass through tubes of evaporators and vacuum steam use as a heating medium to evaporate water in the first few effects. In both industries, superheated vacuum steam on the condensing shell-side of the evaporator is undesirable. Reducing the superheat temperature to the saturation temperature, i.e. desuperheating by indirect contact requires significant heat transfer area and reducing the overall heat transfer duty accordingly. Research parameters about vacuum steam condensation include the key parameters that affect condensation, such as analysis of the temperature profile along the length of a condenser, and the heat transfer rate of the desuperheating and condensing steam sections.

A few researchers have examined the condensation of vapour at pressures below atmosphere. These studies investigated the effects of interfacial resistance, vapour superheat, non-condensable gas (NCG), and thermal diffusion. Minkowycz and Sparrow (1966) improved the laminar film condensation of steam on isothermal vertical plate with consideration of above-mentioned effects on condensation at pressure ranging from 3.44 kPa_g to 7 kPa_g. Berrichon *et al.* (2014) examined vacuum steam condensation at high vacuum pressure 0.035 bar_{abs} (saturation temperature 26.7˚C) in the presence of NCG. However, in the aforementioned industries, the majority of vacuum steam condensation needed is at 0.07 bar_{abs}- 0.47 bar_{abs} (saturation temperature 40˚C-80˚C).

The presence of superheat in the system is inevitable. Industries adopt various desuperheating techniques such as water spray although reduce the dryness fraction. Very little research in the literature has focused on condensation of vacuum steam in a vertical condenser with specific investigation of superheated steam condensation under vacuum pressures.

1.2 Thesis Aim

The aim of the thesis is to examine the heat transfer characteristics of superheated vacuum steam with its associated desuperheating and condensation on the shell-side of a Vertical Shell and Tube Condenser (VSTC). The scope of the research includes the turbulent film condensation of vacuum steam. Particular focus is on the heat transfer characteristics of desuperheating of vacuum steam; analysis of desuperheating section of the condenser, temperature profile along the length of the VSTC during desuperheating, and examination of vacuum steam condensation mechanism for a range of steam flowrate. To achieve the aim, an appropriate test facility that includes steam-handling apparatus, VSTC, coolant loop, and vacuum pump system was built and commissioned by the author at the University of Waikato and used to perform sets of experiments.

1.3 Structure of Thesis

Chapter 2 presents the most significant literature that relates to the thesis aim. It begins by presenting basic knowledge about heat transfer fundamentals and mechanisms. It reviews studies focused on condensation mechanism and parameters, particularly those that affect the rate of condensation.

Chapter 3 describes the experimental method and procedure. This chapter describes the experimental set-up, including the handling of steam, cooling water, condensate, and the vacuum system. A piping and instrument diagram of the test facility summarises the process. Chapter 3 also presents changes in the apparatus as per experiments and a detailed description of the operating procedure of test facility. The final section of Chapter 3 addresses interpretation of experimental data together with error analysis. It finishes by discussing the repeatability of experimental results.

Chapter 4 presents the bulk of the experimental results and discussion. To be understandable, the first part focuses on one particular vacuum steam test pressure and the next section shows averaged results of desuperheating and condensation sections. The overall experimental results section shows systematic assessment of data measured during experiments, formation of desuperheating and condensation sections, calculated heat transfer coefficients and plots of different parameters to generate important correlations. Finally, a detail explanation about the experimental results of high tube wall temperature than steam saturation temperature ($T_2 \geq T_{sat}$) is presented.

Chapter 5 presents an industrial application of the results. Industrial application section presents an actual industry case where the steam condensation mechanism can improve by present conclusions obtained from the investigation.

Chapter 6 put concisely the conclusion of all experimental investigation made on VSTC and expected future work with consideration of different parameters along present topic.

Chapter Two

Literature Review

2.1 Introduction

This literature review includes various phenomena linked with a study of VSTC. The review comprises theories, correlations, mechanisms and equations unfolding the VSTC. The review is organised in following way.

- Fundamentals of Heat transfer.
- Condensation.
- Modes of condensation.
- Factors affecting the condensation mechanism- Geometry of heat exchanger, non-condensable gas (NCG), low atmospheric steam pressures, and superheat of steam.
- Summary of developed correlations for condensation heat transfer.
- Conclusion.

2.2 Heat Transfer

2.2.1 Introduction

The study of heat transfer deals with the transmission of energy from one medium to another with consideration of temperature gradients. This exchange of heat to and from process medium and its transfer rate is an important part of most engineering processes. The fundamentals of heat transfer theory are covered by many authors, for example, Cengel (2007), Holman (1992), and Kern and Quentin (1950). This section reviews the three basic mechanisms of heat transfer, which are conduction, convection and radiation, and their phenomena where combinations of mechanisms applies.

2.2.2 Conduction

Conduction is a transfer of heat through a fixed substance or from one material to another material in physical contact. Heat transfer by conduction has two mechanisms:

a) By lattice vibration - transfer of heat by collisions of molecules moving rapidly in one part of a substance having a greater temperature gradient to molecules moving less rapidly.

b) Transport of free electrons - production of energy flux in the direction of decreasing temperature.

Kern and Quentin (1950) explained the mechanism of conduction using an example of an idealised stationary wall. Heat considered flowing perpendicular to the isothermal wall, which is isotropic and homogenous, from the left side of wall as shown in Figure 2.1. The heat transfer through the wall is proportional to the area of the wall and the temperature difference between the two ends of the wall.

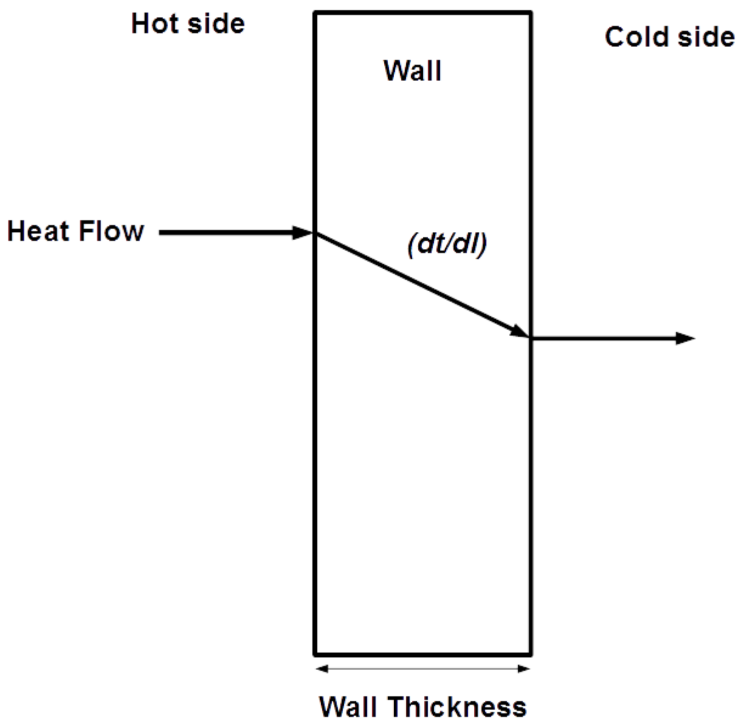

Figure 2.1: Conduction.

Fourier derived the famous equation describing conduction, which is

$$dQ = kA(-dT/dl) \qquad \textbf{(2-1)}$$

Where, dQ = Quantity of heat flow, in W,

k = Thermal conductivity, in W/m ˚C or W/m K

A = Area of wall, in m^2,

dT = change in temperature at any point in the wall, in °C or K,

dl = wall thickness, in m, in direction of heat flow.

The term $\frac{dT}{dl}$ known as the temperature gradient and has negative sign along positive l and so the negative sign included in Eq. 2-1 will give a positive Q. Thermal conductivities are available in engineering reference books for range of a materials.

2.2.3 Convection

Convection is the mechanism of heat transfer where heat flows within a fluid when one portion of fluid mixes with another. The heat flow depends on the properties of the fluid. Convection can thus divided into two sub mechanisms:

a) Natural convection – this occurs when transmission of heat between hot and cold fluids due to natural differences in fluid properties such as density. Heated fluid become less dense due to its thermal expansion and thus mix with the cold fluid, which is denser.
b) Forced convection - if any external work (e.g. by a mixer) is done to increase movement, the rate of convection is increased.

Newton's law of cooling explains convective heat transfer,

$$dQ = (hA)dT \qquad \textbf{(2-2)}$$

Where h is the heat transfer coefficient with typical units of W/m^2 ˚C or W/m^2 K which is affected by the nature of the fluid, its properties and by work done in the case of forced convection. In convection, fluid often observed flowing in an enclosure of a solid surface and a solid surface is a factor that possibly affect fluid flow and thus heat transfer. Considerable the work has been done and is still in progress on the boundary layer mechanism (i.e. the flow region adjacent to the solid surface), fluid properties, and mechanical factors such as stress, and friction (Dharma Rao *et al.* (2008)).

2.2.4 Radiation

Radiation is the transmission of energy in the form of electromagnetic waves or photons through space or a medium causing excitation at atomic and sub-atomic levels of a material. Materials hold radiation phenomenon in different amounts according to their types. The maximum (or idealised) radiation emitted or received by a material called *blackbody* radiation. A common example of radiation is the solar energy incident upon the Earth. The Boltzmann equation used to calculate the heat transfer by radiation based on the second law of thermodynamics is,

$$dQ = \sigma e A T^4 \qquad \textbf{(2-3)}$$

Where, T=Absolute temperature, K,

σ = Stefan-Boltzmann constant, in W/m^2K^4

e = emissivity, ability of surface of a substance to radiate heat. ($0 < \varepsilon < 1$)

2.2.5 Process Heat Transfer

Process heat transfer deals with the investigation of the rate of heat transfer that occurs in the heat exchanger equipment. Thus, more emphasis to find the amount of heat transferred, its rate, driving force, and the physical arrangement of the two medium.

It is very rare to encounter a single type of heat transfer mechanism in practice. Most problems involve combinations of mechanisms of heat transfer. Heat exchangers are devices that direct the thermal energy flow between two fluids or materials. Heat exchangers used in various divisions of engineering. Recuperators or regenerators are designed to best match their transfer processes (e.g. direct or indirect contact), geometry (e.g. tube, plate, finned, etc.), fluid type (e.g. single and two phase), and fluid flow arrangement (e.g. parallel, counter and cross flows). Kakac *et al.* (2002) provide a good explanation of the basic objectives of heat exchanger selection, thermal-hydraulic design, and rating. In the present work, considered process heat transfer is from vacuum steam to tube-side cold water in a VSTC. Thus, the work linked with rating of shell and tube heat exchanger involves determination of the heat transfer rate for each set of conditions, such as temperature of medium, pressure, and fluid flowrates. Thus, it requires understanding of performance calculations of a shell and tube heat exchanger. The difference in temperature in a heat exchanger is strongly dependent on the arrangement of the flow of fluids. Figure 2.2 illustrates two idealised heat exchanger flow arrangements: parallel or co-current and counter flow. The overall energy balance for steady state system of two different fluids with negligible energy change described by Eq. 2-4.

$$dQ = \dot{m} dh \qquad \textbf{(2-4)}$$

Where, $\dot{m}$ is mass flowrate and dh is the rate of change of specific enthalpy. The fluids with same phase and constant specific heat expressed as,

$$Q = \left(\dot{m}\, c_p\right)_h \left(t_{h_1} - t_{h_2}\right) \qquad \textbf{(2-5)}$$

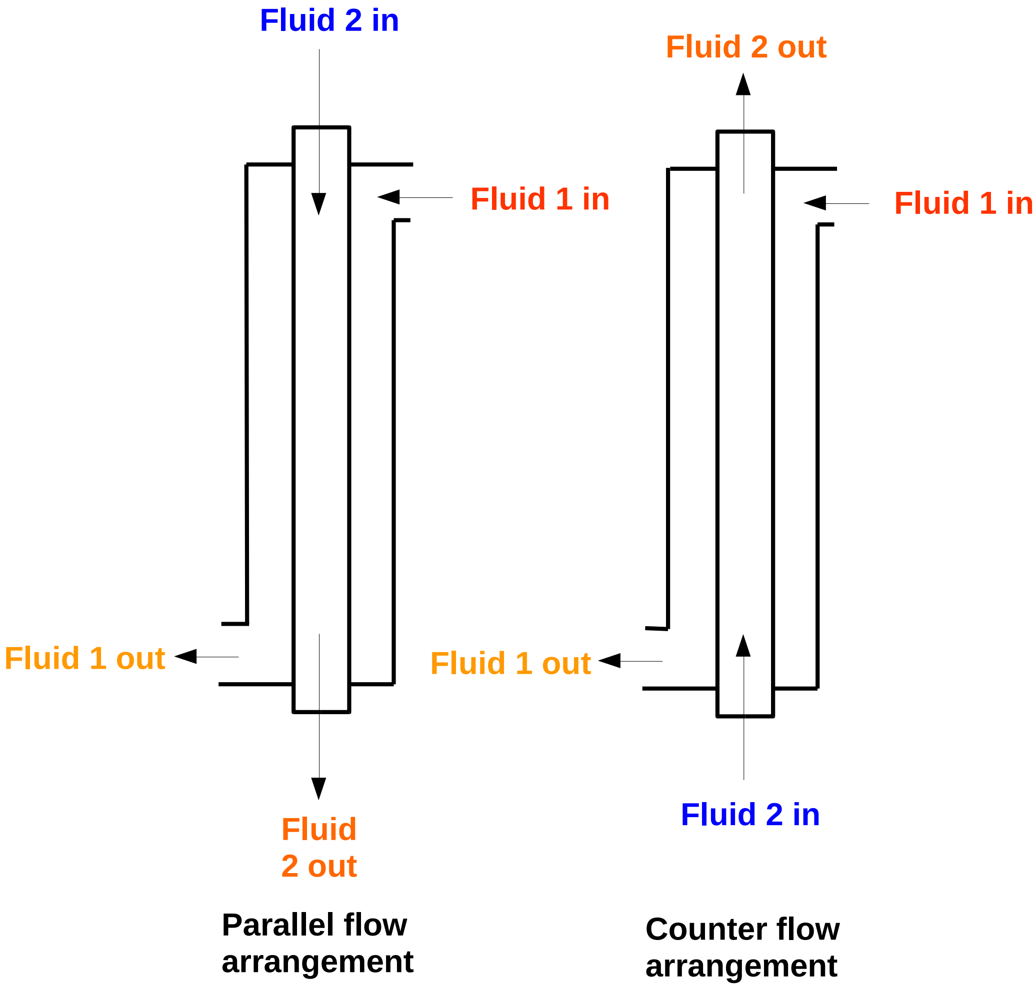

Figure 2.2: Flow arrangements for heat exchangers.

$$Q = (\dot{m}\, c_p)_c\, (t_{c_2} - t_{c_1}) \qquad \textbf{(2-6)}$$

Where c_p symbolises the specific heat of the fluid, subscripts h and c stand for hot and cold fluids respectively, and the numbers 1, and 2 refer to inlet and outlet conditions. Thus, the heat transfer rate for two fluids is calculated and the total heat transfer rate Q governed from the following equation,

$$Q = U\, A\, \Delta T \qquad \textbf{(2-7)}$$

ΔT is the log mean temperature difference between the hot and cold fluids, where it is integrated along a length of exchanger. To establish the temperature difference between two fluids, it is necessary to account for the thermal resistances between the two temperatures of fluids. Resistances encountered in a shell and tube exchanger are tube-wall resistance and fluid-film resistance. The fluid-film resistance is very small and therefore normally ignored. The overall resistance ΣR stated as:

$$\sum R = \frac{1}{h_i A_i} + \frac{t}{kA} + \frac{1}{h_o A_o} \tag{2-8}$$

and the overall heat transfer coefficient U is the inverse of overall resistance:

$$\frac{1}{U} = \frac{1}{h_i A_i} + \frac{\ln\left({}^{r_i}/{}_{r_o}\right)}{2\pi kl} + \frac{1}{h_o A_o} \tag{2-9}$$

Where h_i and h_o are heat transfer coefficients of convection for fluids flowing inside and outside the tube. Eq. 2-9 assumes the heat transfer area for both fluids. In reality, the area for outside and inside tube is different. If the outside area A of inner tube is used, then h_i must multiplied by A_i / A so that h_i would give same value based on the larger area A instead of A_i.

2.2.5.1 Logarithmic Mean Temperature Difference (LMTD)

The temperature difference between hot and cold fluid is not constant along the length of the heat exchanger. The temperature difference along the length of a heat exchanger compute with the help of LMTD. LMTD for counter flow is greater than parallel flow for the same inlet and outlet conditions. Kakac, *et al.* (2002), state that counter flow has a higher heat transfer rate than parallel flow, and can give same heat transfer rate of parallel flow with a smaller heat transfer surface area. LMTD is expressed as:

$$\Delta T_{LMTD} = \frac{(\Delta T_1 - \Delta T_2)}{\ln\left(\frac{\Delta T_1}{\Delta T_2}\right)} \tag{2-10}$$

The temperature difference for parallel flow (Figure 2.3) are,

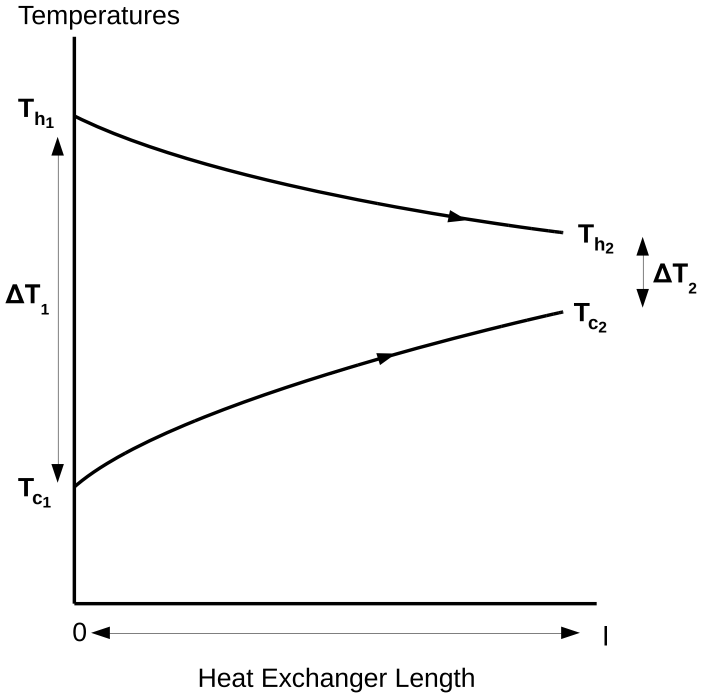

Figure 2.3: Parallel flow.

$$\Delta T_1 = t_{h_1} - t_{c_1} \tag{2-11}$$

$$\Delta T_2 = t_{h_2} - t_{c_2} \tag{2-12}$$

and for counter flow (Figure 2.4) are,

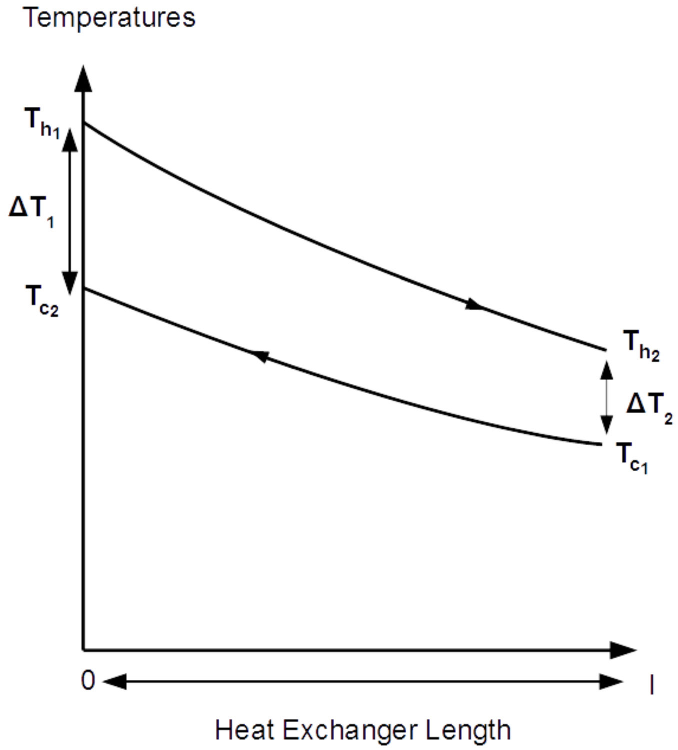

Figure 2.4: Counter flow.

$$\Delta T_1 = t_{h_1} - t_{c_2} \tag{2-13}$$

$$\Delta T_2 = t_{h_2} - t_{c_1} \tag{2-14}$$

2.2.5.2 Effectiveness (ε) - Number of Transfer Units (NTU) Method for Heat Exchanger Analysis

To determine the heat transfer rate, and for the sizing of a heat exchanger, the LMTD method may be used, however without the input and output temperatures of the heat exchanger, further calculations are not possible. With the ε-NTU method (Kays & London, 1984), the heat exchanger analysis simplified since it needs only input temperatures to the heat exchangers and the mass flow rate of streams. The heat capacity ratio (C^*) is defined by Eq. 2-15*:*

$$C^* = \frac{C_{min}}{C_{max}} \tag{2-15}$$

Where, C_{max} and C_{min} are the larger and the smaller of the two magnitudes of heat capacity rates, C_h and C_c respectively

$$C_h = \left(\dot{m}\, c_p\right)_h \tag{2-16}$$

$$C_c = \left(\dot{m}\, c_p\right)_c \tag{2-17}$$

The effectiveness of the heat exchanger expressed as ratio of actual heat transfer (Q) to maximum possible heat transfer (Q_{max}) in a heat exchanger:

$$\varepsilon = \frac{Q}{Q_{max}} \tag{2-18}$$

Actual heat transfer obtained from energy balance on hot and cold fluids and maximum heat transfer rate in a heat exchanger calculated by identifying the maximum temperature difference between the inlet temperatures of hot and cold fluids.

$$Q_{max} = C_{min}\left(T_{h_{in}} - T_{c_{in}}\right) \tag{2-19}$$

The NTU describes the non-dimensional heat transfer size of a heat exchanger,

$$NTU = \frac{U\,A}{C_{min}} \tag{2-20}$$

Thus, it can be shown that effectiveness is a function of number of transfer units (NTU), heat capacity ratio (C^*), and flow arrangement.

$$\varepsilon = f(\ NTU, C^*, Flow\ Arrangement) \qquad \textbf{(2-21)}$$

ε - NTU, relationships have been derived for a variety of heat exchangers and flow configurations and many are presented in Kakac, *et al.* (2002).

2.3 Condensation

2.3.1 Introduction

This section highlights mechanisms of condensation in vertical shell and tube condenser (VSTC), and numerical correlations for film condensation on the shell-side of VSTC. Condensation plays a key role in supplying and removing heat usually via steam in chemical industries, power industries, and nuclear power plants. For example, a refrigerator uses a condenser to remove heat from refrigerant vapour and makes refrigerant into a liquid phase. In milk powder production, steam sent through shell-side evaporators, it supplies heat by condensation in order remove moisture, and concentrate the milk. Condensing steam has a high heat transfer coefficient, typically in the order of 4000 to 8000 W/m^2°C (Sinnott, 2005)

2.3.2 Condensation

Condensation is the process of changing the phase of a fluid from vapour to the liquid state. The phenomenon occurs when its temperature of saturated or superheated vapour reduced to its saturation temperature. In engineering, it is important to understand the mass, energy and momentum transfer through different phases, condensation being one of the example of such types of transfers. During condensation, latent heat transferred as the vapour experiences a phase change to liquid. Condensation occurs at the saturation temperature and therefore heat can be supply at a constant temperature (if there is no cooling of the condensate), as shown in Figure 2.5.

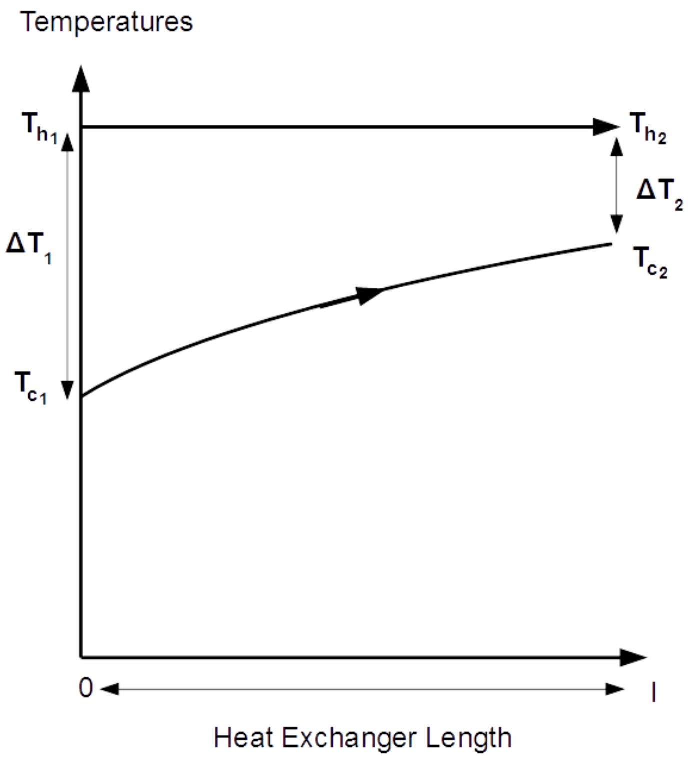

Figure 2.5: Temperature distribution of fluids along the length of condenser.

Muller, (1983) and Taborek, (1991) explained design and operational considerations while handling condenser operations.

1) Condensation modes:
   a) Film-wise condensation
   b) Drop-wise condensation,
2) Condensation regimes:
   a) Gravity controlled or Nusselt flow regime,
   b) Vapour shear controlled regime,
3) Desuperheating: localised condensation of superheated vapour occurs, when the wall temperature of the condenser is below the dew point.
4) Subcooling- subcooling the condensate.
5) Construction: condenser is a two-phase flow heat exchanger that may have any type of orientation in terms of the Tubular Exchanger Manufacturers Association (TEMA) standards, horizontal or vertical with choice of condensation process, on either the shell-side or the tube-side of the condenser.
6) Non-condensable gas (NCG): Presence of NCG in the flow of vapour affects condensation coefficient.

Heat transfer coefficient is the resulting factor for different orientation and allocation of condensing fluid on the shell-side or the tube-side of a condenser. Surface condensation is a common type condensation seen in heat exchangers.

2.3.2.1 Drop-wise Condensation

Condensate will either wet the heat transfer surface and form a continuous film, i.e. ‘film-wise condensation’, or form discrete droplets i.e. ‘dropwise condensation’. In dropwise condensation, the condensed vapour forms droplets on the heat transfer surface. Dropwise condensation is an effective condensation mechanism and large condensing film coefficients can be achieve as little resistance to heat transfer. Since dropwise condensation does not wet the surface, after full growth of droplet, it falls from the surface leaving a clean surface for further condensation (Kern & Quentin, 1950). Large condensing film coefficients leads to high heat transfer rates and a smaller heat transfer area is required for the same amount of heat transferred. The critical factor to achieve dropwise condensation is the surface on which vapour condense. The surface needs to be treated with chemicals or coatings like Teflon, silicones, waxes, and some noble metals. There is a requirement of pure vapour such as steam or the mixture of immiscible vapour and special surfaces to sustain dropwise condensation. Most condensers designed to operate under a film-wise condensation mechanism. With the relevance to the present work, Tanner *et al.* (1968) analysed dropwise condensation at low steam pressures 1.0 kPa_g,1.69 kPa_g, 2.7 kPa_g in the presence and absence of NCG. For effective condensation, their study used a polished condensing surface coated by diamond paste used. The experimental facility also used surface catalysts such as dioctadecyl disulphide, and monton wax to promote drop-wise condensation. Their study found that the rate of condensing heat transfer is higher due to low temperature gradients for drop-wise condensation. In present thesis condensation observed on plain stainless shell-side VSTC under film-wise condensation mode.

2.3.2.2 Film-wise Condensation

In film-wise condensation, the condensate wets the surface and forms a continuous liquid film on the surface. In the case of a vertical flat plate condenser as shown in Figure 2.6, the liquid film flows downwards under the influence of gravity or driving force of vapour. The thickness of condensate film increases as more vapour condenses on surface. The surface on which the vapour condenses covered by liquid film; thus, it creates an additional resistance to heat transfer between the surface and vapour. It is the motion of the film that gives the condensing coefficient for this film-wise condensation. At the start of film formation, the flow of condensate is laminar, the wave starts forming on the surface that introduces disturbance in a laminar flow. It results in a shift from the laminar flow regime to transition flow and lastly to turbulent flow.

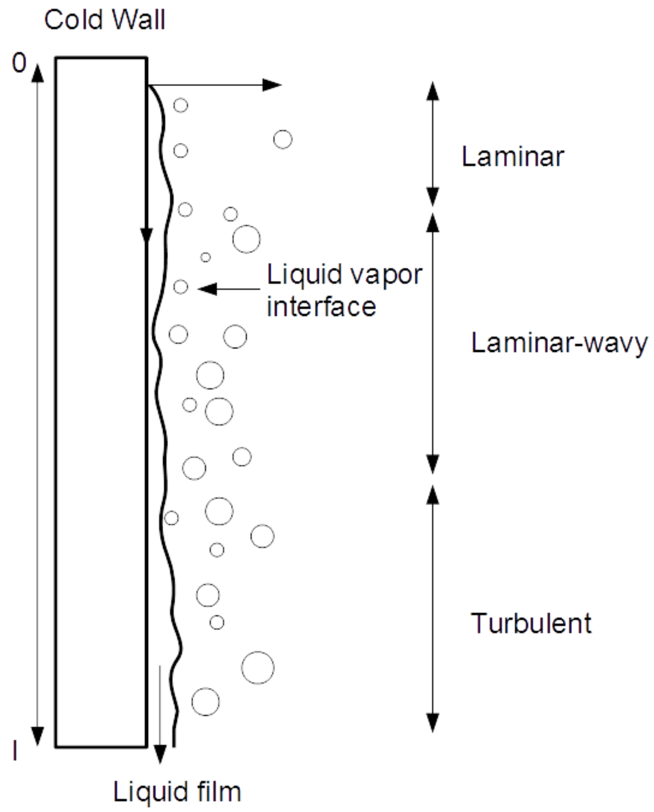

Figure 2.6: Film-wise condensation mechanism.

For the investigation of film-wise condensation heat transfer, a large number of experiments have been performed with various geometries of condenser. Numerous heat transfer correlations have been reported, based on dimensional analysis and the properties of fluids. Nusselt, (1916) developed the basic equations describing laminar film-wise condensation on an isothermal vertical plate. Derived correlations can also apply to horizontal plain tubes. Nusselt neglected the effects of various parameters such as the wavy nature of film, heat capacity rate of condensate, and vapour drag. This leads further explorations to Nusselt work by various authors. Many condensation models have proposed for various conditions, which include laminar and turbulent film condensation in vertical and horizontal geometries. Most of the correlations presented are based on local Nusselt number from which the heat transfer coefficient for film condensation can be calculated. These developed models may be further divided into flat plate type and annular film type condensation and expressed using non-dimensional numbers, mostly Reynolds (Re) and Prandtl (Pr) number. The average heat transfer correlation for turbulent condensation given by Chun and Seban (1971) can be expressed as,

$$Nu_T = 2.297 \times 10^{-3} Re^{0.4} Pr^{0.65} \qquad \textbf{(2-22)}$$

$$\text{For } Re > 1800$$

Chen *et al.* (1987) established an annular-film condensation correlation based on analytical and empirical results for vertical and horizontal type orientation linking the heat transfer coefficient with factors such as interfacial shear stress, waviness, and turbulent transport phenomenon. They formed the correlation for annular film condensation for vertical and horizontal orientation with parallel and counter flow arrangements. For parallel flow turbulent condensation inside vertical tubes, the correlation reported is:

$$Nu_T = {Re_T}^{-0.44} + \frac{{Re_T}^{0.8} Pr^{1.3}}{1.718 \times 10^{-3}} + \frac{A{Re_T}^{1.8} Pr^{1.3}}{2075.3} \qquad \textbf{(2-23)}$$

Chen, *et al.* (1987) analysed the effect of aforementioned factors and compared with Nusselt’s solution, which was a lower estimate than predicted using their correlation.

Chun and Kim (1991) also present a semi-empirical correlation for laminar and turbulent film-wise condensation on a vertical surface. They concluded that there is a lack of compatibility for existing correlations and examined the error associated with each correlation and formed a new correlation that applied to both laminar and turbulent film condensations on a vertical surface. The established relation is valid for sets of data ranging from laminar to turbulent flow regime:

$$Nu = 1.33 Re^{-1/3} + 9.56 \times 10^{-6} Re^{0.89} Pr^{0.94} + 8.22 \times 10^{-2} \qquad \textbf{(2-24)}$$

$$10 < Re < 31{,}000$$

2.3.3 Effect of NCG on Condensation

Typically, the fluid that condensed is a gas mixture, and depending on the conditions, not every part of the vapour condensed during process. The remaining uncondensed gas portion is termed non-condensable gas (NCG). Presence of NCG decreases the vapour pressure of the condenser causing a decrease in saturation temperature. NCG also forms layer (Figure 2.7), which reduce heat transfer rate.

NCG management is an important consideration in the design and operation of condensers.

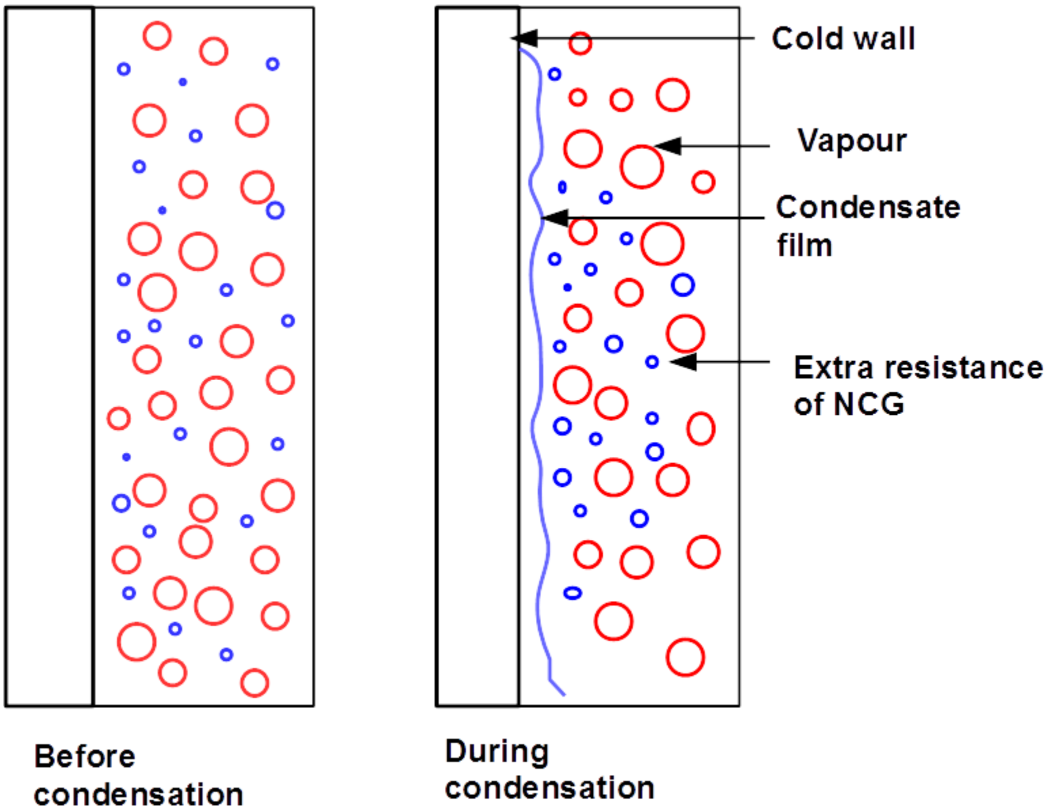

Figure 2.7: Condensation mechanism with consideration of NCG.

Minkowycz and Sparrow (1966), investigated gravity flow laminar film condensation on isothermal plate in the presence of NCG. They observed a reduction in a heat flux corresponding to increase in NCGs fraction, therefore reduction in heat transfer at saturation temperature ranging from 117- 45ºC at 0.5 bar pressure. They also concluded that the collection of NCG cause reductions in vapour pressure and saturation temperature. The reason behind large heat transfer reduction was convective flow of NCG with condensate. The bulk concentration of NCG they tested was from 0.001 to 0.1 fraction of air. Later Sparrow *et al.* (1967), investigated forced convection boundary layer condensation in the presence of NCG and similar conclusions to their earlier work were made. The effect of NCG on heat transfer was most pronounced at sub-atmospheric pressures and as higher temperatures ranging from 60-200ºC. Comparison of effect of NCG showed reduction in heat transfer coefficient in gravity-flow condensation than forced convection condensation. Wang and Chuan (1988), experimentally investigated NCG in a vertical tube, and developed a physical model of laminar film condensation of a vapour–gas mixture in turbulent flow and found similar results as those of Sparrow, *et al.* (1967). Corradini (1984) modelled turbulent condensation on a cold wall in presence of NCG. Reynolds- Colburn analogy for heat and momentum transfer used to generate model. He examined the condensation mechanism for forced and natural convection as a function of mass of air and the steam velocity at 1 m/s and 0.28 bar pressure. The heat transfer coefficient for 0.28 bar was 50% higher than 1 bar.

Dehbi and Guentay (1997) found analytical model for vertical tube condenser in presence for air fractions of 0, 0.05, and 0.1. Their results after model implementation showed, as inlet mass fraction of NCG increased, the performance of vertical tube decreased. Their research also found reduction in the condensation rate with increase in inlet mixture temperature. The study also included effect on condensation by variation in molecular mass of NCG. Maheshwari *et al.* (2004) analysed annular turbulent film condensation in the vertical tube, at 2.6 bar pressure, 0.004 kg/s steam flow, and 11.5 to 23% NCG mass fraction, and developed experimental correlation with consideration of NCG.

$$Nu = 0.15 {Re_{film}}^{0.15} Wa^{-0.85} Ja^{-0.8} {Re_g}^{0.5} \qquad \textbf{(2-25)}$$

For $0.1 < m_a < 0.95$, m_a= Mass fraction of air,

$445 < Re_g < 22700$

$0.004 < Ja < 0.07, Ja$= Jakob number.

Their models based on waviness, rippling, suction effect, local mass flow, and interfacial shear stress. The developed models were compared with existing models of Blangetti and Schlunder (1978), to find local Nusselt number for turbulent regime, which is,

$$Nu_T = 0.00402 \times Re^{0.4} \times Pr^{0.65} \qquad \textbf{(2-26)}$$

The research concluded an increase in heat transfer coefficient due to high turbulence in the boundary layer, which represented by high Reynolds number. Mackereth (1995) discussed different approaches to deal with NCG which were installation of de-aeration ports, and changing air concentration. The study investigated the presence of 0.55% of air in the steam that reduced condensation rate by 33% compared with no air being present. Presence of NCG concentration measured by different techniques that based on temperature and pressure of system, although measurement was somewhat problematic.

Al-Shammari *et al.* (2004) performed condensation of steam in a vertical tube. They examined the condensation of steam at 0.16-0.22 bar pressure and steam air at 0.19-

0.33 bar pressure. It was clear from their work that the presence of NCG produced gas resistance to heat transfer such that it could be reduced almost 50% in the case of pure steam condensation. Thus, reviews suggest decrease in the heat transfer coefficient due to presence of NCG. The presence of NCG may be less however; the growth in NCG over time affects condensation by significant difference, therefore, NCG must be remove at the point it arrives.

2.3.4 Steam Condensation at Vacuum and below Atmospheric Pressures

Buglaev *et al.* (1971) studied the steam-air mixture condensation on a horizontal tube bank under vacuum conditions. The tested pressure range was 1, 0.9, 0.5, 0.25, and 0.12 bar. Investigation found that temperature of tube wall influenced by thermal resistance. Increase in the rate heat transfer at the lower portion of heat exchanger observed. Secondly, they introduced flash steam with existing test facility. They explained the effect of air content on the condensation heat transfer coefficient by forming an equation that was a function of pressure, air content, and temperature gradient obtained from saturation temperature of steam.

Cheng *et al.* (2012) studied heat transfer phenomenon on horizontal tube bundles under vacuum pressure. The process for measuring condensation was intermittent, flowrate of cooling water also changed for different sets of vacuum pressure, which were 70 kPa, 40 kPa and 20 kPa. Results showed an increase in overall heat transfer coefficients by 82% as vacuum pressure enhanced for brass tube bundle and velocity of steam flow through tubes of heat exchanger for 0.02 MPa to 0.07 MPa. The second part of the experiment consisted replacement of Ni-based implanted steel tube with ion implanted brass tube of heat exchanger, and brass tubes were more effective than Ni-based steel tubes.

Recently, Berrichon, *et al.* (2014) examined steam condensation inside a vertical tube surrounded by cooling water flow under forced convection at low pressure for enhancing power plant efficiency in absence of NCG. Small percentage of NCG was however noticeable in the experiment. Experiment conducted with pure water vapour and air mixture at constant inlet vacuum pressure of 0.035 bar. Two cases of film-wise condensation smooth film, and wavy film were considered and respective heat transfer coefficients were found. Berrichon, *et al.* (2014) had good comparison with previous models of condensation and generated new correlation for wavy nature of film condensation at low pressure, which supports the present work.

$$Nu_T = 0.007 \times Re^{0.38} \times Pr^N \qquad \textbf{(2-27)}$$

Where, $N = [1.3 + 0.24 \ln Pr]^{-1}$

In the case of 4% NCG, they achieved about 40% decrease in heat transfer coefficients.

2.3.5 Superheated Steam

When temperature of water increases, the space above the liquid filled with molecules of water vapour. When the number of molecules leaving the liquid surface is more, water molecules evaporates. At this instant water is at saturation temperature. Increase in pressure causes increase in enthalpy of water and saturation temperature, steam at a condition above the saturation temperature is superheated steam. The temperature above saturation temperature known as degree of superheat of steam. Figure 2.8 shows temperature versus duty of condenser. When superheated steam enters the condenser, initially it gets desuperheated and soon attain its saturation temperature by latent heat transfer to corresponding fluid as seen in Figure 2.8.

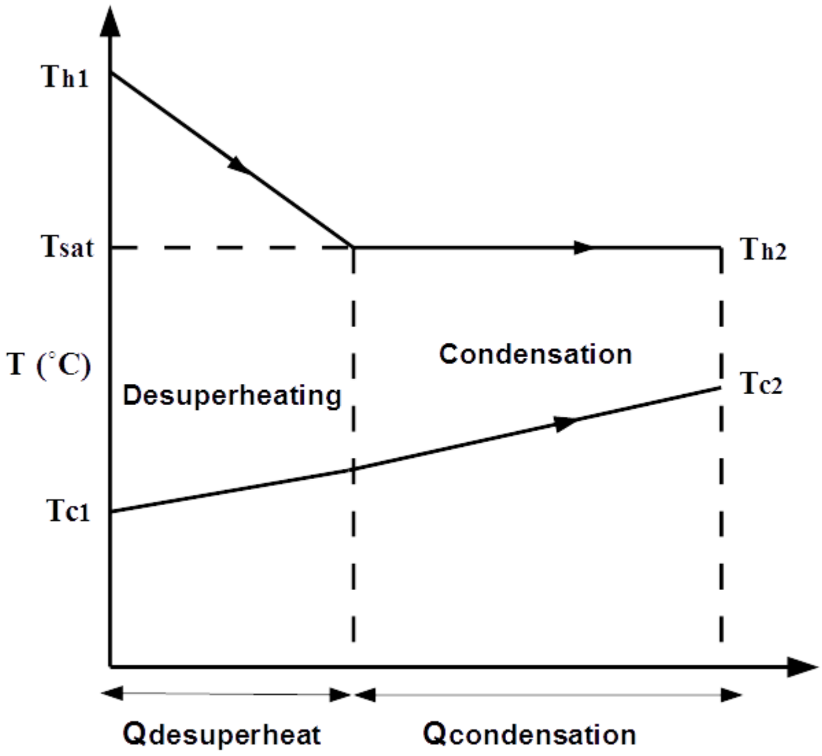

Figure 2.8: Desuperheating in a condenser (Sinnott, 2005).

Superheated steam is unavoidable in several applications, e.g. refrigeration, steam turbines, and dairy industries. Superheated steam has the ability to drive the moisture out of materials effectively. It has advantage in terms of nutrient preservation.

Superheated steam condensation is not suitable due to significant reasons, which are variable heat transfer coefficient, typically low and difficult to quantify correctly that leads to difficulty in accurate sizing and control of heat transfer equipment, and will result in a higher rated and more expensive heat exchanger. The higher temperature of superheated steam may damage sensitive equipment.

Not many investigations made on the influence of superheated steam on condensation. Minkowycz and Sparrow (1966) analysed condensation of vapour and air on isothermal vertical plate at pressure ranging from 3.44 kPa to 7 kPa with consideration of different models that included interfacial resistance, superheating, and free convection, mass and thermal diffusion. They found that about 200˚C superheat brought minor increase in the wall heat transfer without free convection during pure vapour condensation than in presence of NCG. For investigation of interfacial resistance, authors analysed superheated and saturated vapour. However, they could not attain to exact solution. Later, Minkowycz and Sparrow (1969) investigated the effect of vapour superheating for forced convection film condensation on a flat plate in presence of NCG. The effect of superheat represented with the ratio of heat flux of vapour to degree of superheat. The values represented superheating of vapour mainly enhanced the surface heat transfer that was about 10% at high wall temperature. The comparison of effect of superheat on forced convection boundary layer and gravity-induced condensation showed that gravity induced condensation had significant change for superheat. The saturation temperature and mass flowrate also had significant effect in case superheating. Miropolskiy *et al.* (1974) studied superheated steam condensation inside tubes. The testing conditions for finding local heat transfer coefficients were at turbulent flow of fluids at pressure ranging 4 bar to 216 bar and mass velocity ranging 400-4000 kg/m^2 s. Authors divided their investigation into heat transfer from superheated steam at high pressures from 100 to 216 bar, heat transfer from superheated steam at low pressure and low mass velocity, and heat transfer of superheated steam with and without condensation. They investigated the relation between the heat transfer coefficient and the relative enthalpy, it was observed that heat transfer increased with increase in relative enthalpy that ranged from 0-1, and it decreased when it exceeded 1. It was due to formation of thermal resistance of steam layer at wall surface with increased with superheat temperature. Nusselt correlation used for calculating the heat transfer coefficient,

$$Nu_T = C \times Re^{0.8} \times Pr^{0.4} \qquad \textbf{(2-28)}$$

The coefficient C depends on microstructure of the surface. Shang (1997) developed numeral solution for steady state laminar film condensation of a superheated vapour on an isothermal vertical plate. Shang studied the two-phase boundary layer mechanism with consideration of fluid properties and with the help of velocity component method. Assumptions were made while carrying out experimentation; laminar flow within liquid and vapour prompted by gravity at atmospheric pressure, a vertical plate suspended in the volume of superheated vapour. The subcooled water, and steam temperature gradients were in range of 0˚C -100˚C and 0˚C-427˚C. The condensate mass flowrate showed decrement as superheat increased Yang (1997), developed a convection film condensation model on a non-isothermal horizontal tube. Results presented for natural and forced convection film condensation of superheated vapour. The author divided the results into two parts, firstly effect of superheat on condensate film thickness and secondly the heat transfer for same conditions. Investigation found thin condensation film due to conduction effect of superheated vapour. It noted that film condensation for natural convection was steadier with tube than condensation under forced convection. Forced convection involved limited scope for superheat due to larger Reynolds number and reduced thickness of condensate film. Significant increase in heat transfer coefficients observed about 15-20% for a range of pressure gradients and degree of superheat of vapour. Though the developed model could apply to different convective condensation mechanism, author did not explain the replica's use for different geometries allowable with range of pressure.

2.4 Conclusion

To put it briefly, the literature suggests various situations of condensation of turbulent film condensation, condensation in presence and absence of NCG, condensation under low vacuum pressure, and condensation of superheated steam. The literature that consisted low vacuum steam condensation either are for horizontal condensers or steam condensation inside tubes. Variation in NCG is hardly a parameter in the present investigation since literature spoke about NCG effect adequately. Less work has done on superheated steam condensation topic. In addition, negligible research has performed on the study of superheated steam condensation phenomenon under vacuum pressure. The study of superheated steam condensation in vertical shell and tube condenser (VSTC) where steam condensed on shell-side under high vacuum pressure and cooling water flows through tubes represents gap in current knowledge.

Next chapter shows the structure of test facility that has prepared in the large-scale lab at the University of Waikato, to investigate research objectives.

Chapter Three

Methods

3.1 Overview

This section provides an overview of various investigations made on the VSTC. The aim of this study, requires following parameters:

a) the heat transfer coefficients of condensation in VSTC in absence of NCG between 30 kPa_{abs} to 100 kPa_{abs} pressure, and
b) the effect of superheat on the heat transfer coefficient within the same pressure range.

Taking into account the above goals of the investigation, a new experimental facility set-up in the Large Scale Lab (LSL) at the University of Waikato (Figure 3.1). The experimental rig consisted of five major parts:

1) VSTC,
2) steam injection system,
3) the coolant circulation loop,
4) the measurement and data acquisition system, and
5) liquid ring vacuum pump system.

The stainless steel VSTC heat transfer section was 1.14 m high, 0.035 m inner shell diameter, and 3 tubes. Dry vacuum steam is conditioned and injected into the shell-side of VSTC. The cooling water on the tube-side had a constant inlet temperature of 49°C and a flowrate of 15 L/min for all tests.

Figure 3.1: Photograph of experimental test facility.

3.2 Apparatus and Materials

Steam from a boiler at 6 bar_g is dried and reduced to the desired pressure through a pressure reducing valve before entering the shell-side of the VSTC, while cold water is passed on the tube-side for desuperheating and condensing the steam. The vacuum system sets and maintains the desired pressure of the system. Heat is rejected through an air-cooled heat exchanger and a liquid cooled heat exchanger so that the VSTC can be properly controlled and achieve stable operation for the experimental runs. Figure 3.2 shows piping and instrument diagram of test facility. Each part of the system is describe separately in next several sections.

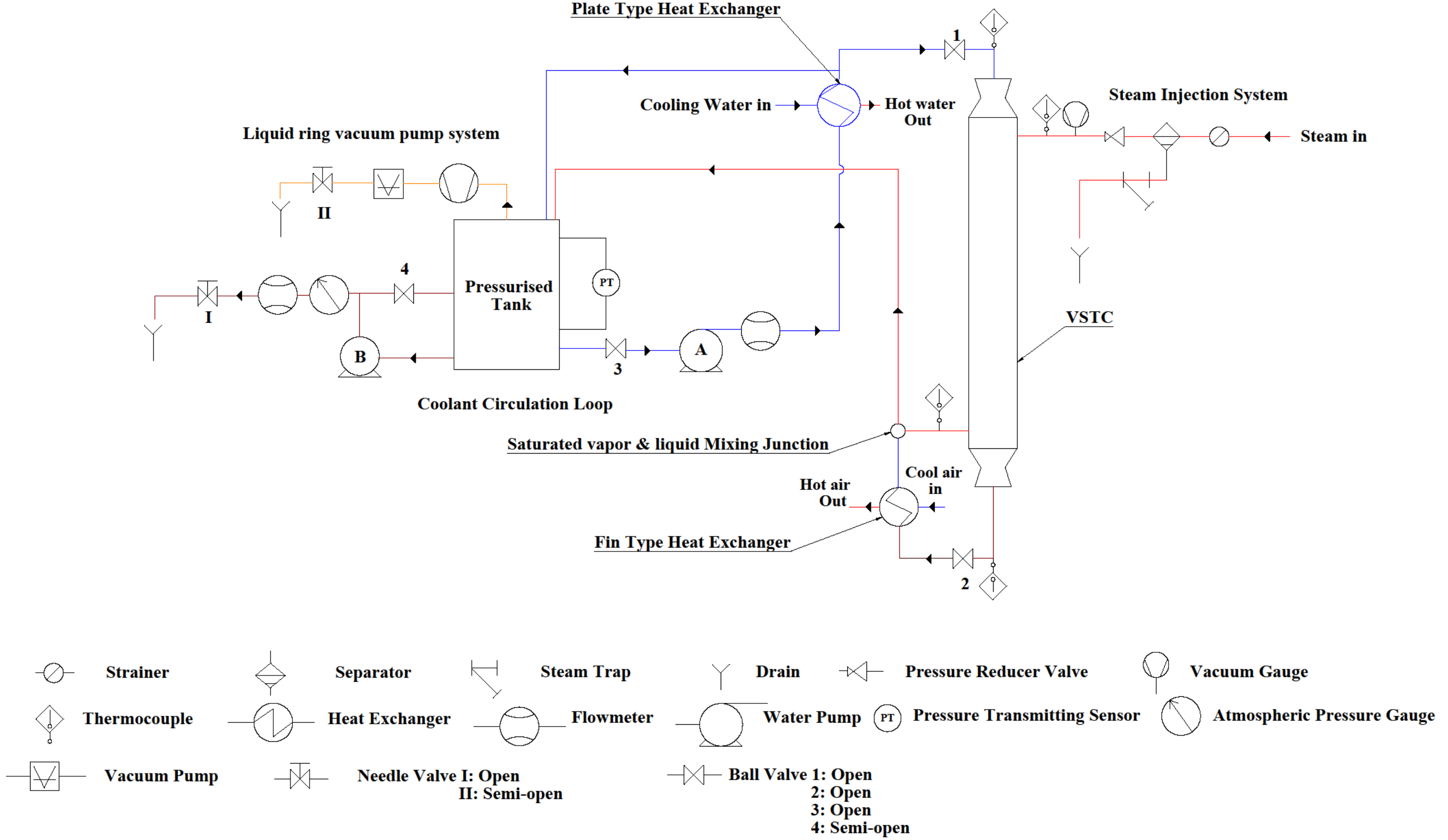

Figure 3.2: Piping and instrument diagram of test facility.

3.2.1 VSTC Design

The stainless steel VSTC heat transfer section used throughout the research as shown in Figure 3.3. Table 3.1 below lists about VSTC dimensions.

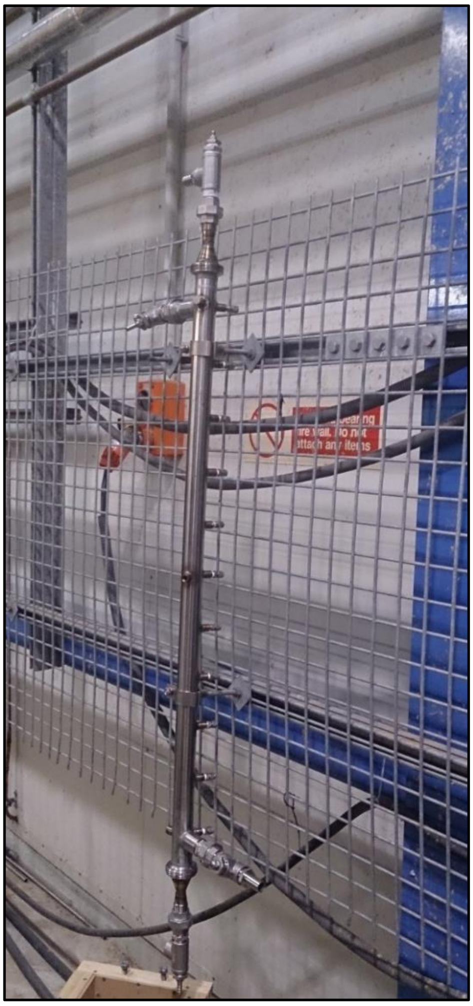

.

Figure 3.3: VSTC.

Table 3.1: VSTC details

Feed Arrangement in VSTC	Parallel flow
VSTC Length, $\boldsymbol{L}$	1.14 m
Tube inner diameter, $\boldsymbol{d_i}$	0.010 m
Tube outer diameter, $\boldsymbol{d_o}$	0.013 m
Number of Tubes, $\boldsymbol{N_t}$	3
Inner shell diameter, $\boldsymbol{D_{is}}$	0.035 m
VSTC material	316 Stainless steel
Water flowrate through tubes, $\boldsymbol{\dot{m}_{water}}$	0.25 kg/s
Wall thickness of tube	1.2 mm

Tubes have an equilateral triangular pitch (Figure 3.4). The centre-to-centre tube spacing were 20 mm. To separate shell-side and tube-side, the top and the bottom of tubes were welded plates.

Figure 3.4: Tubes arrangements in a condenser.

The VSTC had 11 mountings for thermocouples spaced 100 mm apart evenly along the length of the exchanger. Figure 3.5 shows the schematic details of VSTC used for experiment. The rig was pressure tested using compressed air to find and seal any leaks. Leak detection performed before experimental runs were undertaken whenever a change or replacement carried out with the test facility.

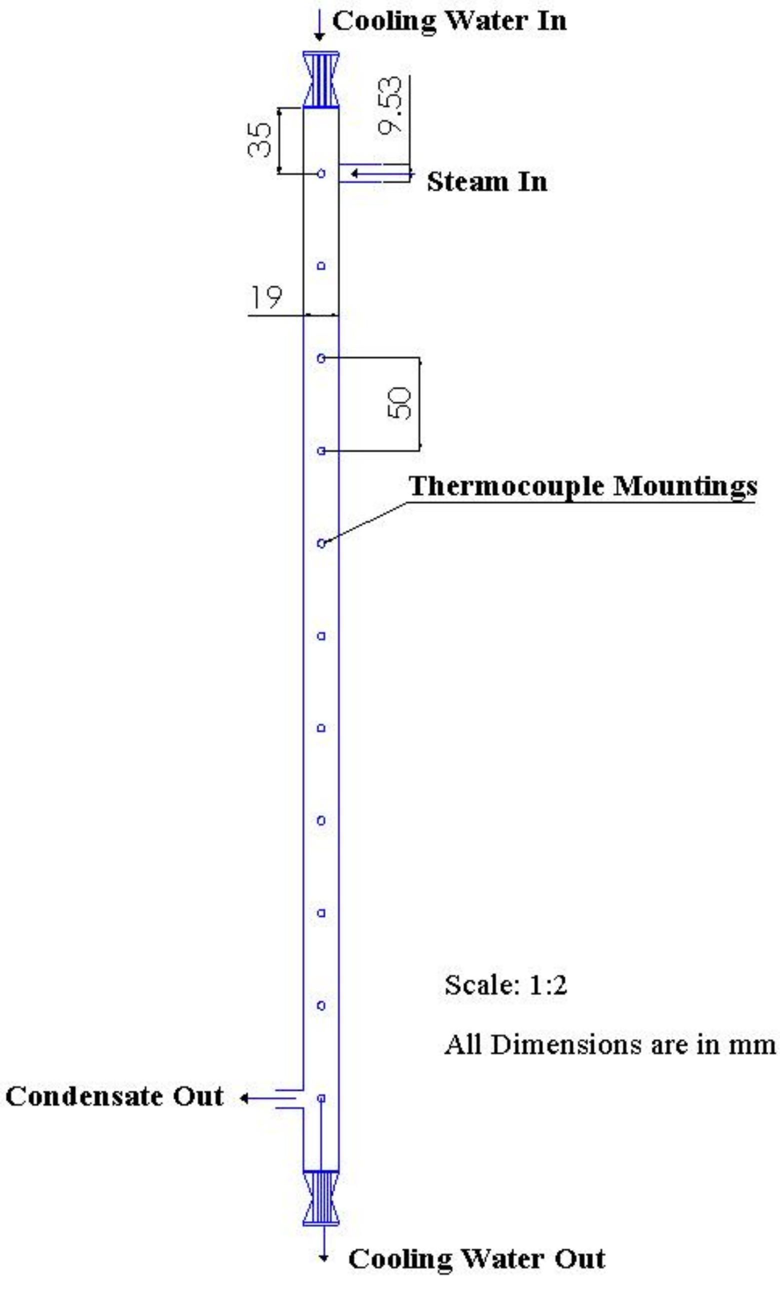

Figure 3.5: Detailed VSTC.

The lab has installed an AQUAHEAT VPX steam generator that generates low quality steam, ~0.90. The generator provided steam at 6 bar_g. The steam was conditioned before entering the VSTC using a strainer, separator, steam trap, and PRV (Pressure Reducing Valve) as shown in Figure 3.6.

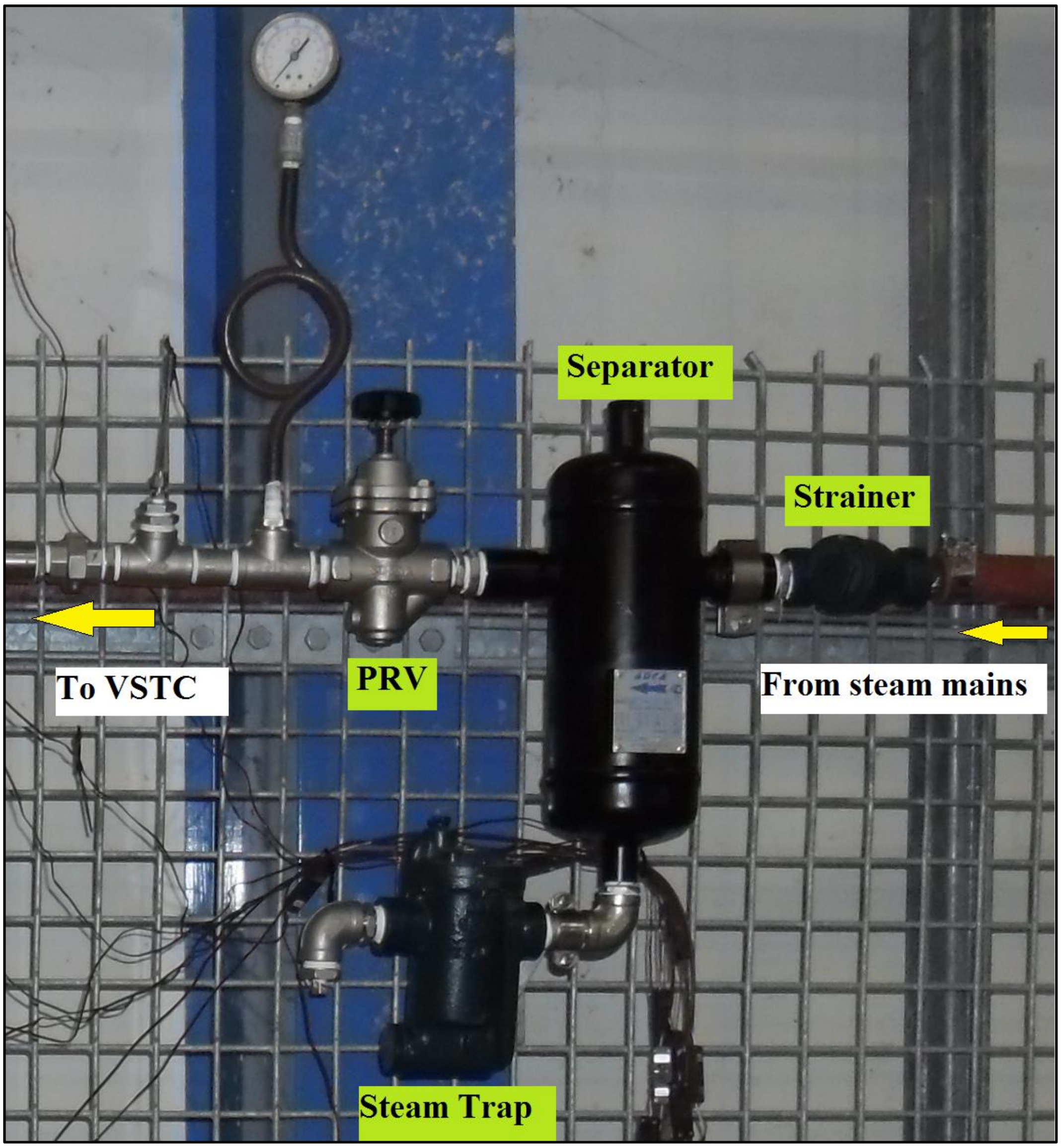

Figure 3.6: Steam handling system.

3.2.1.1 Strainer

Strainer is a form of inline screen. The strainer blocks the pipeline debris such as scale, rust, jointing compound, weld metal and other solids in flowing liquids and gases. It contains a mesh, which obstruct these solids, and allowing clean steam to pass through the process. Y-type strainer used for the experiment as shown in Figure 3.7, which is standard, compact, strong and sustained for high pressures. Y-type strainer has two orientation for installation. For steam and gases, horizontal to pipeline, which stops water collecting in pocket. For liquids, pocket should be vertically downwards. Vertically downward orientation prevents drawing debris back to the flow. Due to low dirt holding capacity, Y-type strainers requires regular cleaning, current strainer cleaned at regular interval during experiments.

Figure 3.7: Strainer.

3.2.1.2 Separator

A VALSTEAM ADCA ENG. S.A. made S16/S baffle steam separator is used. It is the most efficient type of separator over wide range of steam velocities. Figure 3.8 shows the separator that used in the experiment.

Figure 3.8: Steam Separator.

3.2.1.3 Steam Trap

An inverted bucket-type steam trap also used to discharge condensed water to the drain without losing dry steam.

Figure 3.9 shows the photo of inverted bucket-type steam trap that was used for the experiment.

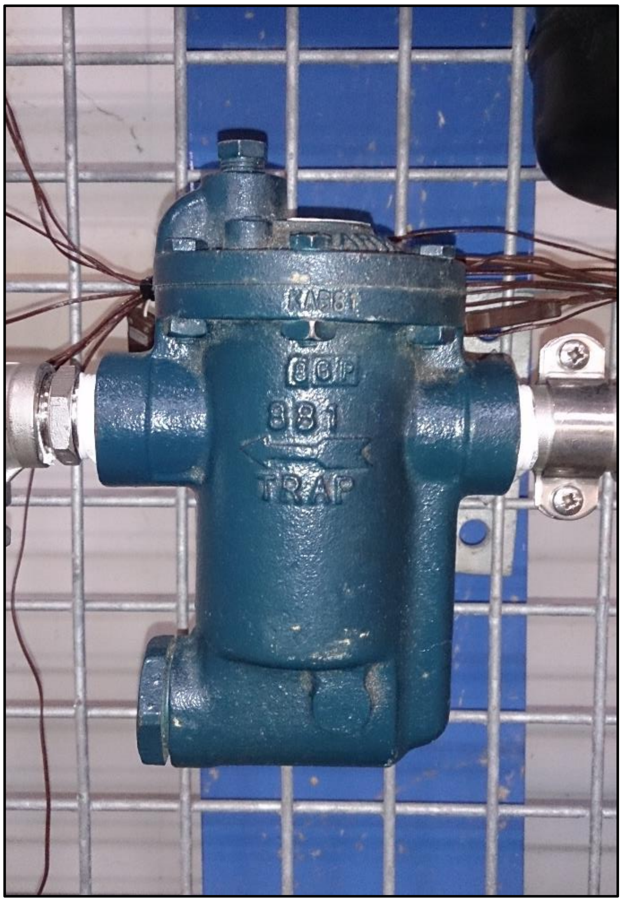

Figure 3.9: Steam trap.

3.2.1.4 Pressure Reducing Valve

A direct acting DR20 PN-DR pressure-reducing valve (PRV) was used to reduce the pressure of the incoming steam from a nominal 6 bar_g to the desired pressure (with the aid of the vacuum pump system) and also to control flow of steam.

The PRV has restricting element that provides restricted flow of steam to the system. PRV comes with pressure adjustment handle connected to diaphragm. The movement of diaphragm is use to regulate the pressure. Figure 3.10 shows the PRV used on the experimental rig, the downward pressure on the diaphragm can increase by adjusting the handle position upwards. With no inlet pressure, the spring above the diaphragm pushes it down on the poppet valve, holding it open. Once steam introduced, the open poppet allows flow to the diaphragm and the pressure in the upper chamber increases, the diaphragm pushed upward against the spring, causing the poppet to reduce a flow, finally stopping further increase of pressure (Spirax-Sarco, 2007)

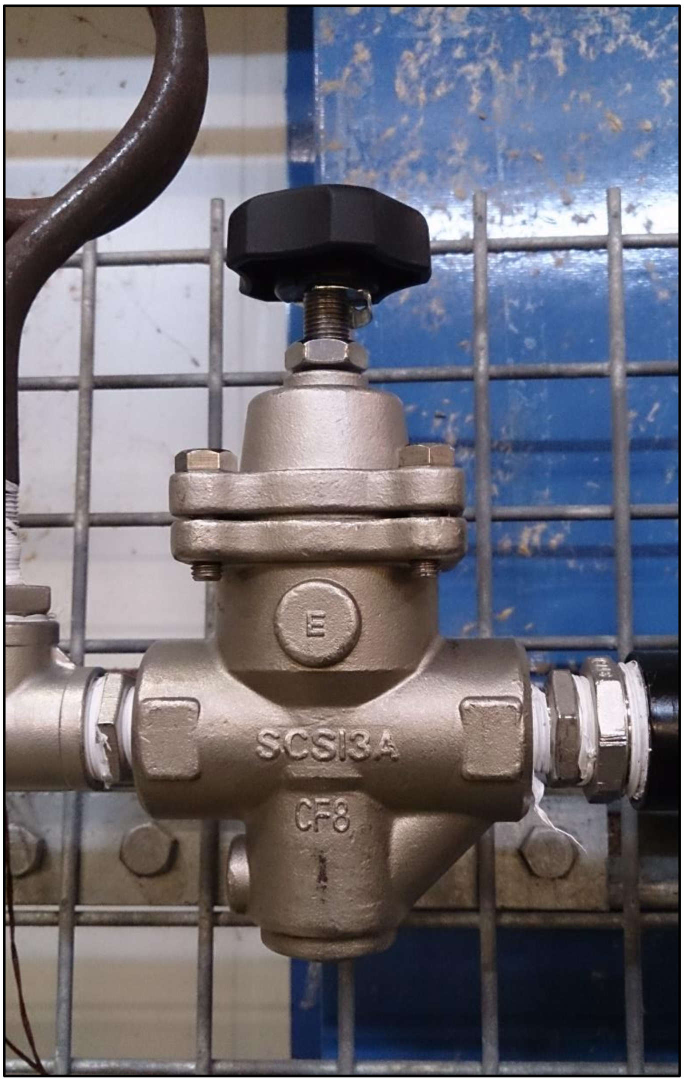

Figure 3.10: Pressure reducer valve.

3.2.2 Coolant Loop

The test facility was equipped with a liquid water coolant to operate in a closed loop configuration. The liquid handling system consisted of a 40 L tank and two pumps for recirculating the coolant and discharge of the coolant. A 40 L tank initially filled with approximately 18 L of water. The water level in the tank measured using a differential pressure transmitter that measure the pressure difference between two mediums, inside tank. Figure 3.11 describes the flow of water in the system. Water pumped directly from tank to the tubes of the condenser. A CDX/A 70703 Lowara pump (A) extracted water from the tank, passing it through the inner tubes of the condenser. On leaving the tubes, the hot water was sent to cool through a fin and tube heat exchanger (HEX 1), mixed with the condensate which were coming out from shell of the VSTC, and then to a plate heat exchanger (HEX2). The temperature of tube-side water was controlled by adjusting the external cooling water flowrate and airflow over plate, and fin and tube heat exchanger respectively. A centrifugal fan used to blow cool air over fin and tube heat exchanger. A 0.37 kW three phase EBARA CDX 70/05 series centrifugal pump (B), controlled by VSD-Altivar 61, as a discharge pump was used to expel water from tank. The pump controlled using a PID feedback loop to the VSD based on the reading of the differential pressure transmitter, which measured the tank level. The pump runs at its maximum frequency of 50 Hz when the PID feedback is much greater than the set PID reference. Similarly, the pump would stop when the PID feedback is well below the set PID reference. A bypass line from the pump discharge some water to tank via a partially closed valve.

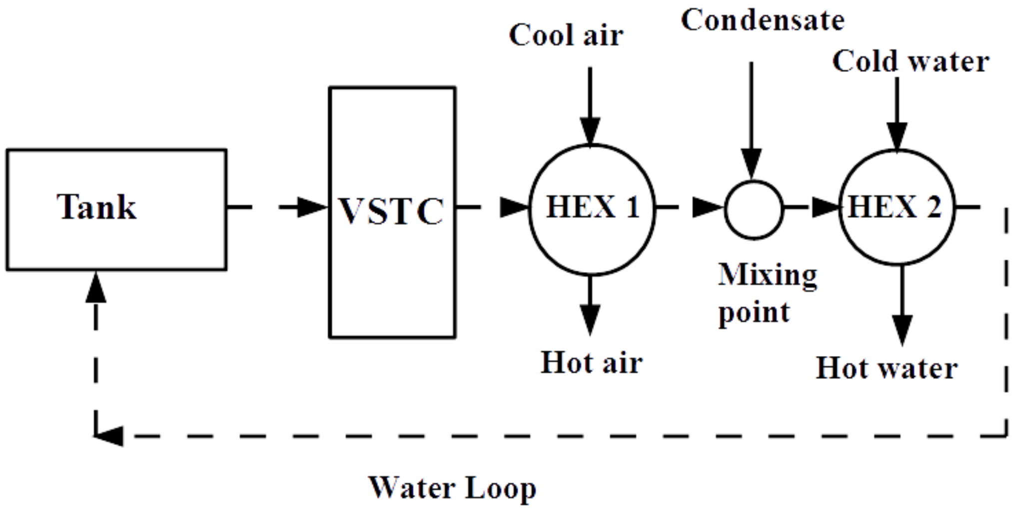

Figure 3.11: Cooling water circulation of a system.

3.2.3 Vacuum System

A vacuum system used to reduce the system pressure below atmospheric pressure. The vacuum system included water tank (under vacuum), and a vacuum pump. Pressure was measured by a vacuum gauge on top of the water tank. A TRMX257-1-C-RX single stage liquid ring vacuum pump provides the vacuum in the system. With seal, water provided by a separate tank as seen in the Figure 3.12. The system provided a needle valve to provide precise control the vacuum.

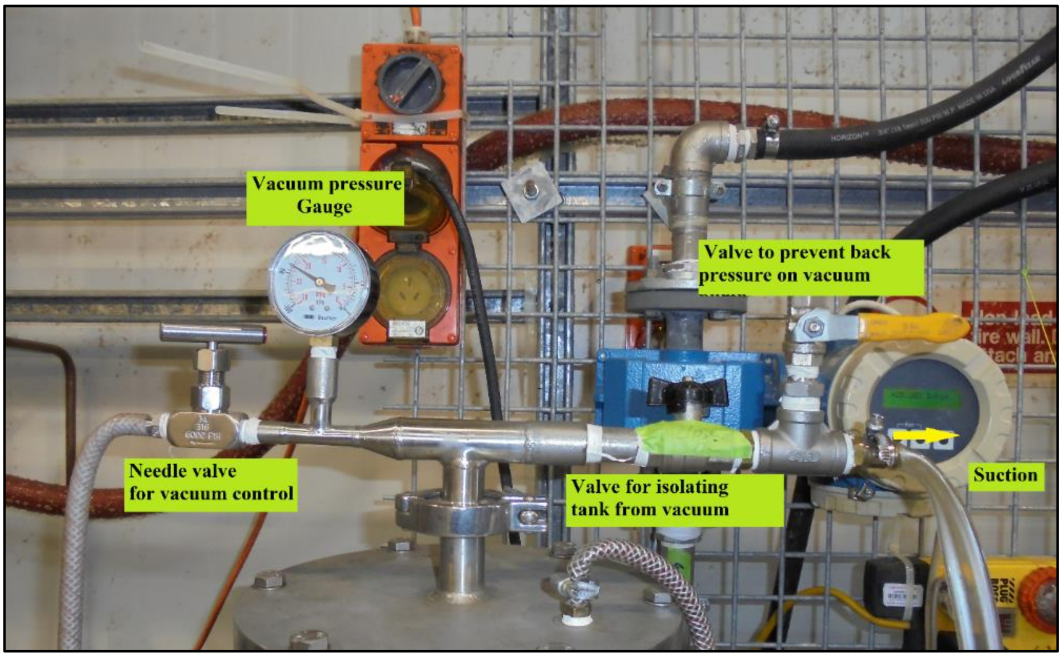

A. Suction from top of the tank

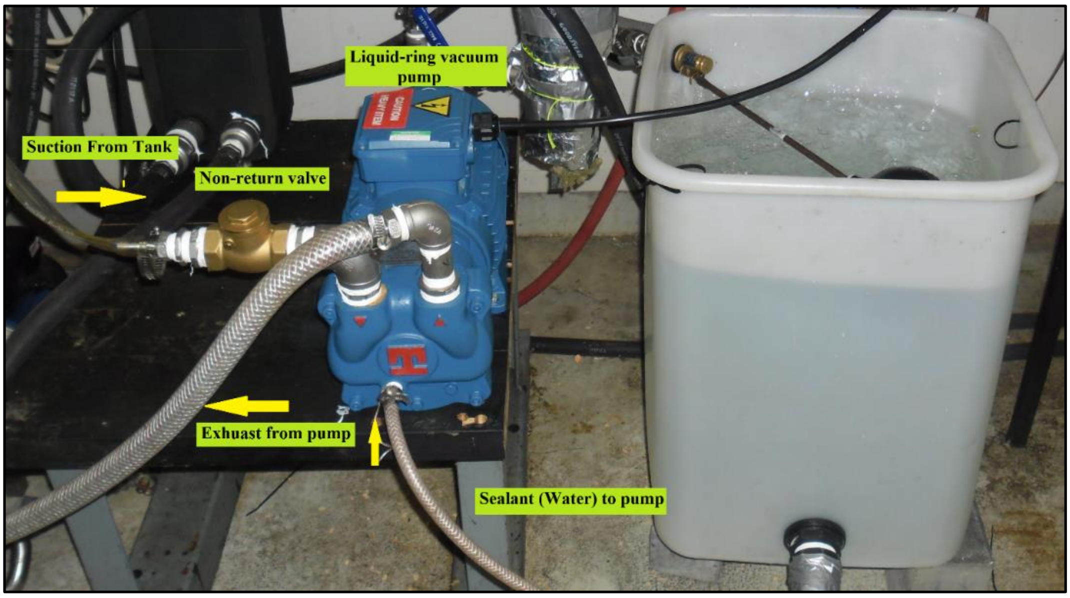

B. Liquid-ring Vacuum Pump

Figure 3.12: Vacuum system.

3.2.4 Condensate Handling

On leaving the VSTC, the condensed steam and uncondensed saturated vapour from outlet of the shell-side mixed with cooling water that was entering the tank after dumping heat at plate, and fin and tube heat exchanger after flowing through tubes of the condenser. The arrangement for mixing the condensate/steam mixture into water loop is presented in Figure 3.13.

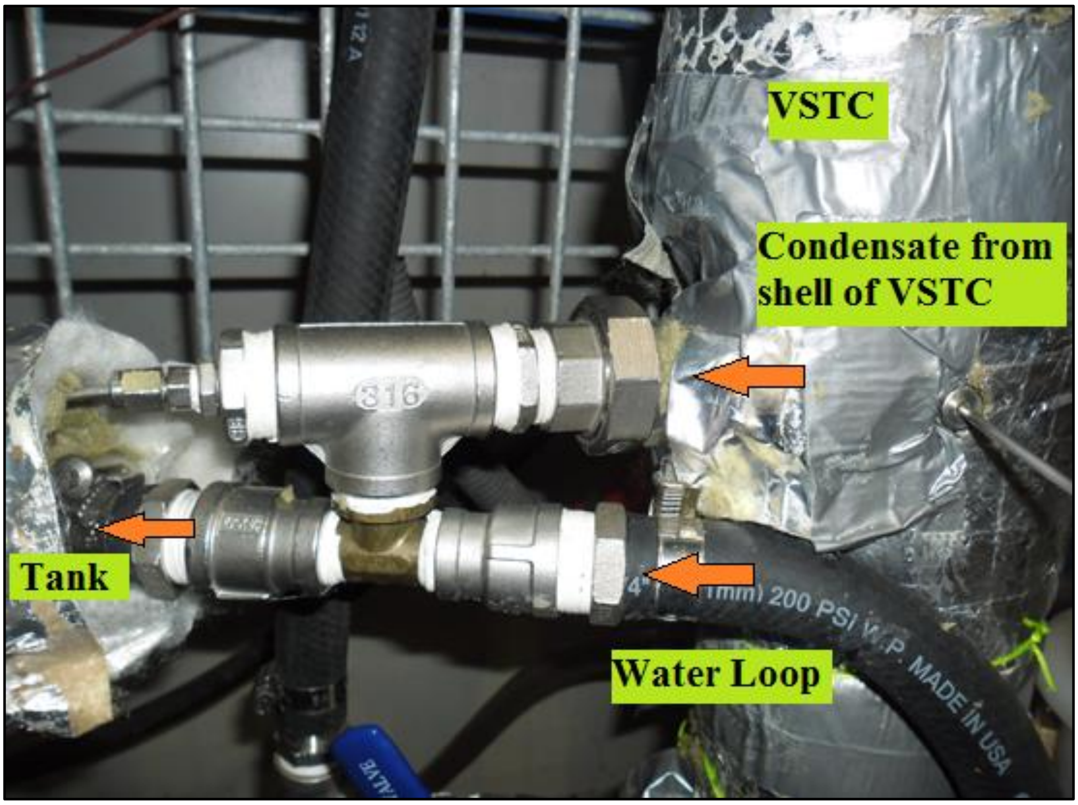

Figure 3.13: Mixing region of condensate and water.

3.2.5 Insulation

The test rig and steam handling system were insulated by 50 mm fibre glass wool (Figure 3.14). The insulation can withstand high temperature, 450°C.

Figure 3.14: Insulation to the system.

3.3 Instrumentation and Process Control

3.3.1 Temperature

Fifteen (15) sheathed Class 1 T-type thermocouples used for measuring temperature, at different position of system. Eleven (11) thermocouples were placed along the length of VSTC, at equal distance. The remaining four of thermocouples are placed axially at the steam inlet and condensate outlet, and inlet and outlet of tube-side water respectively.

An Agilent 34970A data logger is used to record thermocouple measurements using 20 channel multiplexer. T-type thermocouples with 3 mm probe diameter embedded in a VSTC with the help of compression fittings (Figure 3.15). The depth of thermocouple probe into the annulus selected to avoid contact with tube wall.

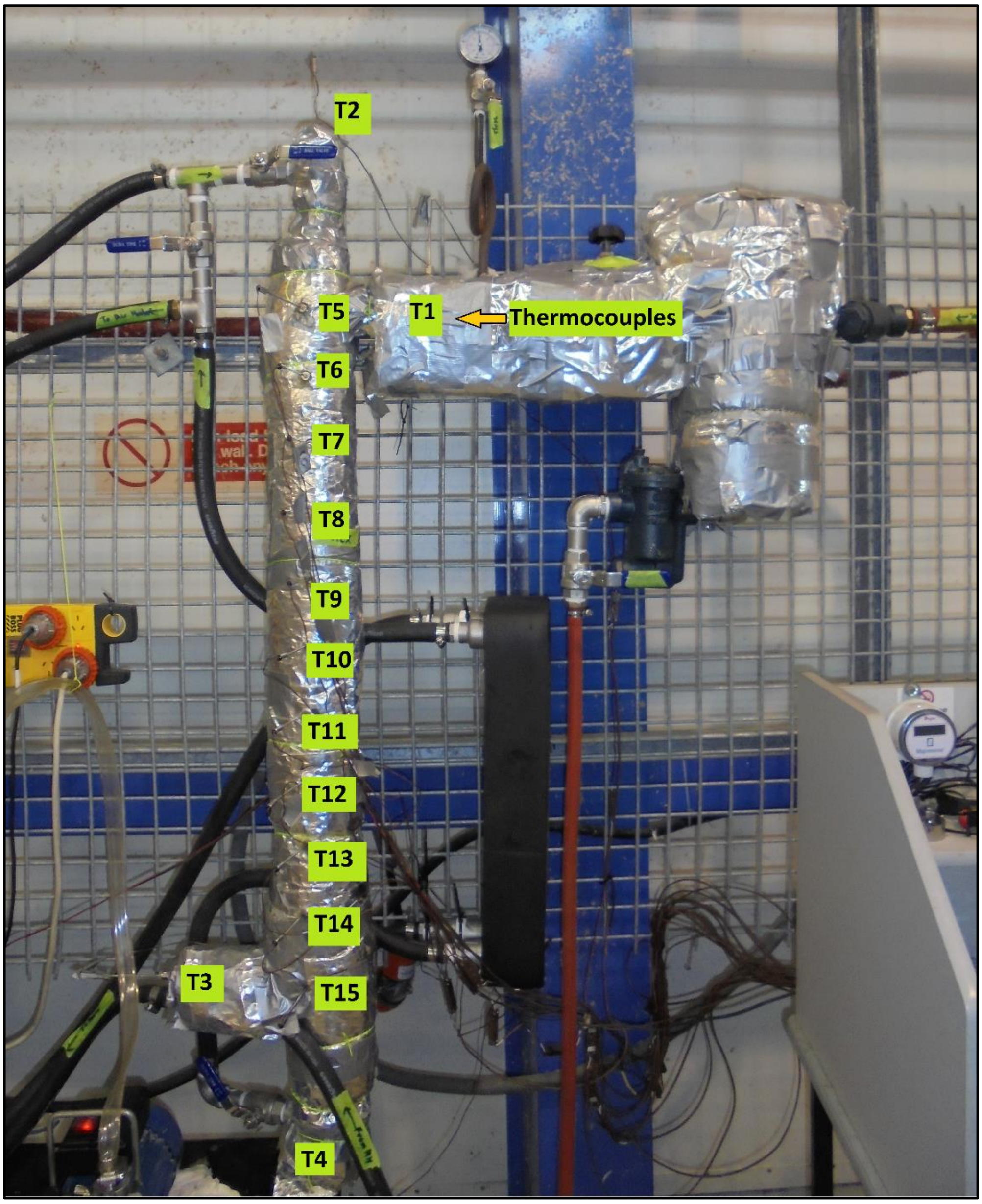

Figure 3.15: Thermocouples mounting in VSTC.

Thermocouples were calibrated carefully before actual use for accuracy purpose, based on isothermal check the error associated with thermocouples was 0.2%. All thermocouples calibrated by putting them into boiling water and water/ice mixture before mounting on the system (Figure 3.16). Individual thermocouples were then corrected based on this initial calibration. The maximum thermocouple correction was 0.44°C.

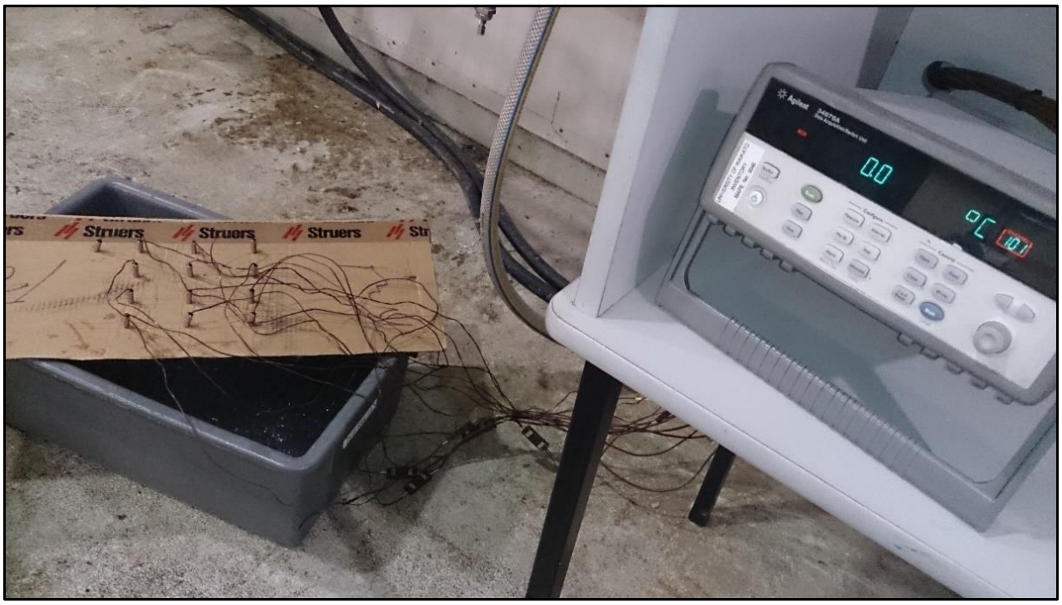

Figure 3.16: Calibration of thermocouples with Agilent 34970A (data logger on the right side in picture).

3.3.2 Pressure

Mechanical pressure gauges, which are two vacuum gauges, and two above atmospheric pressure gauges as shown in Figure 3:17 used to measure the system pressure. These vacuum pressure gauges at the inlet of VSTC, and top of the water tank, displayed vacuum pressure in kPa and in Hg, while atmospheric pressure gauge at similar location read in kPa and psi.

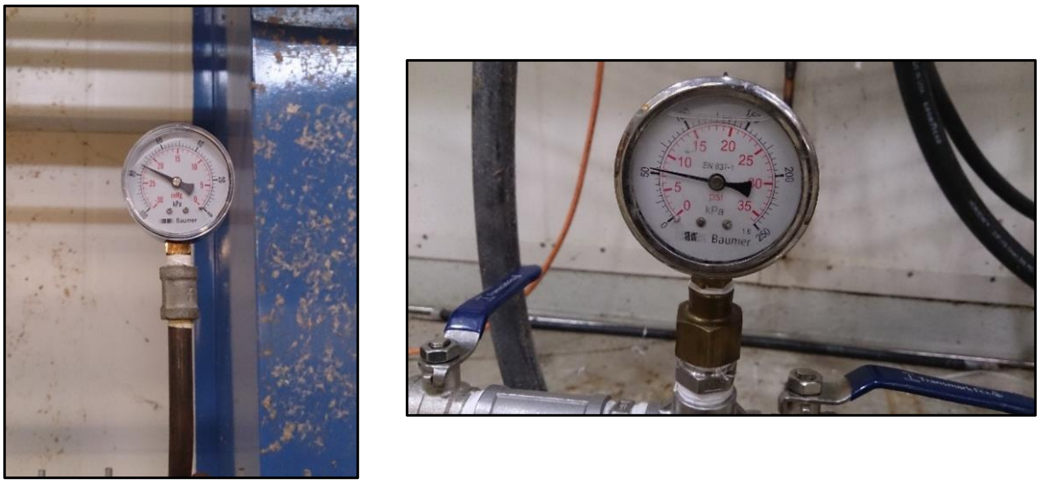

Figure 3.17: Pressure gauges.

3.3.3 Flow Measurement

Flow meters from Endress+Hauser, Promag 50 measured the flowrate entering the tube-side of VSTC, and the condensate coming out from tank, which is equivalent to the total steam mass flowrate (Figure 3.18).

Figure 3.18: Flowmeter.

For the experiment, the Promag 50 measured flowrate in L/min. Adjustment of a ball valve at the entry of tube-side of the VSTC controls the cold-water flow rate and a needle valve control the condensate flowrate to the drain exiting the tank. The condensate flow was also logged. Flow meter programed such that it can read flow rate of water for range of 0-5 L/min. using 4-20 mA loop with the logger.

3.4 Investigations Made on VSTC

3.4.1 Experiment 1: Vacuum Steam Condensation

First experiment was about inspecting vacuum steam condensation for various steam pressures. Each experiment took about 40 minutes to attain steady state. It was essential while running the experiments to ensure 1) enough water level inside tank, 2) to set required shell-side system pressure, flowrate of water at set value through tubes of condenser, and the pressurised steam to the system. In the case of measurements from test facility, except PID feedback, and pressure gauge measurements, all other parameters noted with help of data logger. Table 3.2 enlists the fixed and variable parameters for experiment.

Table 3.2: List of parameters for running the experiment

Parameters	Units	Range
A) Constant Parameters		
Water flowrate through tubes of condenser $\dot{m}_w$	L/min	15
Pressure inside tank, P	kPa_{abs}	21
Water inlet temperature, T_2	°C	49
B) Variable Parameters		
Superheated steam pressures, P	kPa_{abs}	31-101
Superheated steam temperatures, T_1	°C	100-140
Water outlet temperature, T_4	°C	55-75
Condensate temperature, T_3	°C	65-120
Steam temperatures along the VSTC, $T_5 - T_{15}$	°C	70-120
Condensate flowrate, m_{cond}	L/min	2

There were certain alterations carried out in test facility over time. The changes have done for effective cooling of water to the required temperature.

3.4.2 Experiment 2: Vacuum Steam Condensation at Reduced Steam Flowrate

The second part of the experiment was to vary the steam flowrate entering the shell-side. Suitable bypass arrangement made to steam main that diverted certain amount of steam to the coil arrangement, which immersed inside cold-water tank as seen in Figure 3.19. Opening the ball type valve caused splitting of steam stream and reduction in the steam flow to the VSTC. Rest all other parameters were same.

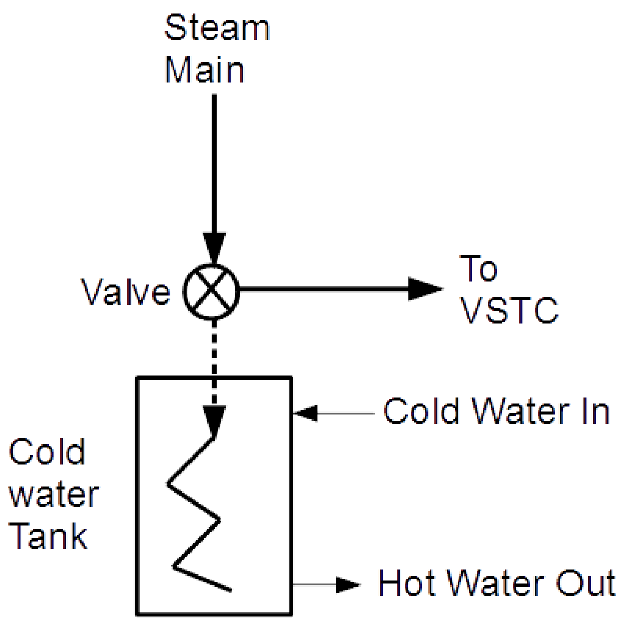

Figure 3.19: Steam flowrate reduction arrangement.

3.4.3 Experiment 3: Investigating Dry Heat Transfer Mechanism for Vacuum Steam Condensation ($T_2 \geq T_{sat}$)

Third experiment particularly performed to examine dry heat transfer. The cooling water through tubes heated up to saturation temperature of steam so that wall of the tubes would dry. To perform this experiment, changes made with existing test facility as seen in Figure 3.20. The shell-side and tube-side of VSTC were separated. The hot water from open tank pumped to the tube-side and returned to the same tank. The saturated steam from shell-side returned to the existing tank, the tank was under vacuum and initially filled by cold water. The water from tank has circulated through two heat exchangers (HEX 1 and HEX 2) to maintain the tank water temperature.

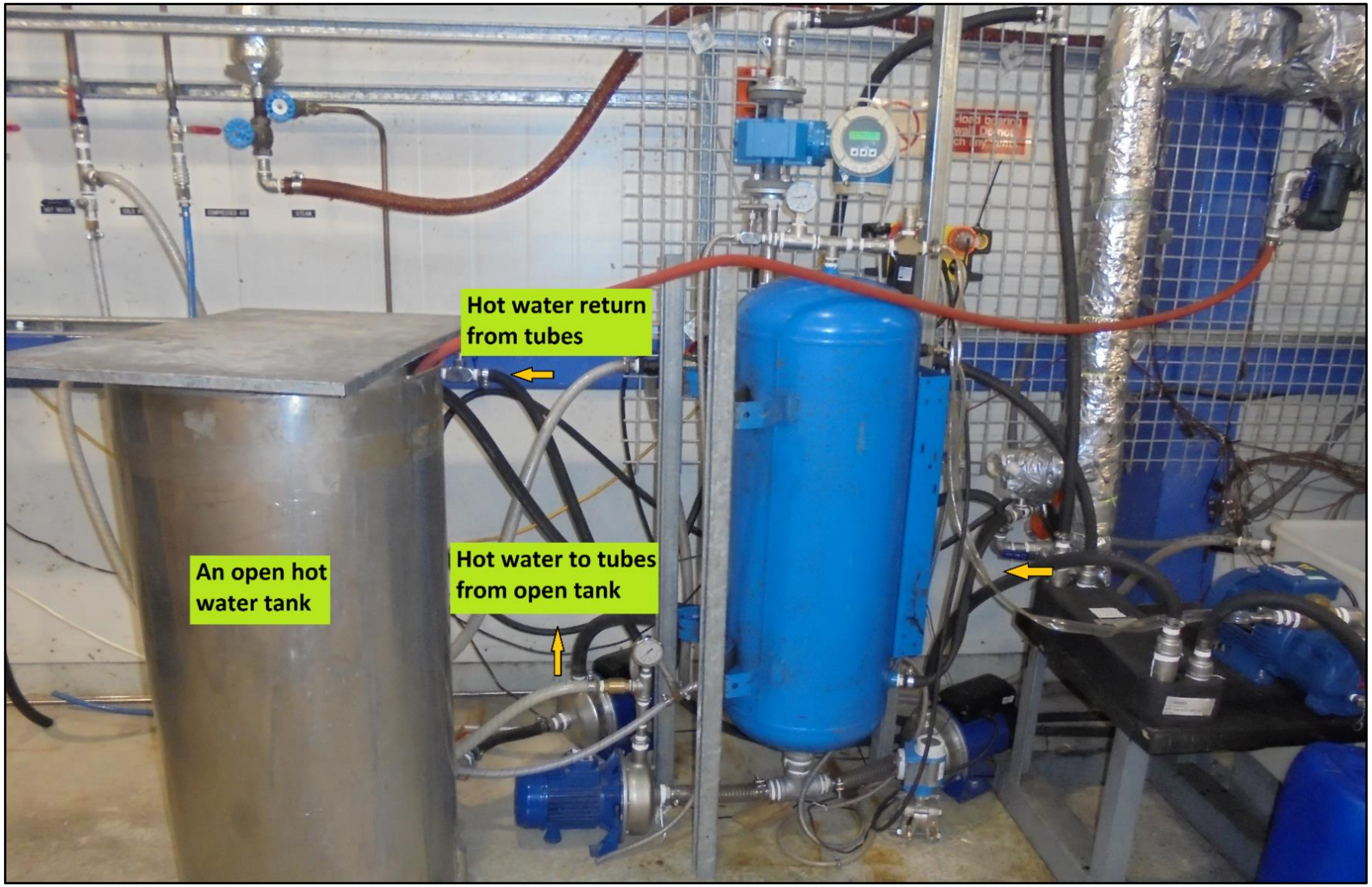

Figure 3.20 Experimental setup for investigating vacuum steam condensation at high tube wall temperatures ($T_2 \geq T_{sat}$).

In the present work, Excel-spreadsheets with Microsoft visual basics enabled used. Different heat exchanger equations coded. The Excel-macros workbook contains steam table stored that makes easier to get all properties of steam at different conditions.

3.5 Experimental Procedure

The steps in carrying out the experiments were as follows:

Steam, normal water, and compressed air were used for the experiments.

1. The boiler was started for steam generation.
2. The design has been pressure tested and made suitable for vacuum system by isolating from atmosphere and injecting compressed air through the system for leak detection. This step performed at initial stage of building of a rig, and after replacement or change in position of any part of test facility.
3. A Bench link data logger was switched on and Agilent IO libraries suite was started to ensure the connectivity of all measuring devices like thermocouples, and flowmeter to computer.
4. At first, the water level in the tank adjusted and initially noted using differential pressure transmitter.
5. Water flow inside the tubes of VSTC initiated by switching the water pump on.
6. PID loop initiated by tuning the Altivar 61 variable speed drive, to start the secondary water pump (EBARA I-38023).
7. The steam trap valve shut off and vacuum pump started. Required vacuum pressure maintained inside the water tank.
8. After achieving steady state of require pressure in tank, steam introduced to the rig by opening main steam valve. Steam trap valve also adjusted simultaneously to maintain the vacuum established in the system.
9. The temperature of water in the tank maintained by passing it through plate heat exchanger, and fin and tube heat exchanger driven by fan.
10. Data acquired from system after the steady state achieved.

Pressure of the system changed through PRV for sets of reading.

3.6 Error Analysis

Present topic involved wide range of experimental testing under different operating conditions. Moreover, the test apparatus changed several times to overcome operational problems, replacement of some individual pieces of equipment. The following section discusses the various sources of error associated with experiment as well as the reproducibility of the results.

3.6.1 Heat Balance

The energy balance based on the amount of steam entering the VSTC, condensate collected from the outlet of the VSTC and the cooling water flowrate through tubes. Since present system is a closed system, the cooling water after passing through tubes mixed with the mixture of saturated vapour and liquid condensate from shell-side. As steam did not condensed completely in VSTC, a part of saturated vapour along with condensate mixed with water and entered the tank. The steam flowrate therefore calculated based on the energy balance on the tube-side cooling water.

3.6.2 Leakages of Test Equipment

Over the time, different experiments run through apparatus. Due to high temperatures, loosening of hose clamps and other fittings cause leakages. Every joint of apparatus has tightened at time interval and after any change in setup and air leakage test performed to maintain the desired vacuum pressure of an apparatus.

3.6.3 Temperature Sensors

Thermocouples calibrated before installing them on VSTC as mentioned earlier. The offset value gained from calibration of each thermocouple added to the respective channel in data logger to get corrected temperature. The temperature profile of steam condensing at shell of the VSTC showed waviness, temperature for every alternate thermocouple was increasing or decreasing. The desuperheating section in result chapter will be discussing about it. To ensure thermocouples are not in contact with any metal part of VSTC, thermocouple positions were changed, and thermocouples were switched and pattern of variation was similar.

3.6.4 Pressure

Less error associated with pressure measurement in the experiment. Pressure gauge was reading test pressure decently of VSTC for first experiment. Pressure drop along the length of hose that connects tank and VSTC was foremost concern during building a rig. About 10 kPa_g drop in pressure observed in VSTC. For second experiment due reduction in flowrate of steam to the VSTC, pressure variation occurred. For heat transfer analysis, saturation pressures for respective temperatures considered.

3.6.5 Re-testing

Although experiment of each test pressure has done distinctly on a separate day, to check the effect of ambient conditions such as temperature, the experiments repeated again. Figure 3.21 shown below illustrates two temperature profile of 33 kPa_{abs} pressure (–66 kPa_g) for same experiment examined on different days. Similarly, remaining test pressures tested again. (See Appendix F)

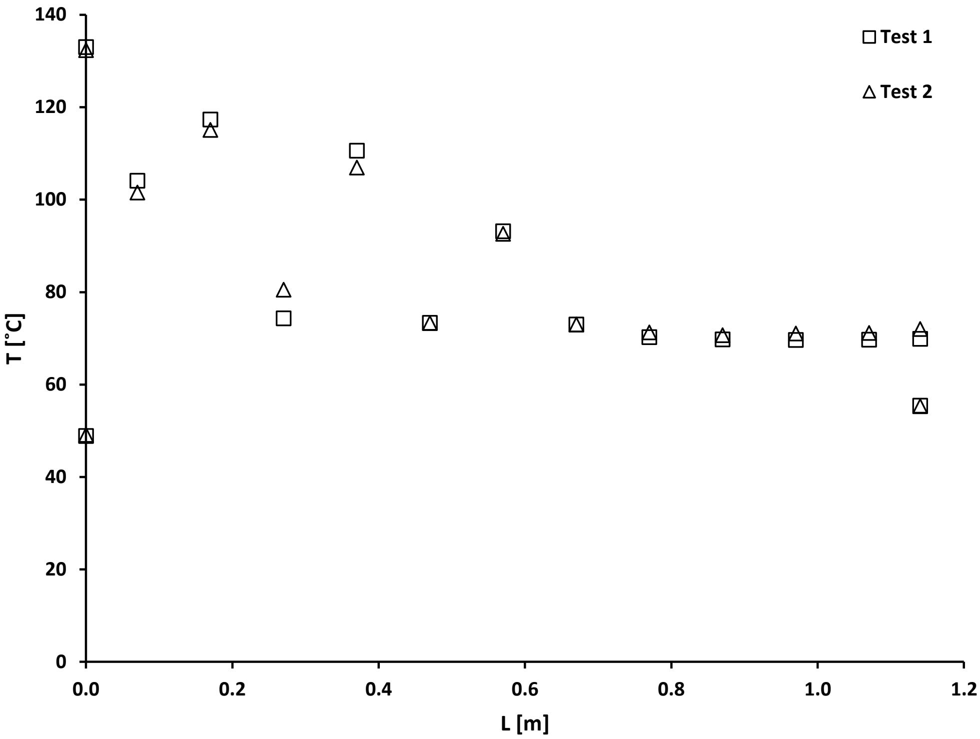

Figure 3.21: Temperature profiles of 33 kPa_{abs} pressure (–66 kPa_g).

As seen in the figure good reproducibility was achieved with the greatest difference in temperatures occurring in the desuperheating section.

3.6.6 Re-testing Test Pressures after Replacement of Equipment

During the latter part of the experimental programme, the replacement of the tank became necessary due to it being required elsewhere. A re-purposed 100 L compressed air receiver was used as a replacement tank in vertical alignment (Figure 3.22). The suction sides of pump were made big enough to ensure minimum pressure drop at discharge.

Figure 3.22: New setup of a tank.

After discharge from the pump- A, (see Figure 3.2) previously water used to pass through flowmeter and tubes directly, but due building up temperature inside tank it was necessary to cool the tank temperature. Therefore, small quantity of water after discharge from pump-A bypassed and it mixed with hot water that was coming from tube exit (Figure 3.23). It reduced hot water temperature and further drop in temperature by a HEX 1. The new setup of the experiment has showed similar results like previous setup (Figure 3.24)

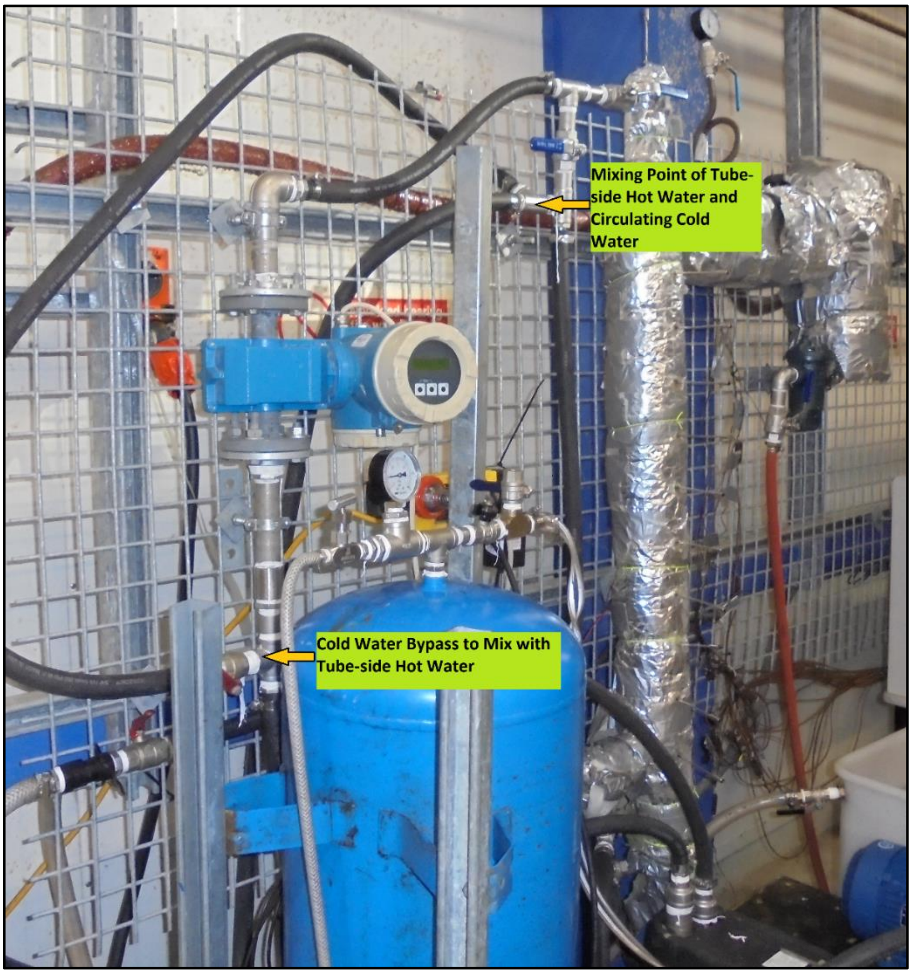

Figure 3.23: Mixing cold water with hot water that is coming from tube exits.

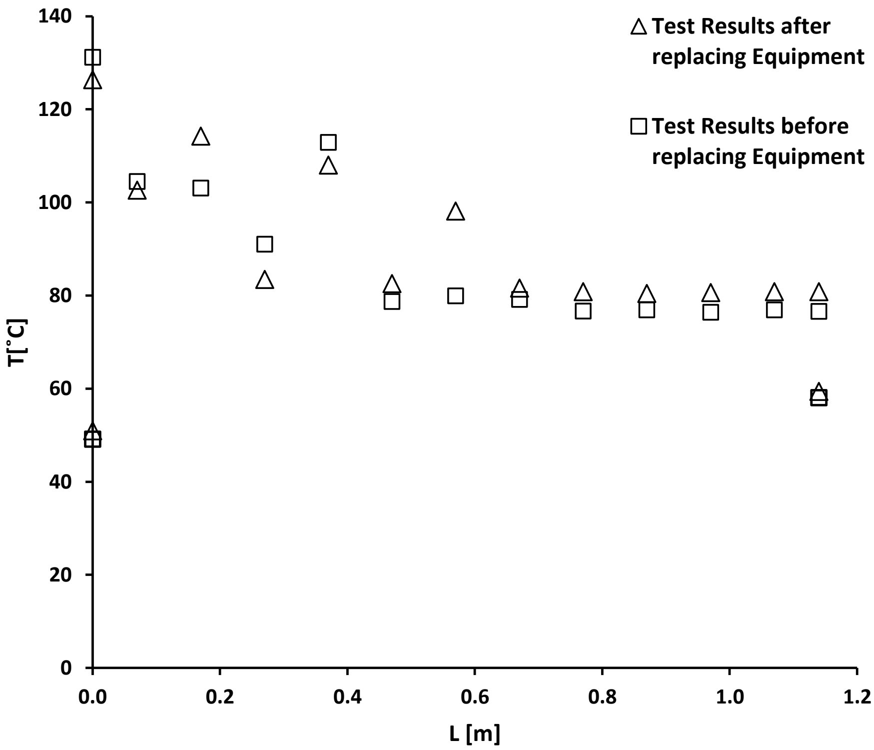

Figure 3.24: Plot of results of 0.41 kPa$_{abs}$ pressure (–50 kPa$_g$) before and after change in setup.

3.7 Summary

This chapter has described the VSTC setup and other equipment used for this study. Detailed installation of used equipment and their purpose described in this chapter. Detailed steps for operations have explained in procedure section. Changes in the test facility have been made as research progressed. The next chapter presents and discusses analysis of the data recorded from experiments. Desuperheating section of VSTC and respective averaged heat transfer coefficients will be examine in detail.

Chapter Four

Experimental Results and Discussion

4.1 Overview

This chapter presents and discusses results of the experimental programme. A total of 32 individual tests at different pressures were conducted on the vertical shell and tube condenser (VSTC) for the first part of the experimental programme. The results for a single experiment will be presented first to demonstrate what data collected and the detail analysis was performed for each condition. Later all experimental results will be presented together using averaged desuperheating and condensation sections of VSTC to show important effects.

The second set of experiments consisted of reducing steam flowrate entering the VSTC. Existing test equipment altered for four reduced steam flowrate experiments for same test pressures. Finally, to investigate and remove any effect from condensation during the desuperheating section due to the tube wall temperature less than steam saturation temperature, the tube-side inlet water temperature was raised above the steam saturation temperature. Four test pressures were tested for these experiments.

4.2 Temperature and Flowrate Scrutiny of 51 kPa_{abs} Pressure (-42 kPa_g)

Temperatures and flowrate data were logged at 5-second intervals throughout each experimental run. Figure 4.1 shows the recorded temperature over time for a test condition of 51 kPa_{abs} pressure (-42 kPa_g). The tube-side water temperatures (T_2 and T_4) were constant during experiment but shell-side temperatures (T_5 and T_{15}) slightly fluctuated. As illustrated in the Figure 4.1, a start-up time to reach steady state was required, which was about 40 minutes in some cases. Individual thermocouple readings were averaged over a 90 minutes period to be used for further analysis. Figure 4.2 describes steam flowrate entering in the VSTC recorded over time for the same test condition of 51 kPa_{abs} pressure (-42 kPa_g). The variable nature of the condensate flowrate was due to PID feedback of a tank level to variable speed drive (VSD) and respective discharge of condensate from water pump (B) (see Figure 3.2).

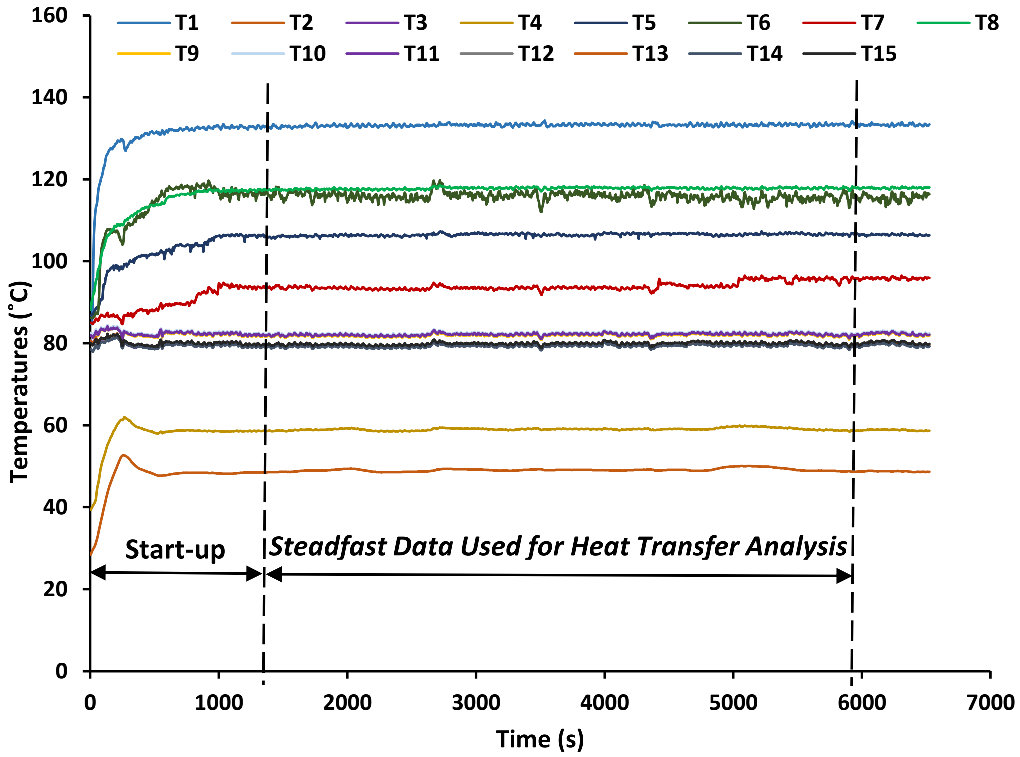

Figure 4.1: Temperatures during a typical trial. {51 kPa$_{abs}$ pressure (-42 kPa$_g$)}

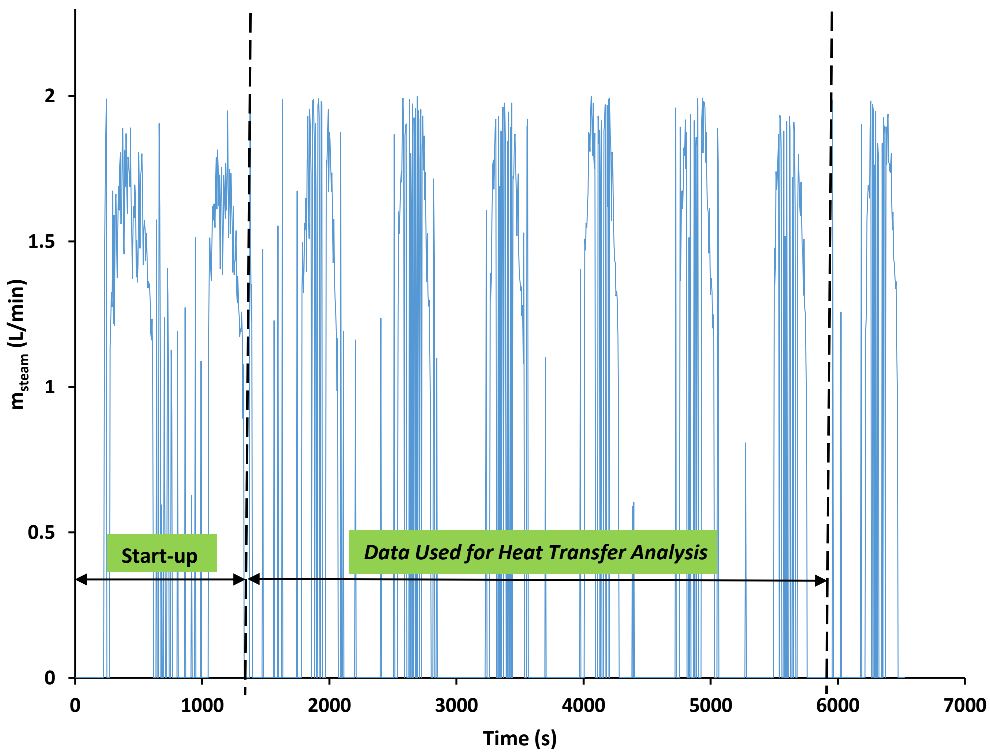

Figure 4.2: Flowrate of the condensate during a typical trial. {51 kPa$_{abs}$ pressure (-42 kPa$_g$)}

Figure 4.3 shows averaged temperatures of the shell-side steam at 51 kPa$_{abs}$ pressure along the length of VSTC, and cooling water temperatures for the tube-side. For 51 kPa$_{abs}$ test pressure, the superheated steam entered the VSTC shell at a temperature about 132°C, starts cooling to a saturation temperature of 82°C, then partially condenses at constant temperature. The cooling water enters at 49°C and heated to an exit temperature of 59°C. The temperature profile of the cooling water is assumed linear as a first approximation. There are two distinct temperature regions for the shell-side. The overall duty of the VSTC for 51 kPa_{abs} pressure was 10.1 kW.

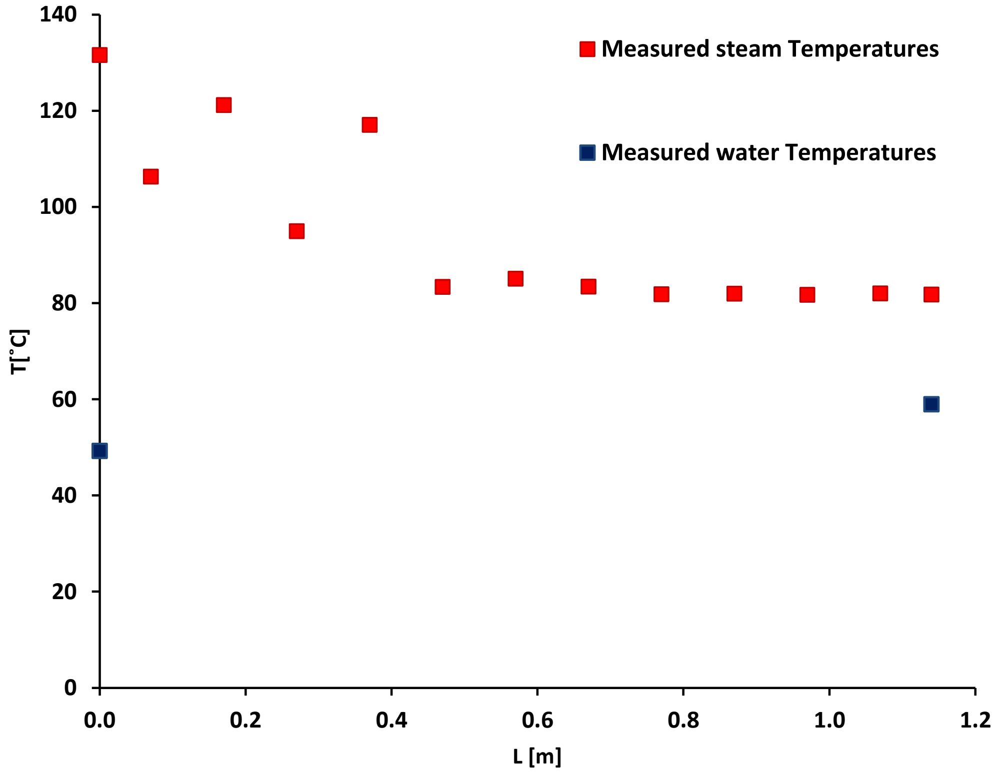

Figure 4.3: Temperature profile along the length of VSTC.
{51 kPa_{abs} pressure (-42 kPa_g)}

The VSTC temperature profile can be divided into two distinct sections as illustrated in the Figure 4.4:

- **Desuperheating section**: the steam is desuperheated with a decreasing temperature along the length, the measured temperature profile in this section is variable, but has a general decreasing trend to the saturation temperature;
- **Condensation section**: once the vapour has reached the saturation temperature, the steam is condensed. For all test cases, only a portion of the steam was condensed and there is two-phase flow from exiting the shell-side of the VSTC.

The temperature profile of each experimental test is presented in Appendix D. The variation in the temperature profile during the desuperheating section appeared to be greater at lower absolute pressures (e.g. 0.41 bar_{abs}).

Due to variation in vapour properties such as velocity and density of steam, each test pressure has slightly different temperature profiles and rate of condensation.

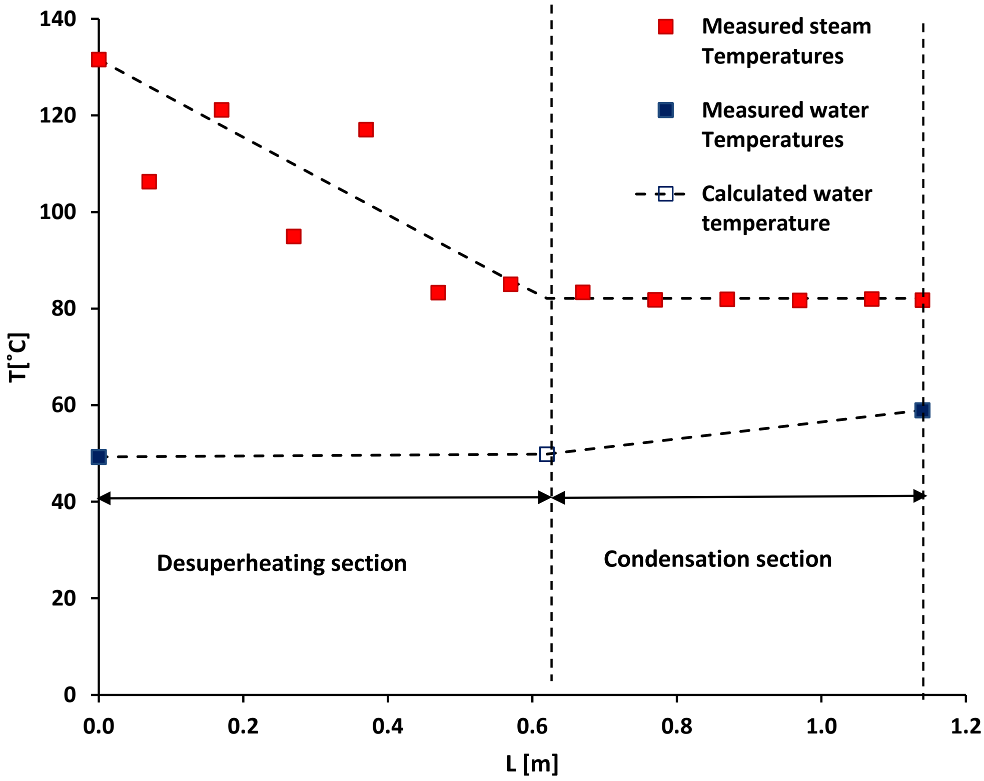

Figure 4.4: Heat transfer sections of VSTC. {51 kPa_{abs} pressure (-42 kPa_g)}

On average, about 60% of VSTC length was desuperheating steam and the rest is condensation of steam at the corresponding saturation temperature for pressure tested. Only a portion of the steam condensed during the trial and two-phase flow existed out of the shell-side outlet of VSTC. Typically only about 44% of the mass of the steam actually condensed in the shell of VSTC for a test condition of 51 kPa_{abs} pressure (-42 kPa_g).

The uniqueness of the condensation region is similar with normal steam condensation process at constant steam saturation temperature.

Figure 4.5 shows the variability of the heat flux along the length of VSTC. Due to the variation of temperatures along VSTC, heat flux per unit area between two thermocouples shows deviation including negative flux for some section. The local heat transfer coefficient (h") for the same section was also calculated and shown in Figure 4.6. Once again both positive and negative heat transfer coefficients occurred along the length. The right hand side secondary axis in both Figure 4.5 and Figure 4.6 shows scale for respective condensation section value. Clearly, this is not feasible because heat transfer will be one-directional from the shell-side to the tube-side, along the entire length of the VSTC due to the temperature difference.

The irregularity is because during the desuperheating section, the measured shell-side temperatures alternate with a decrease and then an increase in temperature. If an energy balance were performed, based only on the measured shell-side temperatures, then the heat transfer appears to be form the cold side to the hot side, which is infeasible.

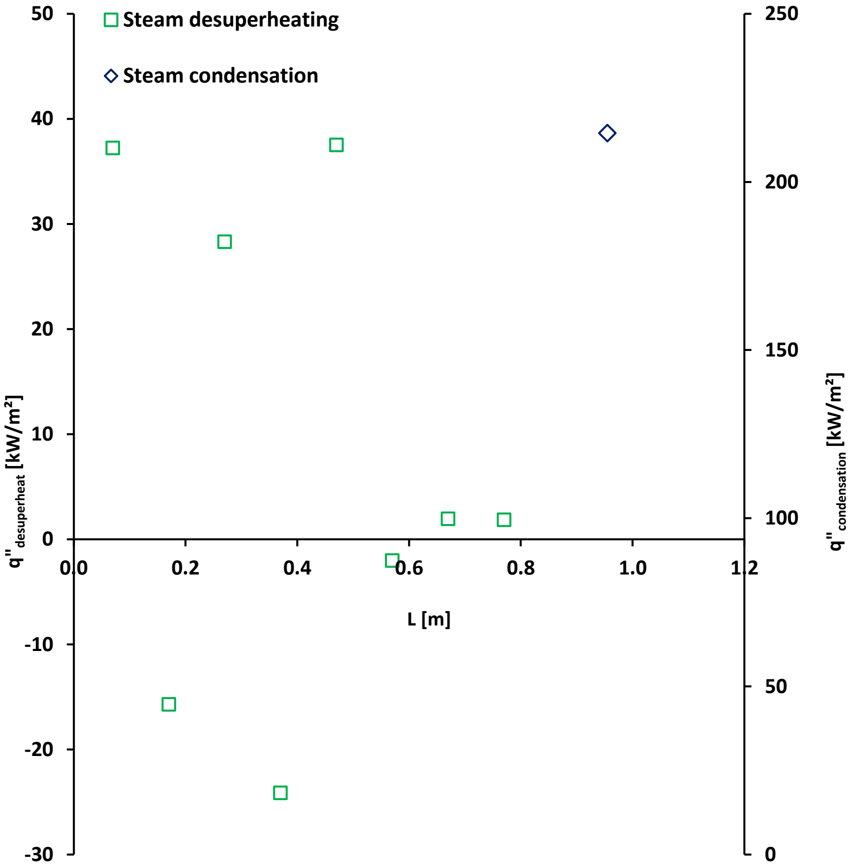

Figure 4.5: Heat flux along the VSTC. {51 kPa$_{abs}$ pressure (-42 kPa$_g$)}

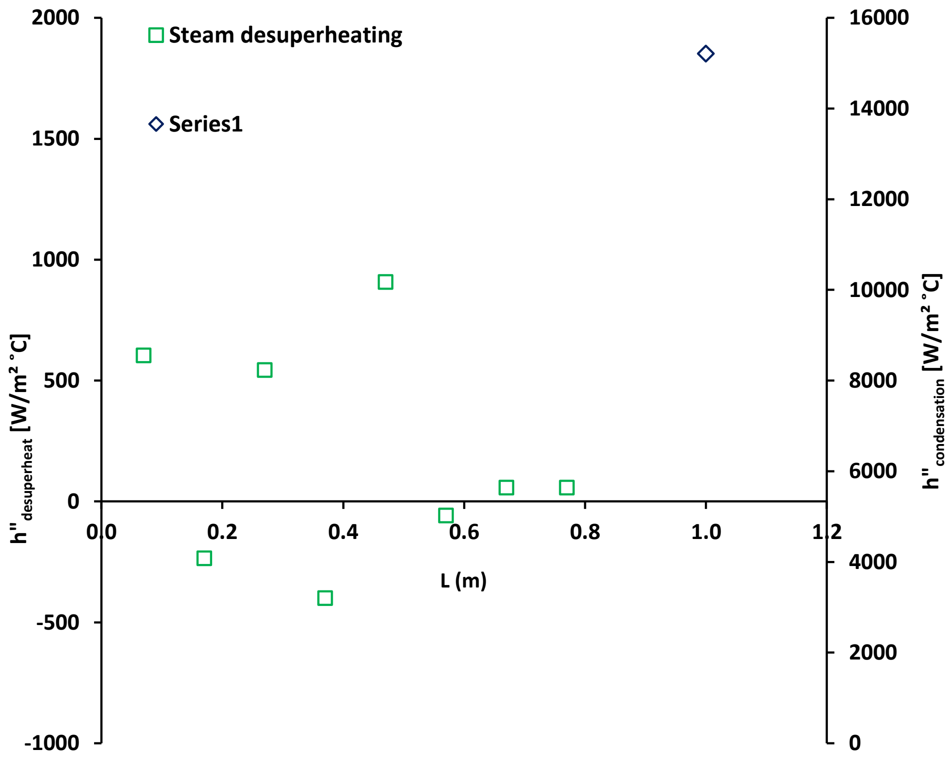

Figure 4.6: Local heat transfer coefficient along the VSTC.
{51 kPa_{abs} pressure (-42 kPa_g)}

The variation in the temperature of the desuperheating section could be due to number of reasons. Initially, it was supposed that it might occur due to contact between the thermocouple and the tube wall. The tube wall is expected to be somewhat less than the saturation temperature due to the relatively low temperature of the tube-side fluid compared to the superheat temperature. The shell-side tube wall temperature (T_{wall}) estimated using the correlation of Minkowycz et al. (1966) as shown in Eq. 5-1 where T_1 is the temperature of the bulk hot side fluid and T_2 is the bulk temperature of the cold side fluid.

$$T_{wall} = T_2 + 0.31 \times (T_1 - T_2) \qquad \textbf{(5-1)}$$

Shell-side tube wall temperatures were less than saturation temperature of steam for tested pressures and for a test condition of 51 kPa_{abs} pressure; the shell-side tube wall temperature would follow the profile shown in Figure 4.7. Furthermore, the thermocouples were mounted such that they were 2 mm away from the tube wall.

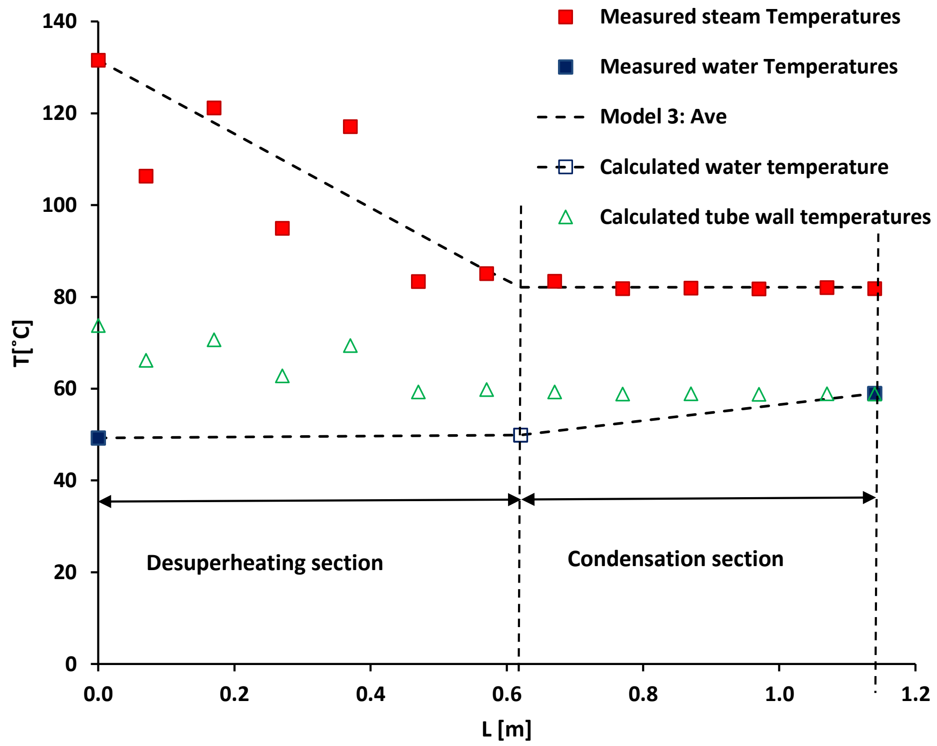

Figure 4.7: Shell-side tube wall temperatures along the VSTC. {51 kPa_{abs} pressure (-42 kPa_{g})}

It was further postulated that there could be condensate bridging the gap between the tube wall and the thermocouple via capillary action and becoming subcooled thus giving the lower temperatures. Using the method suggested by Kirkbride (1934), average condensate film thickness was calculated and estimated to be in the order of 0.14 mm. Thus, the chance of attachment of subcooled droplets to the junction of the thermocouple is extremely slim.

The reason for the irregular temperature profile in the desuperheating section is likely due to the simultaneous process of evaporation and condensation at the surface of cold tubes (see Figure 4.8). The temperature of the tube wall during desuperheating was lower than saturation temperature of the steam. Therefore, condensate, which was dripping down along the tube wall, has a sensible heat transfer by flashing into vapours (Kern & Quentin, 1950).

In order to make the temperature profiles feasible several models of the profiles in the desuperheating sections were developed based on the measured temperatures.

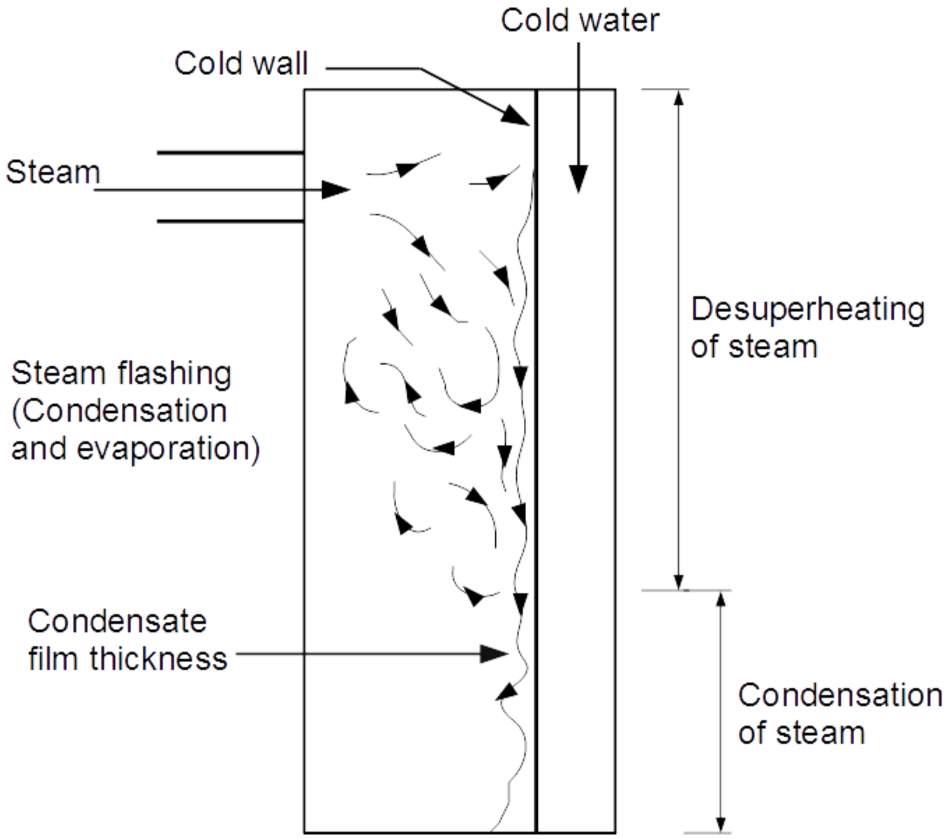

Figure 4.8: Vacuum steam condensation mechanism.

4.2.1 Modelling Temperature Profiles of Desuperheating Section of VSTC

In this section, the temperature profile of steam for desuperheating section is analysed. The desuperheating section was determined to be from the inlet of steam to the point where the steam temperature becomes constant, which assumed to be the saturation temperature. Due to the variation in temperatures along the length, the following models were developed for desuperheating section to simplify analysis.

Three methods for modelling the temperature profile, based on the temperature measurements are described below. These profiles are illustrated in Figure 4.9; linear models are developed for 51 kPa_{abs} pressure. Appendix D shows generated models for remaining test pressures.

- **Model 1: Low–** represents the practical case that divide desuperheating and condensation sections from the sensed temperature by thermocouple probe at 0.77 m from top of VSTC.
- **Model 2: High–** generated by computing the point that has a chance of saturation temperature by reducing the area of desuperheating regime.

- **Model 3: Ave–** is the model generated by averaging the Model 1: Low, and Model 2: High. This model will be representing overall results of each test pressure. Model 1: Low and model 2: High are the actual boundary conditions, in between there is strong chance of steam saturation.

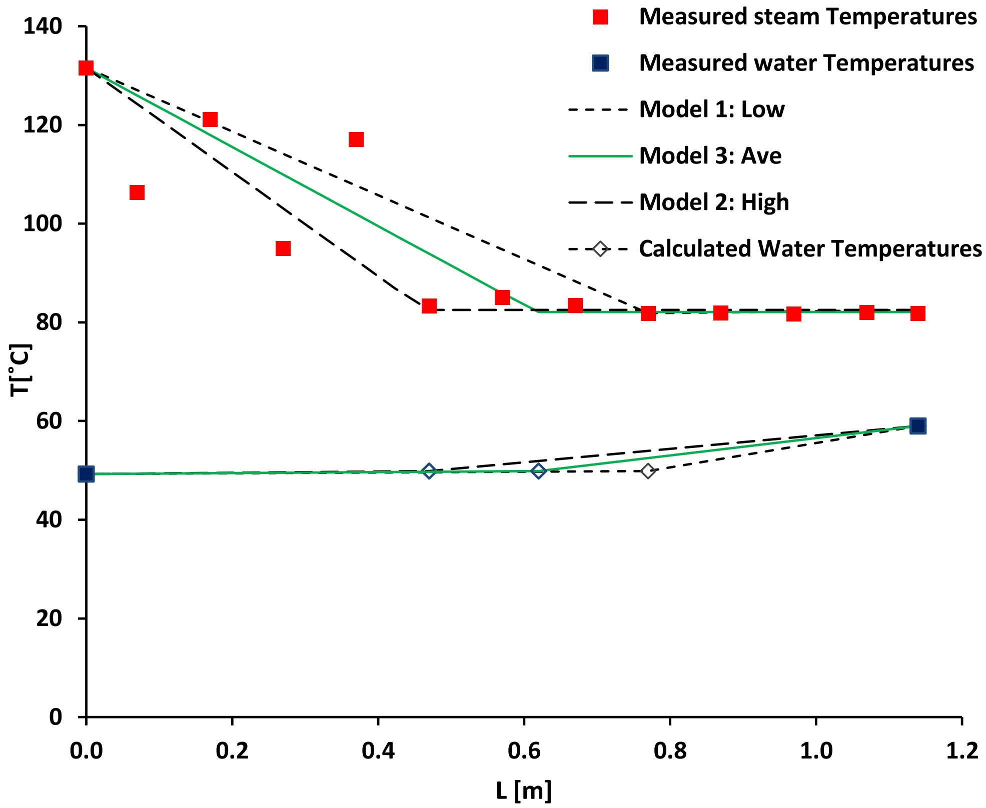

Figure 4.9: Developed condensation models. {51 kPa_{abs} pressure (-42 kPa_g)}

Table 4.1 lists the temperature of steam, the corresponding amount of superheat and the length of each models of desuperheating section.

Table 4.1: Desuperheating models

Desuperheating								
Model 1: Low			**Model 2: high**			**Model 3: Ave**		
L (m)	**T (°C)**	**$\Delta T_{superheat}$ (°C)**	**L (m)**	**T (°C)**	**$\Delta T_{superheat}$ (°C)**	**L (m)**	**T (°C)**	**$\Delta T_{superheat}$ (°C)**
0.00	132	50	0.00	132	49	0.00	132	49
0.08	127	45	0.05	127	44	0.06	127	45
0.15	122	40	0.09	122	39	0.12	122	40
0.23	117	35	0.14	117	34	0.19	117	35

Desuperheating								
Model 1: Low			**Model 2: high**			**Model 3: Ave**		
L (m)	**T (°C)**	**$\Delta T_{superheat}$ (°C)**	**L (m)**	**T (°C)**	**$\Delta T_{superheat}$ (°C)**	**L (m)**	**T (°C)**	**$\Delta T_{superheat}$ (°C)**
0.31	112	30	0.19	112	29	0.25	112	30
0.39	107	25	0.24	107	24	0.31	107	25
0.46	102	20	0.28	102	19	0.37	102	20
0.54	97	15	0.33	97	14	0.43	97	15
0.62	92	10	0.38	92	9	0.50	92	10
0.69	87	5	0.42	87	4	0.56	87	5
0.77	82	0	0.47	83	0	0.62	82	0

4.2.2 Heat Transfer Analysis of 51kPa$_{abs}$ Pressure (-42 kPa$_g$)

Both the heat flux and characteristic heat transfer coefficient are recalculated by model temperature profiles. Figure 4.10 shows the effect of superheat on the heat flux for the desuperheating and condensing regions at 51 kPa$_{abs}$ pressure and shows the effect of superheat on the heat flux for the desuperheating section and on the right hand side secondary axis condensation region at 51 kPa$_{abs}$ pressure. There is a marginal increase in the heat flux in the desuperheating section until condensing commences when there is almost an order of magnitude change in the heat flux due to the phase change and latent heat of the vapour. In Figure 4.10, the vertical bars indicate the span of heat flux for Model 1: Low (negative vertical bar), and Model 2: High (positive vertical bar). The horizontal uncertainty bars Model 1: Low (negative horizontal bar), and Model 2: High (positive horizontal bar) are estimated from respective change in length of sections. The change in heat flux for linear models are noticeable.

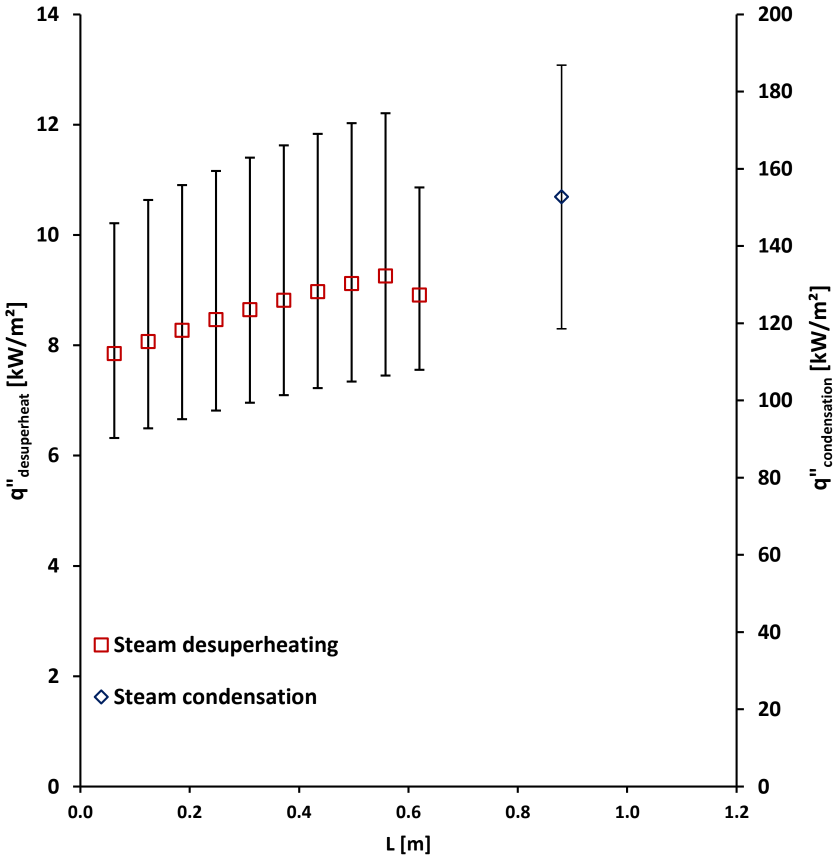

Figure 4.10: Heat flux of desuperheating and condensing section of VSTC.
{51 kPa_{abs} pressure (-42 kPa_g)}

Figure 4.11 illustrates the characteristic heat transfer coefficients for these two sections of VSTC. As seen in the Figure 4.111, a significant rise occurs in the characteristic heat transfer coefficient, as steam is desuperheated. Characteristic heat transfer coefficients also follow the same trend as the heat flux with a gradual increase in the desuperheating section followed by a large increase in the condensing section (right side vertical secondary axis). The characteristic heat transfer coefficient increased from around 90 $W/m^{2}°C$ to 300 $W/m^{2}°C$ in the desuperheating section to approximately 5500 $W/m^{2}°C$ in the condensing section. This value of 5500 $W/m^{2}°C$ is in good agreement with recommended design values for condensing steam (Sinnott, 2005).

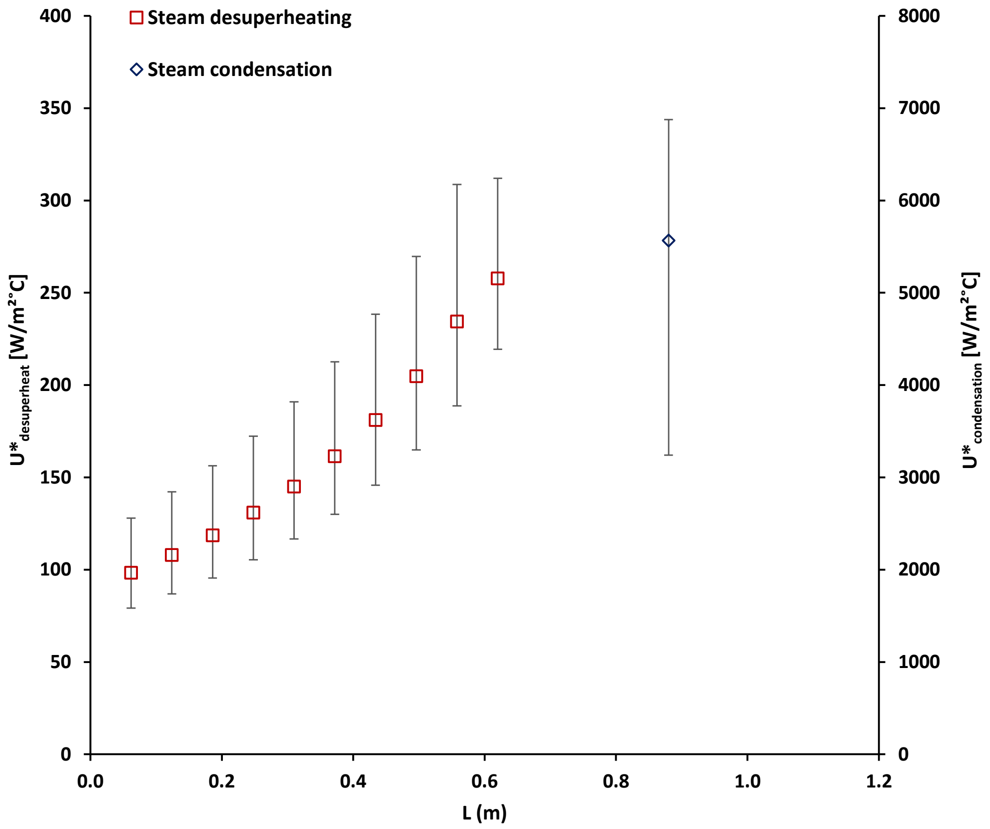

Figure 4.11: Characteristic heat transfer coefficient along the length of VSTC of two sections of condensation. {51 kPa_{abs} pressure (-42 kPa_g)}

Reynolds number of the shell-side vapour were calculated and values were in the order of 21,000 to 25,000 indicating turbulent flow. Figure 4.12 shows overall heat transfer coefficient versus Reynolds number for 51 kPa_{abs} test pressure.

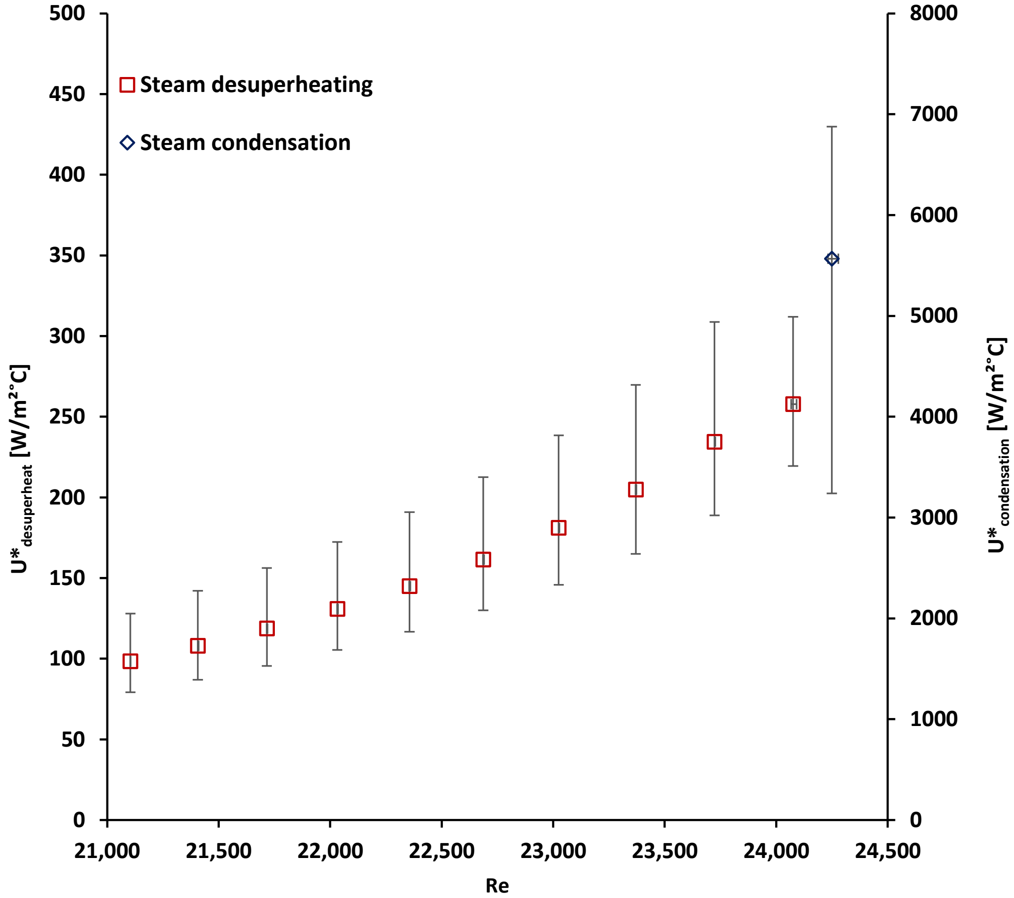

Figure 4.12: Plot of calculated Reynolds number and characteristic heat transfer coefficient across length of VSTC. {51 kPa_{abs} pressure (-42 kPa_g)}

The result section of each test pressure is same as describe above for 51 kPa_{abs} pressure (-42 kPa_g). Figure 4.13 clarifies the analysis of measured temperatures of shell and tube-side VSTC. Temperature profiles of each test pressure analysed by dividing desuperheating section in to 10 divisions. Table 4.2 and Table 4.3 below summarised the averaged results of 51 kPa_{abs} pressure of complete desuperheating section and condensation section respectively. In upcoming overall result section, similar averaged results are used to analyse overall desuperheating and condensation of VSTC of each test pressure.

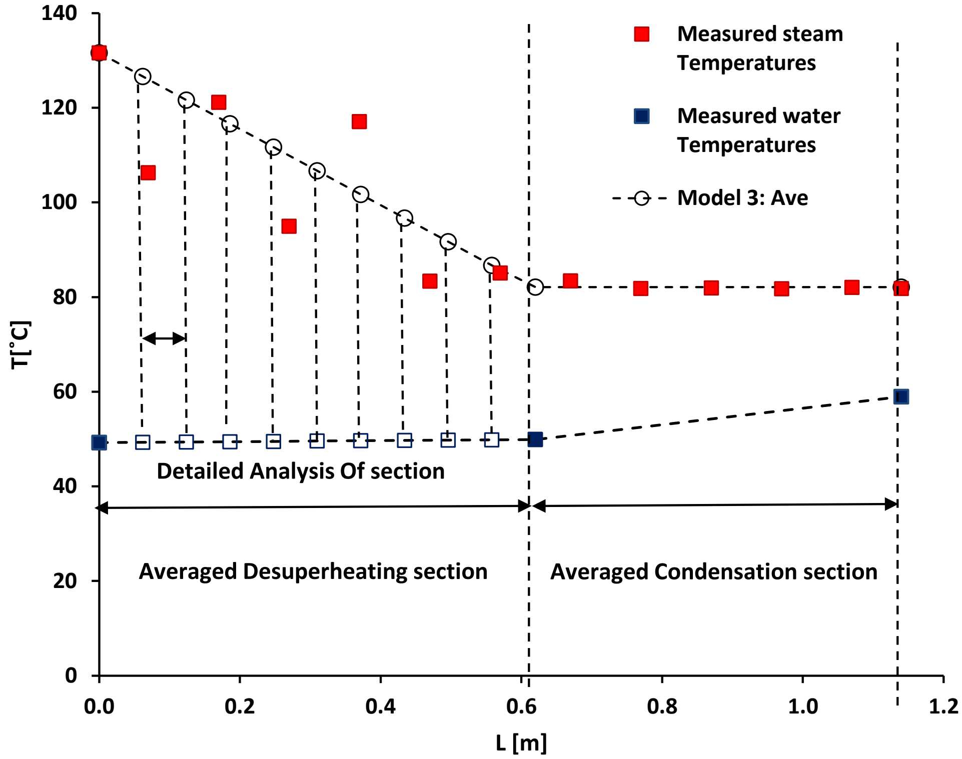

Figure 4.13: Analysis of measured temperatures. {51 kPa_{abs} pressure (-42 kPa_g)}

Table 4.2: Summary of averaged desuperheating section {51kPa_{abs} pressure (-42 kPa_g)}

Region		**Desuperheating**		
Model		Low	High	Ave
$T_{water\ in}$	°C	49	49	49
$T_{water\ out}$		50	50	50
$T_{steam\ in}$	°C	132	132	132
T_{sat}		81.9	82.5	82.1
$\Delta T_{superheat}$	°C	50	49	49
A	m^2	0.092	0.056	0.074
Q	kW	0.6	0.6	0.6
Q_{max}	kW	1.1	1.1	1.1
q''	kW/m²	7	11.3	8.6
LMTD	°C	53	54	53
U”	W/m² °C	131	210	162
ε		0.60	0.60	0.60
NTU		0.93	0.91	0.93
h_{shell}	W/m² °C	312	518	390

Region		Desuperheating		
Model		Low	High	Ave
Re(shell)		22,519	22,499	22,512
Pr(shell)		0.99	0.99	0.99

Table 4.3: Summary of condensation section {51kPa$_{abs}$ pressure (-42 kPa$_g$)}

Region		Condensation		
Model		Low	High	Average
$T_{water\ in}$	°C	50	50	50
$T_{water\ out}$		59	59	59
A	m^2	0.044	0.08	0.062
Q	kW	9.5	9.5	9.5
Q_{max}	kW	33.4	34.1	33.7
q''	kW/m²	214.5	118.6	152.7
LMTD	°C	27	28	27
U”	W/m²°C	7893	4256	5566
ε		0.28	0.28	0.28
NTU		0.33	0.33	0.33
h_{shell}	W/m²°C	15,213	23,522	19,367.5
Re(shell)		24,267	24,220	24,249
Pr(shell)		1.02	1.02	1.02

4.3 Overall Experimental Results at Shell-side Tube Wall Temperatures Less than Steam Saturation Temperatures and at Reduced Steam Flowrate

To relate the total results of remaining test pressures, it is appropriate to consider total desuperheating section and condensation section. Therefore, similar analysis executed like 51 kPa$_{abs}$ pressure and averaged heat transfer results are presented for both desuperheating and condensation sections. Parametric relations are developed between the averaged heat transfer coefficient of steam desuperheating and steam condensation and factors affecting condensation process. Effect of reduced steam flowrate at same test pressure examined on desuperheating and condensation of the steam in the second experiment. To reduce the amount of steam to the VSTC, valve settings were changed as described in section 3.4.2. A total of four pressures were retested at reduced steam flowrates. Unfortunately due to limitations of the testing apparatus and also time constraints further tests at higher absolute pressures could not be performed.

4.3.1 Temperature Profiles and Rate of Heat Transfer

Figure 4.14, shows shell-side steam temperature profile for each test pressure. Each test pressure has a different amount of superheat and different saturation temperatures involved. At high vacuum steam pressures, the temperature fluctuates for every alternate thermocouple probe and the fluctuation reduces as vacuum steam pressure decreased.

Figure 4.15 shows the inlet and outlet tube-side water temperatures for all tested pressure including a linear approximation of the temperature profile. The shell-side tube wall temperatures for each test pressure were less than respective steam saturation temperatures. The target inlet temperature of the tube-side water was 49°C, which was achieved within ± 0.5°C. As absolute steam pressure increased, the overall duty of the VSTC increased resulting in a higher outlet water temperature as seen in the Figure 4.16. After reduction in steam flowrates, the desuperheating section of the VSTC has reduction of about 0.1m that elevated heat transfer duty for same test pressures. Approximately 15% increase in the overall duty of VSTC seen after reduction in the steam flowrate.

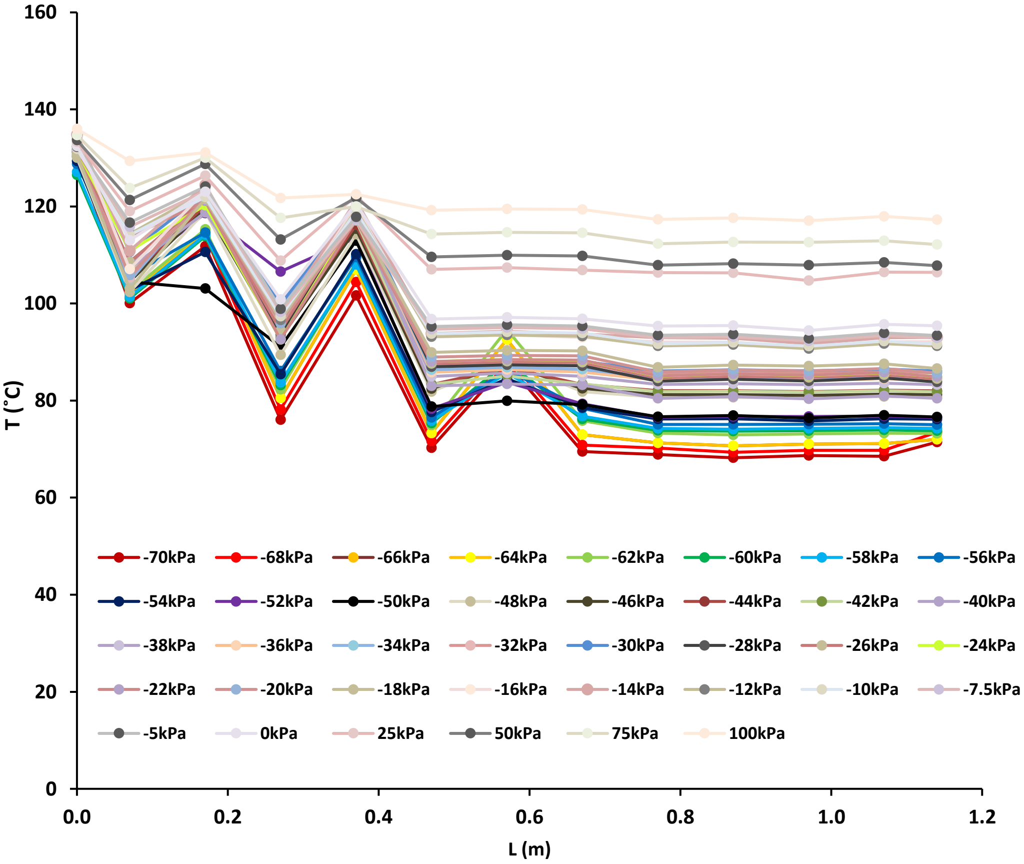

Figure 4.14: Temperature profiles of steam condensation along the length of VSTC at tested pressures.

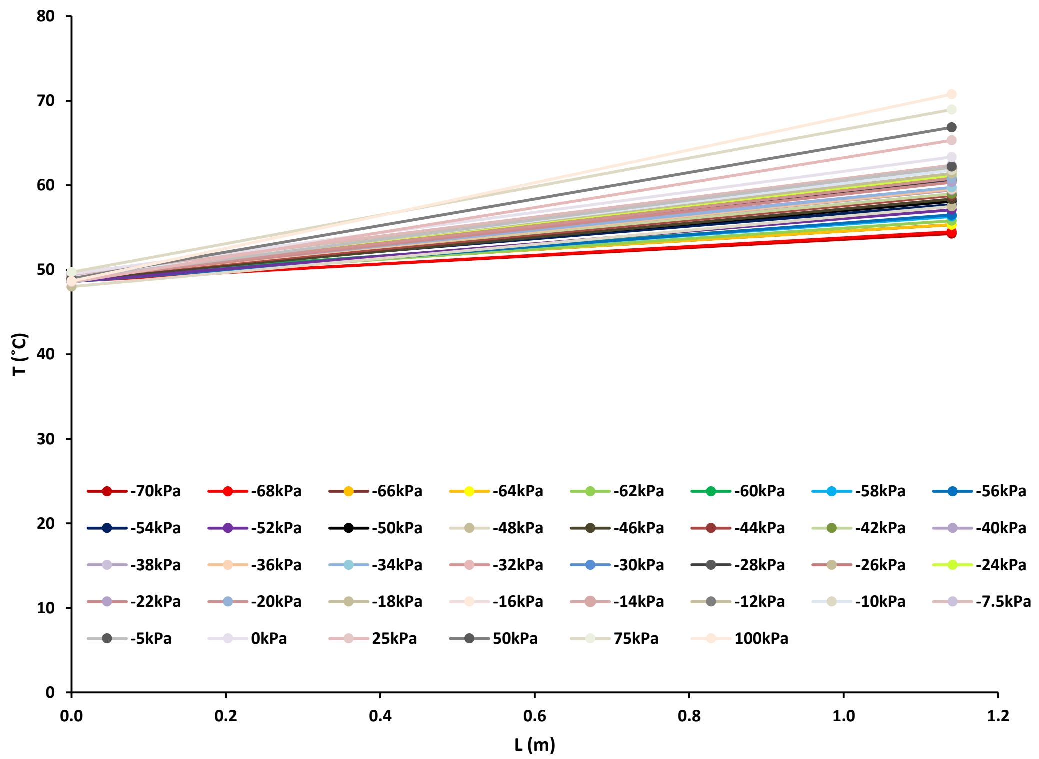

Figure 4.15: Temperature profiles of cooling water loop along the length of VSTC at tested pressures.

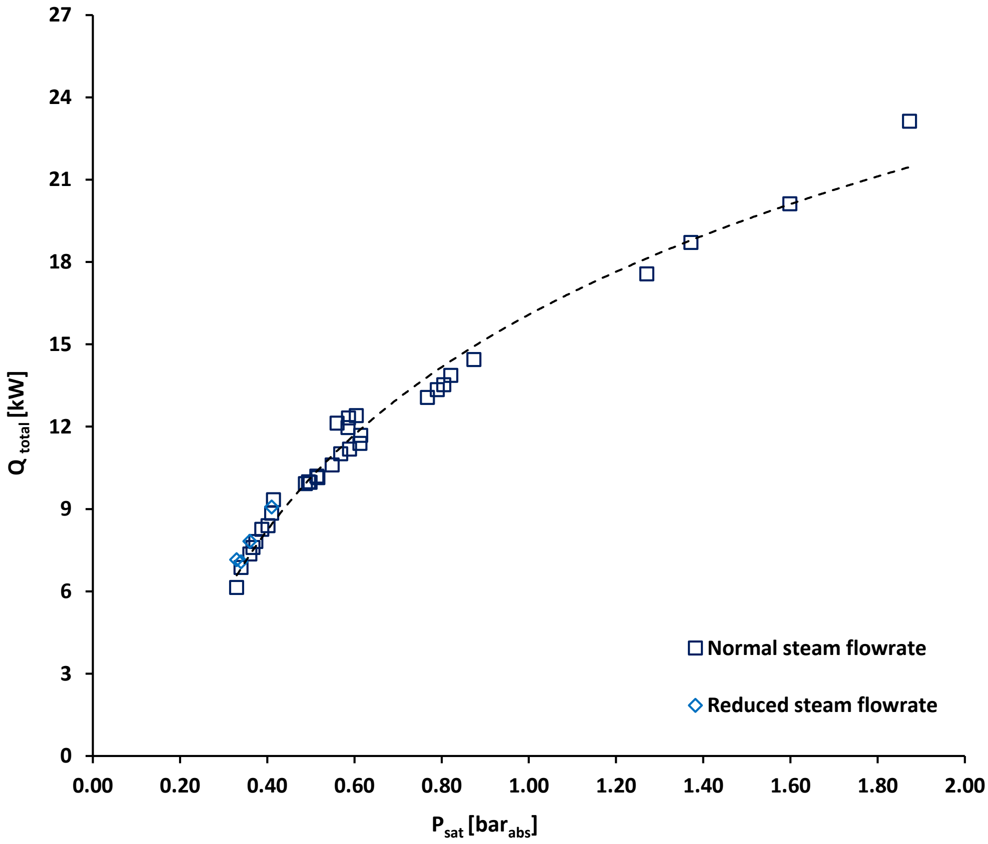

Figure 4.16 Overall duty of VSTC.

4.3.2 Steam and Condensate Mass Flowrate

The steam flowrate to the VSTC was typically between 0.005 kg/s to 0.015 kg/s as illustrated in Figure 4.17, although it was up to 0.026 kg/s at above ambient pressure. The condensate flowrate (i.e. the amount of steam condensed in the condensing section of the VSTC) is also shown in the figure along with the associated vapour fraction (on the secondary axis) leaving from the shell-side of the VSTC. The generated trend between measured mass flowrates and saturation pressure shows similarity with operating curve of Pressure Reducer Valve (PRV). Low mass flowrates obtained at high vacuum steam pressures due to partially opened diaphragm of PRV, Figure 4.17 also shows relevant values of reduced mass flowrates, condensate flowrates and vapour fractions for second test conditions. Furthermore, each result section comprised particular results of reduced steam flowrates. Appendix C provides all mass flowrates and percentage condensation in tabulated form for all test pressures.

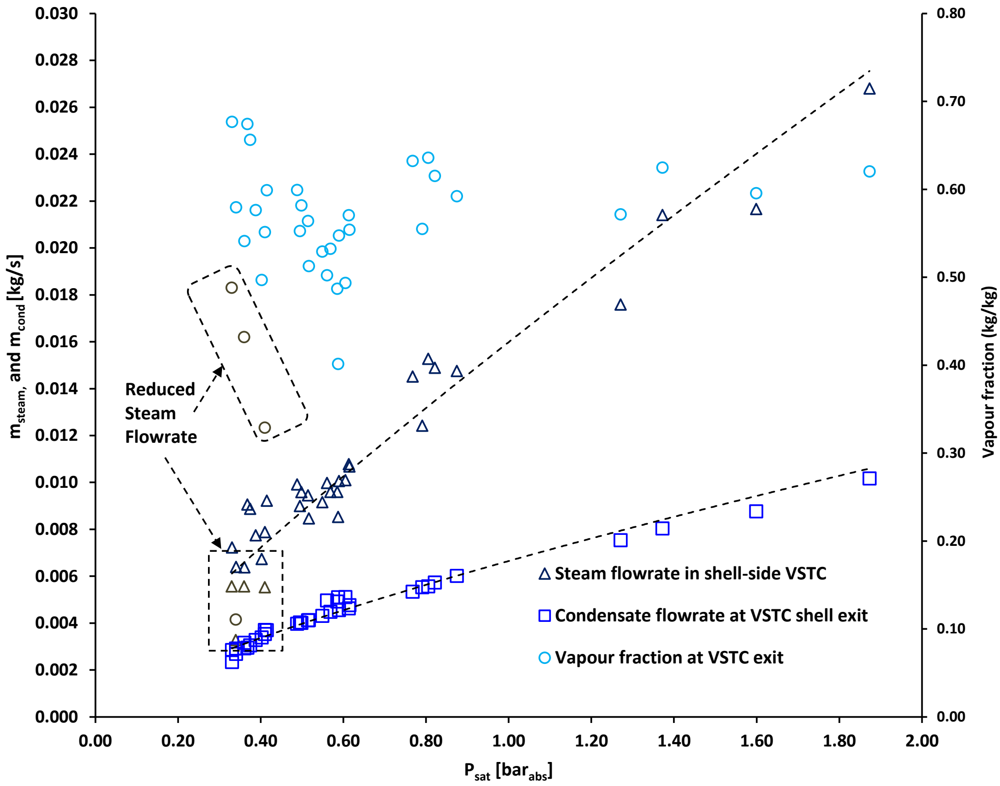

Figure 4.17: Steam, condensate flowrate and vapour fraction (secondary axis) for test pressures.

4.3.3 Desuperheating Section

This section focuses on the desuperheating section of the VSTC at different pressures tested. Due to change in vacuum steam pressures corresponding saturation temperature changed. Therefore, each pressure have different amount of superheat. Figure 4.18 shows the amount of superheat associated with each test pressure. At high vacuum steam pressures (e.g. 0.38 bar_{abs}), the superheat in the steam was more and it reduces as vacuum steam pressure decreases. After reduction in steam flowrate, amount of superheat varies by 1%. Figure 4.19 illustrates overall duty of the desuperheating section for each test pressures. Due to variation in the steam flowrates, entering VSTC and associated degree of superheat, the rate of heat transfer in the desuperheating section varied. Due to change in steam flowrate, about 50% and corresponding minor change in superheat for same test conditions, duty in the desuperheating section dropped approximately by 20%.

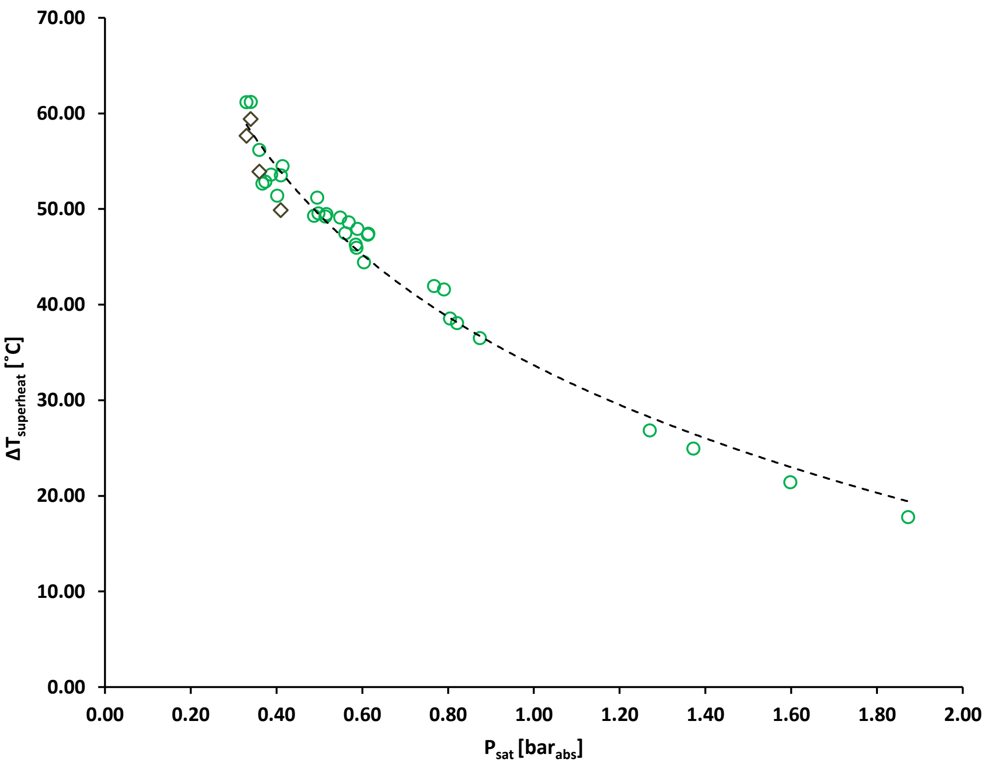

Figure 4.18: Plot of superheat for each test pressures.

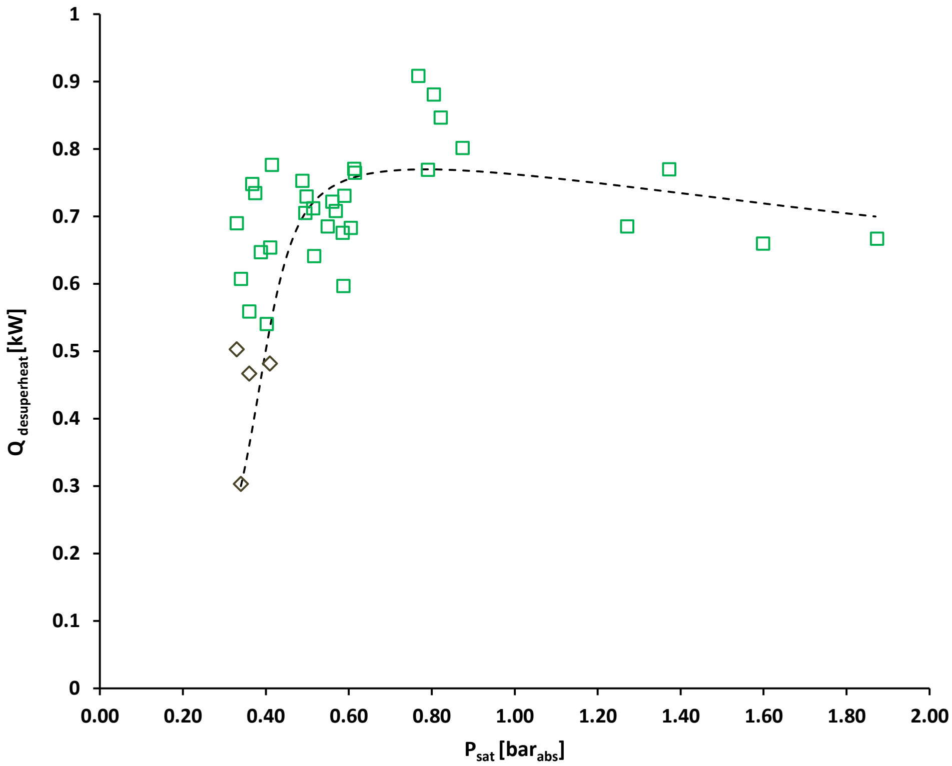

Figure 4.19: Heat transfer of desuperheating sections for test pressures.

Figure 4.20 shows graph of averaged desuperheating heat transfer coefficients versus vacuum steam pressure. Decreasing vacuum steam pressures (e.g. from 0.38 bar_{abs} to 0.80 bar_{abs}) induced significant reduction in logarithmic mean temperature difference along desuperheating section. Therefore, the averaged heat transfer coefficients increase with change in vacuum steam pressures. Averaged heat transfer coefficients presented are the averaged over the entire length of the desuperheating section of the VSTC. Some of the variation in the averaged heat transfer coefficients is mostly likely due to slightly differing steam mass flowrates.

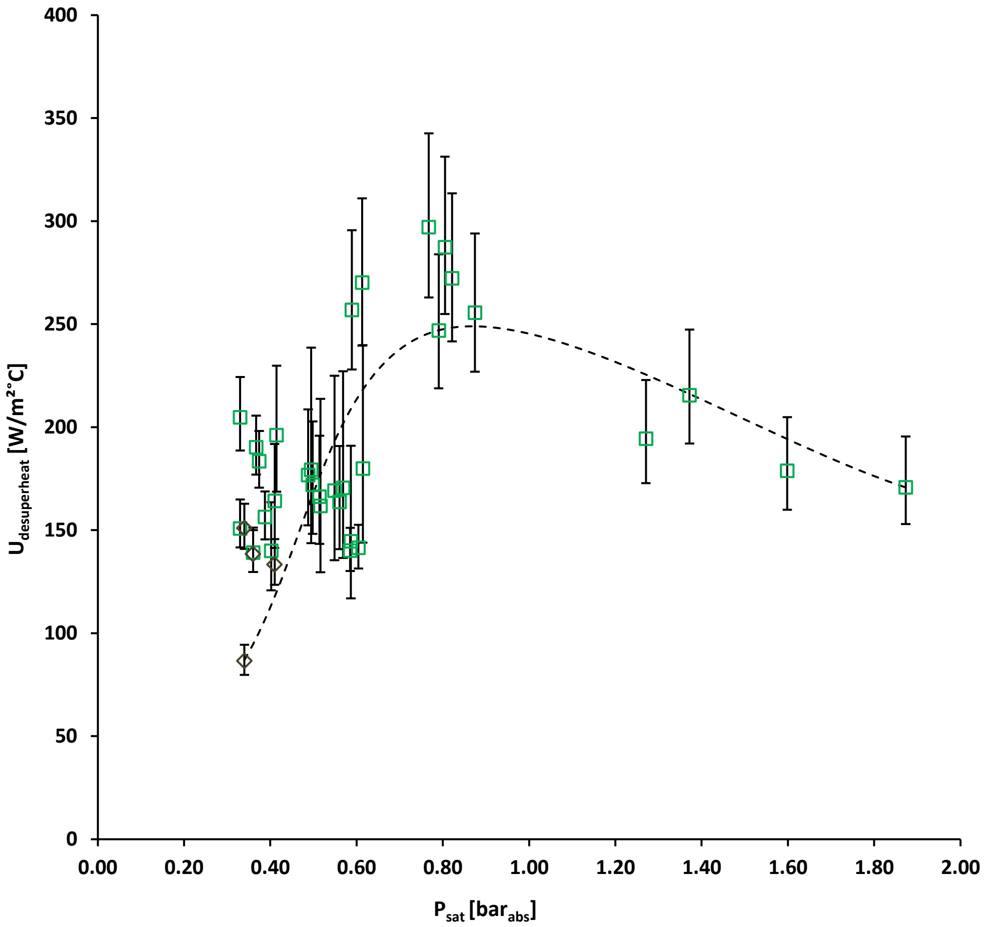

Figure 4.20: Averaged heat transfer coefficients versus saturation pressures of desuperheating section.

Figure 4.21 shows experimental verification of reliability of Reynolds number on the steam flowrate. Steam viscosity was constant for all test pressures. Change in steam mass velocity occurred due to increasing steam flowrates. Thus, Reynolds number increased with reduction in Vacuum steam pressures.

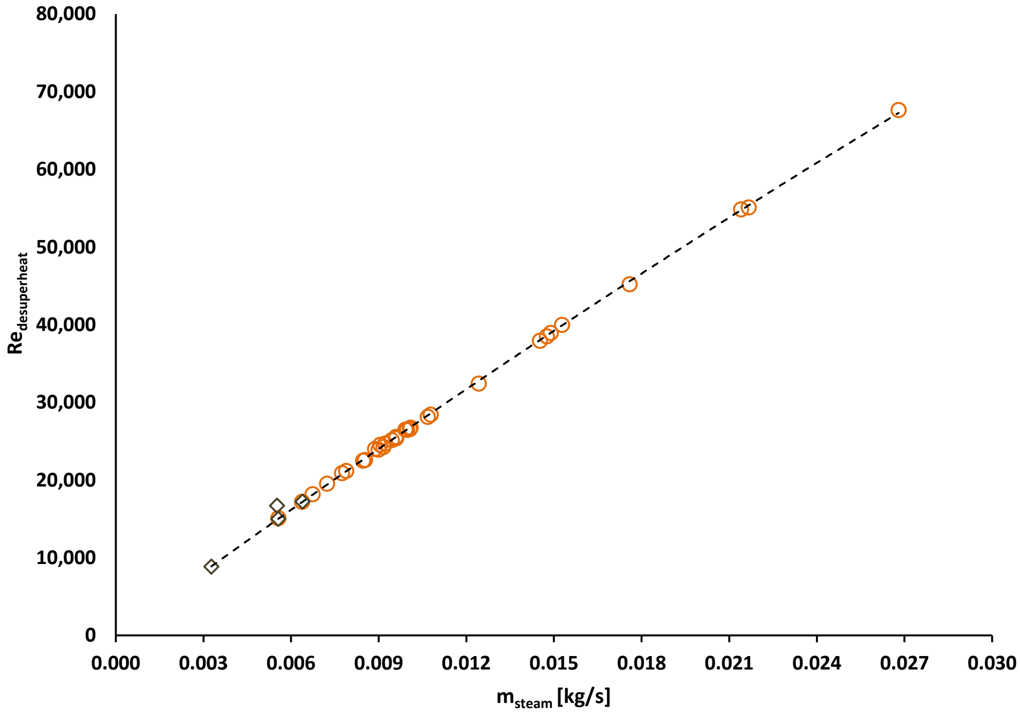

Figure 4.21: Graph of Reynolds number for desuperheating section versus steam flowrate entering VSTC.

Figure 4.22 shows the heat flux versus Reynolds number for the desuperheating section. Influence of desuperheating section area on the heat flux has seen as area of desuperheating section reduced corresponding to degree of superheat. The nature of plot is similar to duty of desuperheating section as seen previously. Figure 4.23 shows the averaged heat transfer coefficient versus Reynolds number of the desuperheating section. Reynolds number varied from 10,000-70,000, indicating turbulent vapour flow under vacuum conditions. After reduction in steam mass velocity, Reynolds number of desuperheating section reduced by 15%. Averaged heat transfer coefficients reduced by approximately 20% by reducing steam flowrate by about 50%.

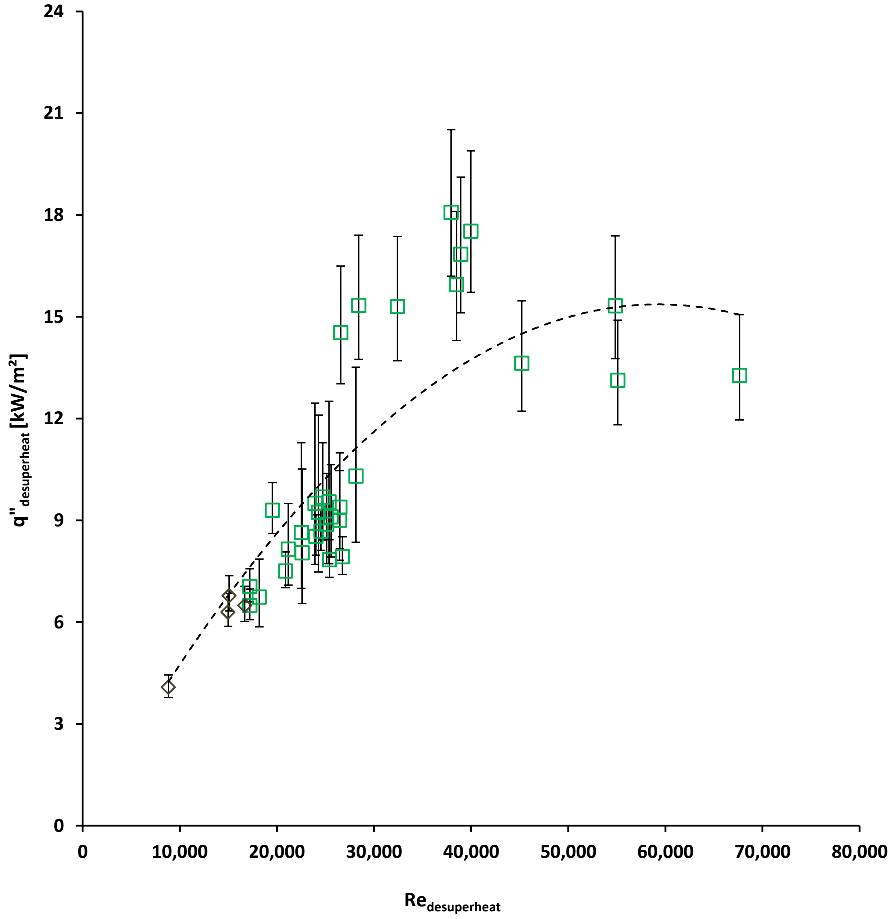

Figure 4.22: Heat flux versus Reynolds number of desuperheating section.

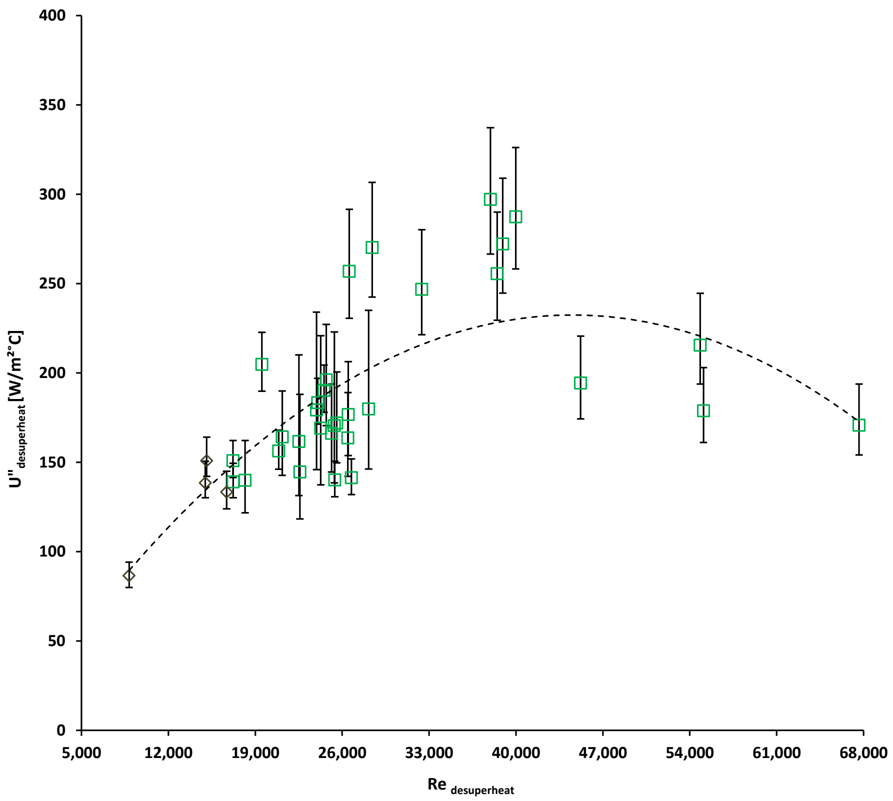

Figure 4.23: Averaged heat transfer coefficients versus Reynolds number of desuperheating section.

4.3.4 Condensation Section

The experimental results for the condensation section of VSTC are outlined in the following section. Rate of condensation increased as vacuum steam pressure lowered (degree of superheat decreased) as presented in Figure 4.24. Increase in condensation section of VSTC observed after steam flowrate reduction.

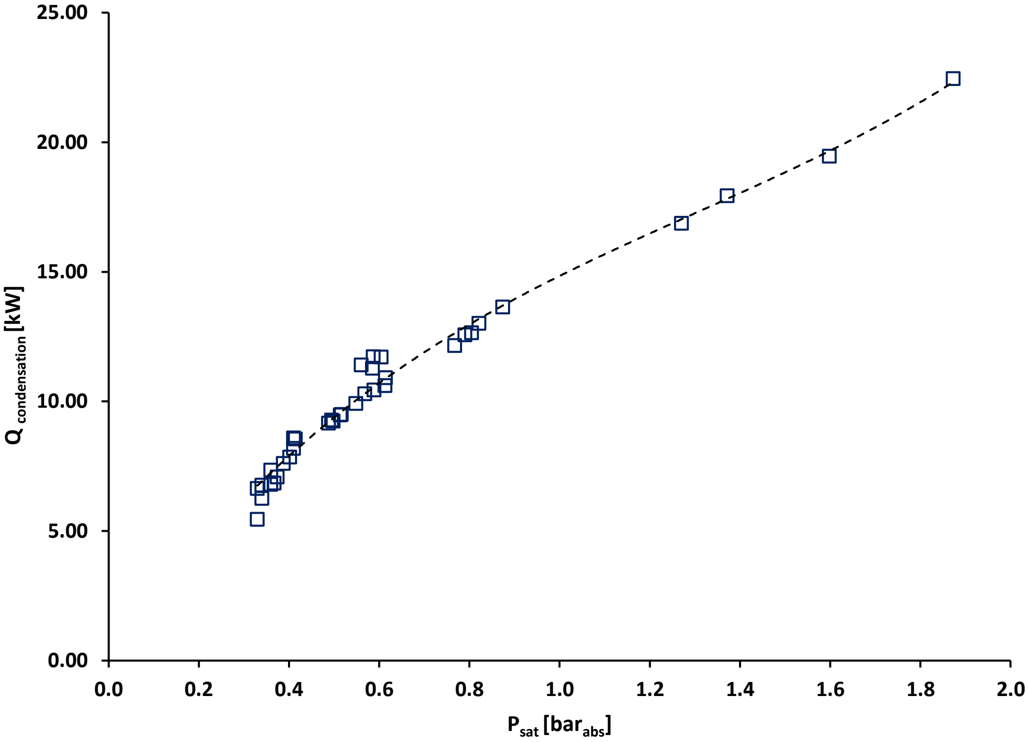

Figure 4.24: Condensation section heat transfer for test pressures.

Figure 4.24 shows the average condensation coefficients for experimental test pressures. It varies in the range of 4000-7000 W/m^2°C. No exact trend in condensation coefficients were observed due to influence of vacuum steam pressure and steam flowrates. Figure 4.26 presented averaged condensation coefficient versus condensate flowrate at shell exit of VSTC. The averaged condensation coefficients varied with increase in condensate flowrate. Figure 4.27 shows graph of averaged condensation coefficient versus Reynolds number of condensation section. No significant change observed in condensation coefficients.

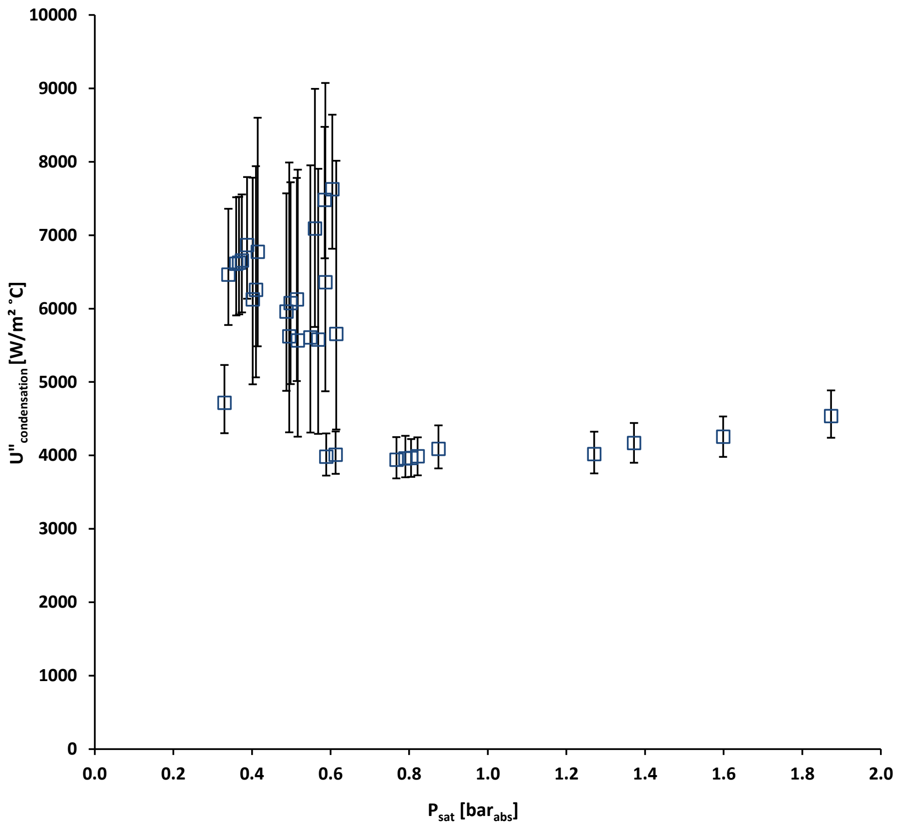

Figure 4.25: Averaged heat transfer coefficients of condensation Section versus saturation pressures.

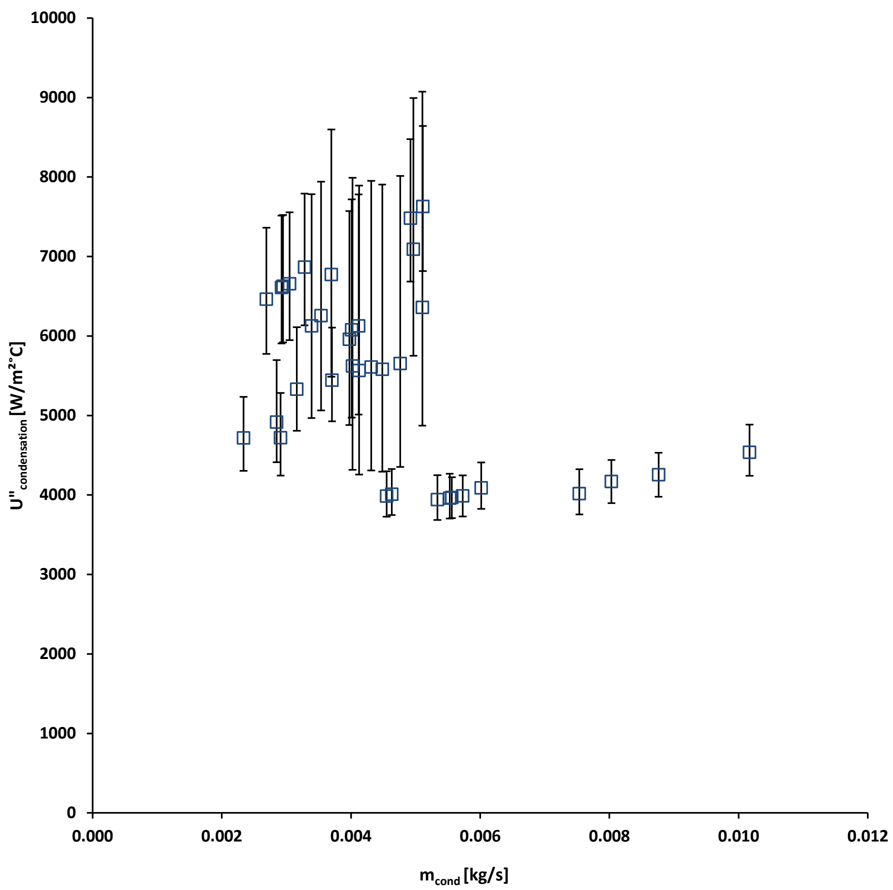

Figure 4.26: Averaged condensation coefficient versus condensate flowrate shell exit of VSTC

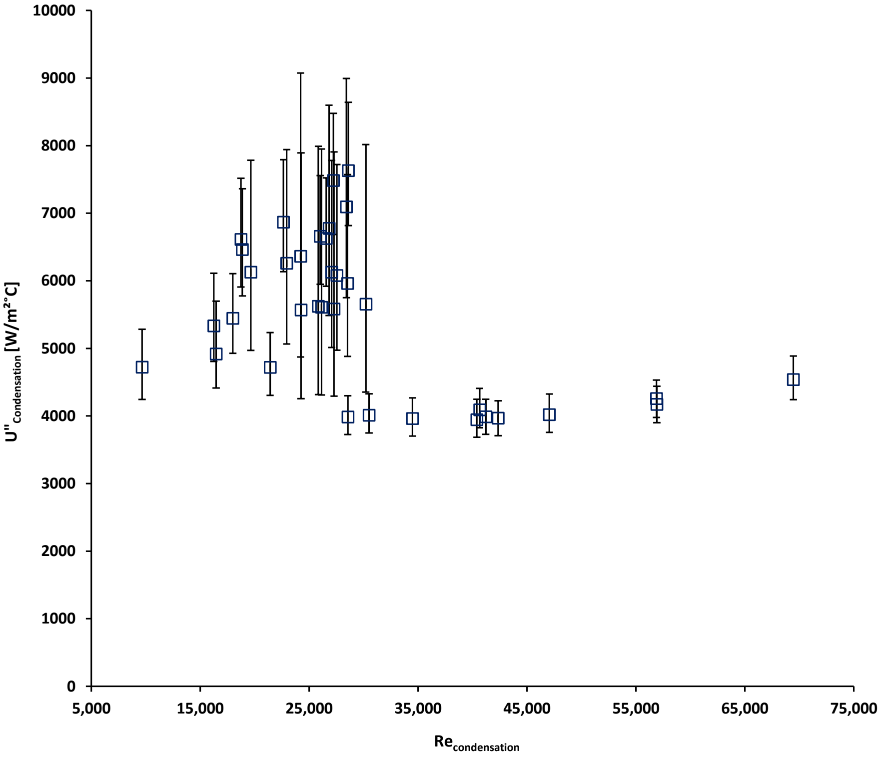

Figure 4.27: Averaged heat transfer coefficients versus Reynolds number of condensation section.

4.4 Generated Correlation from Experimental Investigation for Vacuum Steam Desuperheating

Figure 4.28 shows the developed relation between Nusselt number and Reynolds number of desuperheating section. The graph also shows the tested pressures at low steam flowrate (diamond markers), which are in agreement with the tests without reducing steam flowrate. Typically, Nusselt number varies from 150 to 580. Trend for developed Eq. 4-1 shows steady increase with Reynolds number for vacuum pressures, but it sinks as vacuum steam pressures reduced.

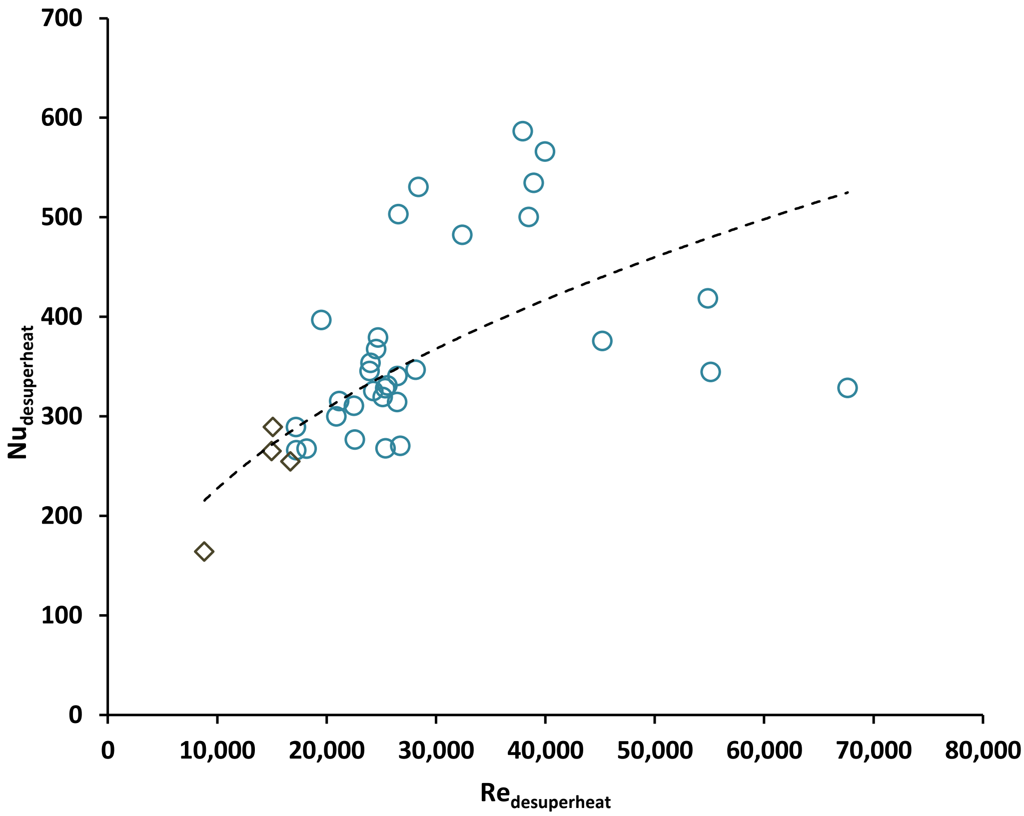

Figure 4.28: Developed correlation between Nusselt number and Reynolds number.

$$\mathrm{Nu} = 4.0455 \times Re^{0.4375} \tag{4-1}$$

4.5 Experimental Results of Vacuum Steam Condensation at $T_2 \geq T_{sat}$

As discussed previously, it was thought that the main cause of the temperature fluctuations in the desuperheating region was due to tube wall temperatures being lower than the saturation temperature. This caused some steam to condense to its saturation temperature in the desuperheating section and exchange heat by alternate evaporation and condensation phenomenon. Therefore, temperature jump across every alternate thermocouple was significant. In order to investigate this further the temperature of the tube-side water was increased above (or close to) the saturation temperature of the steam entering the VSTC.

Figure 4.29 shows shell-side steam temperature, tube-side water temperature and respective shell-side tube wall temperature outline of 37 kPa_{abs} pressure. The tube wall temperature was raised above the saturation temperature of steam by rising tube-side water temperature. As explained in the method section, tube-side and shell-side of VSTC were separated, and separate hot water tank arrangement made to circulate hot water through tubes.

If the tube wall temperature is greater than the saturation temperature then no condensation should occur and desuperheating will take place with the steam remaining completely dry (i.e. vapour fraction equal to 1). The tube wall should also be completely dry on the shell-side.

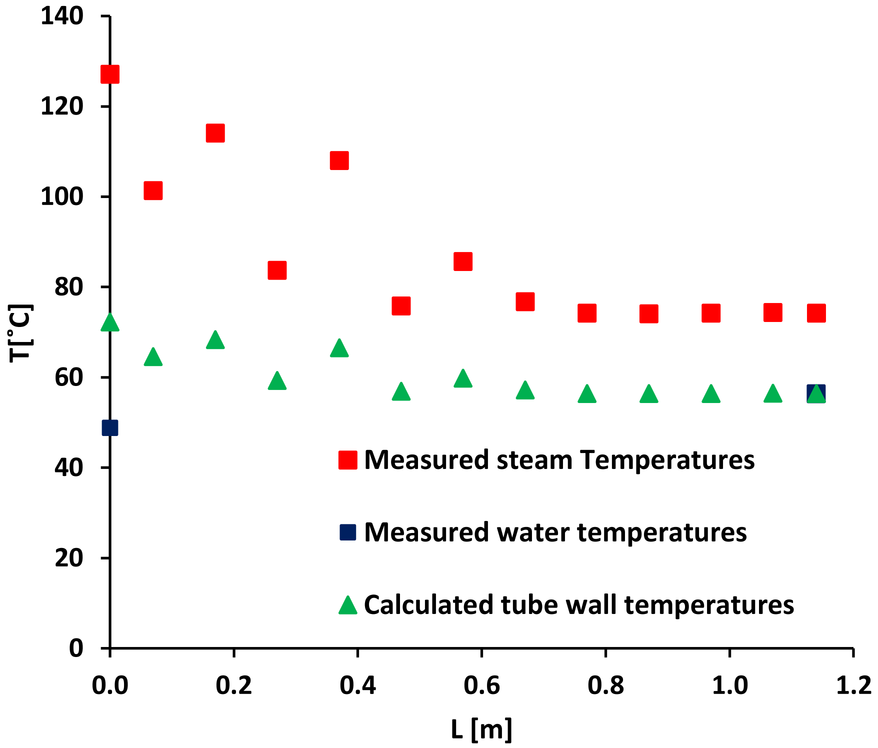

Figure 4.29: Steam, tube-side water, and tube wall temperature outline before rising wall temperature of tube. {37 kPa_{abs} pressure (-58 kPa_g)}

Figure 4.30 shows steam temperatures and wall temperatures outline of 37 kPa_{abs} pressure where reduction in temperature variation across every alternate temperature probe during the desuperheating is observed. The shell-side tube wall temperature profile as seen in Figure 4.30 is also smoother than previous outline. If tube-side water temperature could raise above steam saturation temperature, the temperature profile across desuperheating section would be more flat. Due to the limitations of the heating source, higher inlet water temperatures were not achievable. Figure 4.31 illustrates condensation models generated of 37 kPa_{abs} test pressure. From Figure 4.31, it appears no change in the length of desuperheating and condensation sections before and after rising tube-side water temperature.

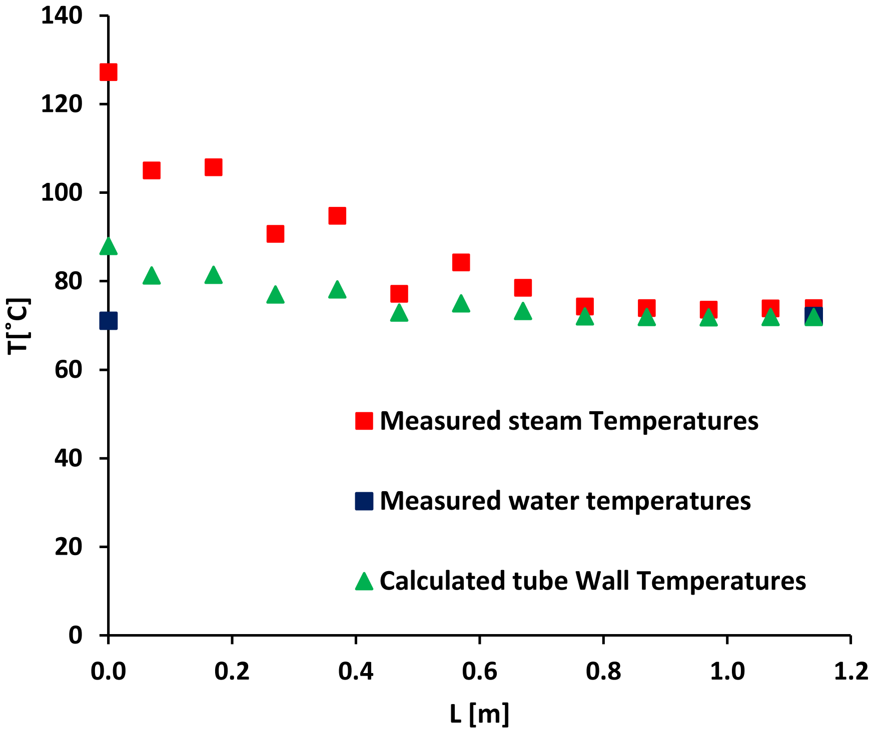

Figure 4.30: Steam, tube-side water, and tube wall temperature outline after rising wall temperature of tube up to steam saturation temperature. {37 kPa$_{abs}$ pressure (-58 kPag)}

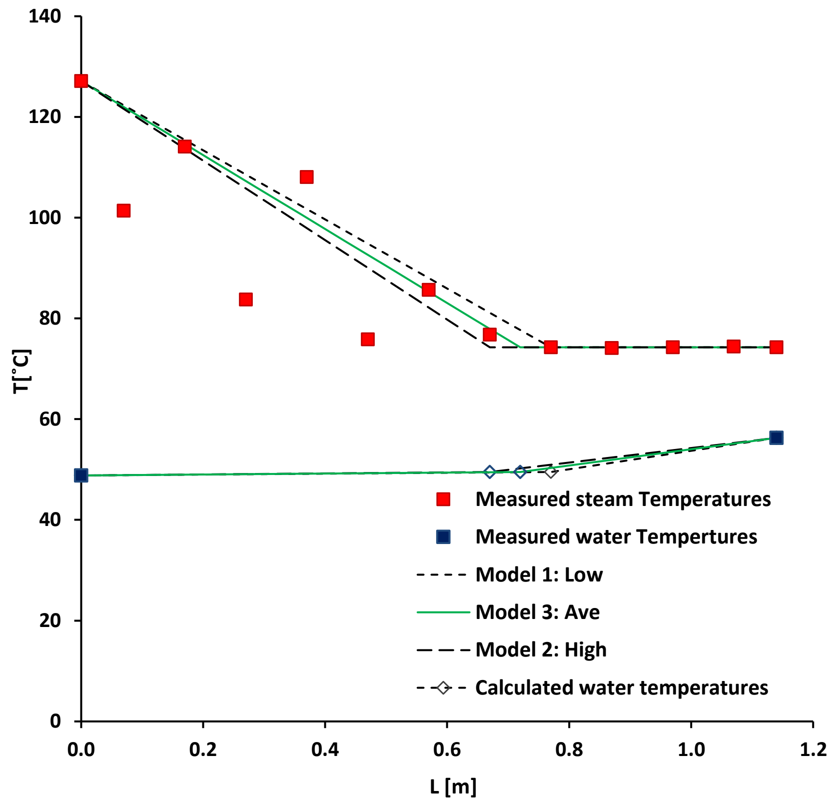

A) Before

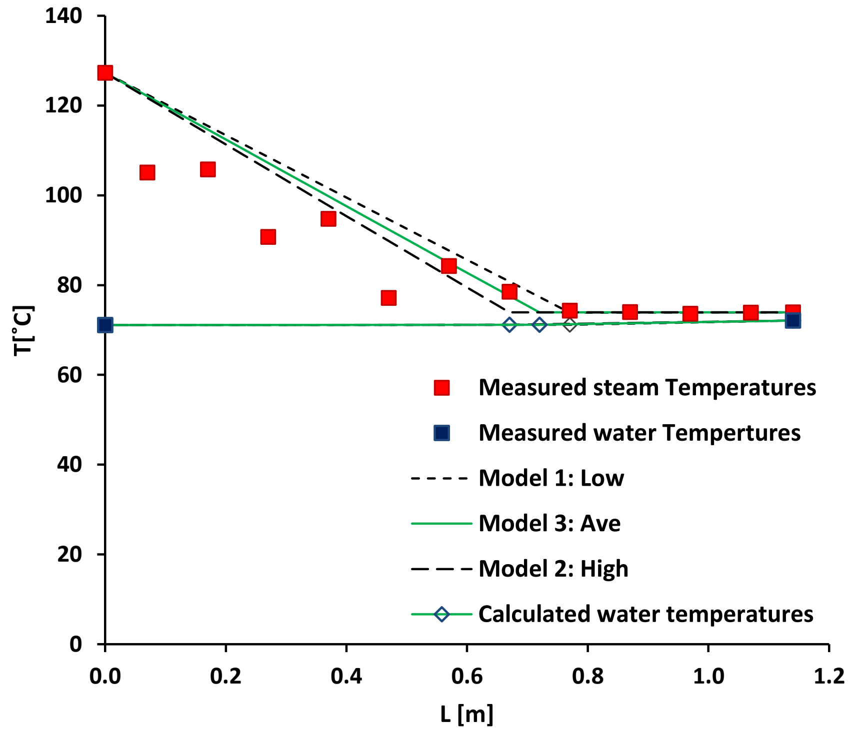

B) After

Figure 4.31: Measured temperature and model temperature profiles before (A), and after (B) increasing tube-side water temperature. {37 kPa$_{abs}$ pressure (-58 kPag)}

Figure 4.32 shows hypothesised condensation mechanism considering effect of two different tube wall temperatures. Normally surface condensation of vapour is done by directing vapour on the surface whose temperature is less than the saturation temperature. In the case of desuperheating, the superheat has to be removed by sensible cooling for it to reach its saturation temperature, before it will condense.

A) Case 1: Tube Wall Temperature Less than Steam Saturation Temperature ($T_{wall} < T_{sat}$)

In present case of low tube wall temperature than steam saturation temperature, steam desuperheating has to overcome the interface effect where heat transfer occurred from subcooled vapour on the tube wall to the adjacent liquid molecules. Therefore, junction of superheated steam and saturated vapour formed next to condensate film. Steam velocity added swirling action around tubes that can be affecting the heat transfer mechanism. In this case, thermocouples are sensitive to their positioning for temperature measurement, due to steep temperature profile.

B) Case 2: Tube Wall Temperature Equals to Steam Saturation Temperature ($T_{wall} = T_{sat}$)

On the other hand, if shell-side tube wall temperature is raised above steam saturation temperature, the vapour subcooling on the tube wall is diminished and no opposing trend of heat transfer from subcooled vapour to gas vapour and condensate film on shell-side are observed. In addition, no heat transferred from superheated steam to the tube-side. Thus, only sensible cooling of the steam is observed .

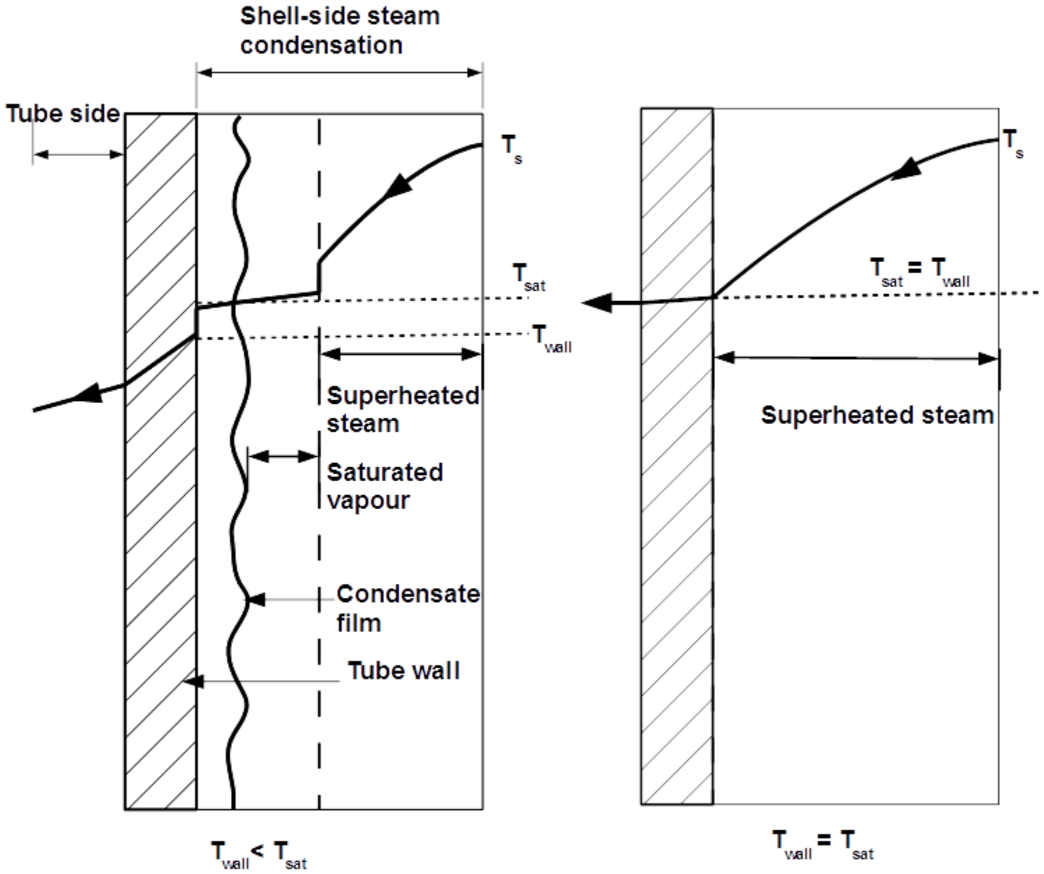

Figure 4.32: Condensation mechanism for different tube wall temperatures.

There occurred a reduction in the heat flux for desuperheating section about 90% as well as condensation section by 85% as seen in Figure 4.33. There was hardly any heat transfer in the desuperheating section whereas heat transfer in condensation section lowered by 80%.

Figure 4.34 shows averaged heat transfer coefficients of 37 kPa_{abs} pressure before and after rising water temperature up to steam saturation temperature. Steam acted as a perfect dry gas in the desuperheating section after rising tube-side water temperature and has a sensible heat transfer along desuperheating section of the condenser, while average condensation heat transfer coefficient increased by 30%. It is clear that a complex process of condensation and evaporation during the desuperheating section causes variability in the measured temperature profiles and therefore, large reduction in the local heat transfer coefficient in the desuperheating section.

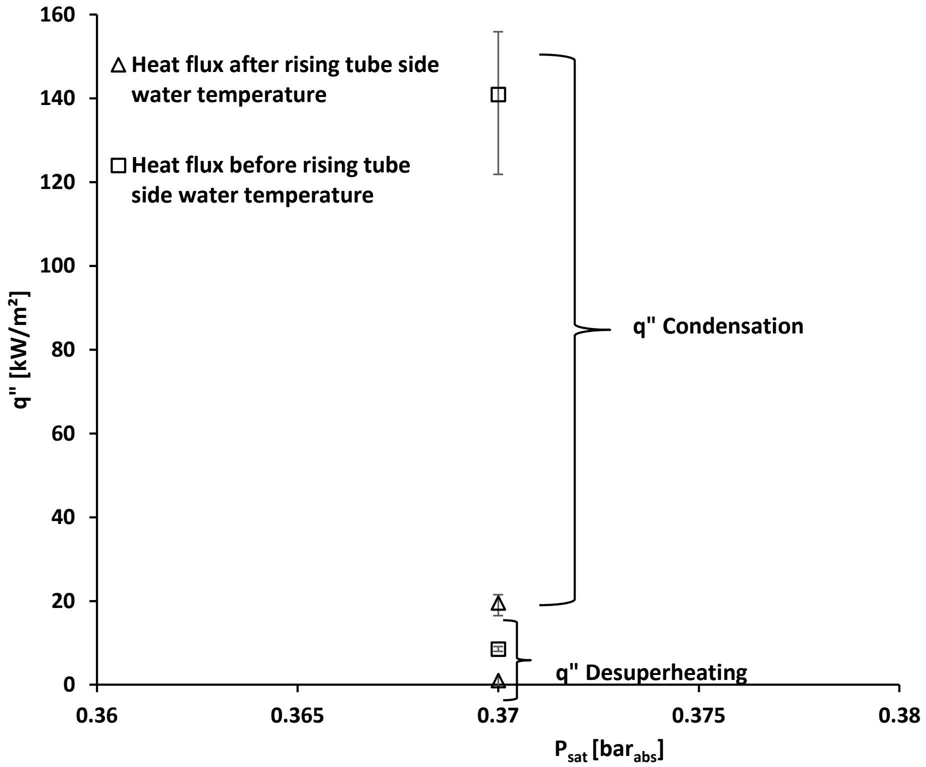

Figure 4.33: Heat flux before and after rising tube-side water temperature. {37 kPa_{abs} pressure (-58 kPag)}

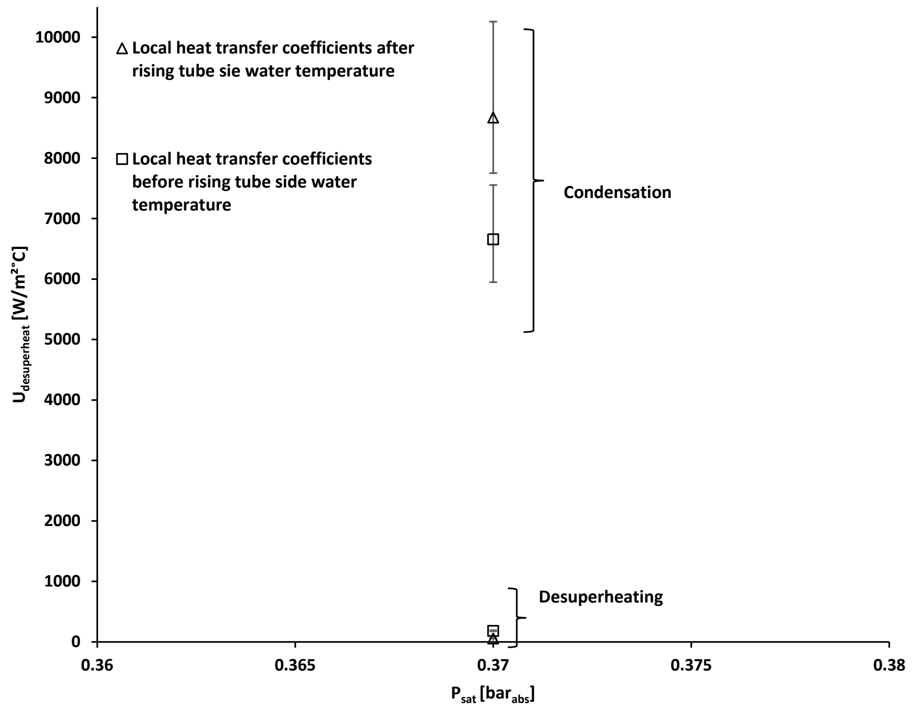

Figure 4.34: Average heat transfer coefficients of before and after rising tube-side water temperature. {37 kPa_{abs} pressure (-58 kPag)}

4.6 Conclusion

This chapter has described several detailed investigation made on VSTC. Heat transfer mechanisms of vertical shell and tube condenser (VSTC) examined by dividing shell-side measured temperatures into desuperheating and condensation sections, and generating different VSTC temperature models. Effect of low steam flowrates on desuperheating and condensation is verified by testing four vacuum steam pressures. Detailed mechanism of influence of shell-side tube wall temperature on steam desuperheating has been also discussed in this chapter. In the next chapter, these results will be applied to a hypothetical milk evaporator, to demonstrate the adverse effect of superheated steam on milk evaporation process.

Chapter Five

Industrial Application

5.1 Introduction

Several industries have active condensation mechanism going through heat exchangers to enhance throughput. This chapter presents application of vacuum steam desuperheating and condensation investigation to the milk powder plants. The effects of superheated vacuum steam condensation on the shell-side of evaporator are estimated in this chapter. Because of low heat transfer coefficients during desuperheating as demonstrated in the previous chapter, two significant problems may arise:

1) Evaporation capacity/ duty reduction (for fixed heat exchanger area) or

2) Larger evaporation area (for fixed heat transfer duty) to sustain desired throughput. These problems will be demonstrated ahead with consideration heat transfer parameters of milk evaporator.

5.2 Industrial Application to Dairy Processing

In the dairy industry, vacuum evaporation processes are used to remove water from milk. Typically falling film type evaporators/milk evaporators are utilised for evaporation. The milk feed flows uniformly as a thin film through vertical tube bundle and steam is passed through the shell-side of evaporator. Shell-side condensation of the steam plays a role of supplying heat to the tube-side feed. Milk evaporators boil the milk under vacuum pressure and at reduced temperature. Vacuum steam on shell-side of evaporator maintains the desired steam temperature at low pressure. The removal of water content requires multiple evaporation cycles/effects, thus saturated vapour may be mechanically (MVR) or thermally (TVR) compressed and used to improve steam economy. MVR is preferred over TVR due to advantages such as, minimum energy consumption, no additional requirement of steam or cooling water, and good capacity control. MVR operates similar to a heat pump, a centrifugal fan or compressor mechanically recompresses saturated vapour exiting from the tube side of the evaporator effects, to a higher pressure and temperature before reinjecting to the shell-side evaporator. In TVR, only a portion of vapour exiting from evaporator effect is recompressed using a steam recompression nozzle, and as such require primary steam to provide the upgrading.

A) Effect of Superheated Vacuum Steam Condensation on Rate of Milk Evaporation (Fixed Area of Evaporation)

Figure 5.1 presents layout of general multi-effect evaporator system used in the dairy industry, incorporating both MVR and TVR stages. Most evaporators for milk powder process operate under vacuum pressure of 0.31 bar_{abs} with the boiling temperature of milk around 65˚C-70˚C. It is then passed through several effects/passes to increase percentage solid contents of milk typically from around 13% to 50% solids. On other hand, saturated steam exiting tube-side is sent through the MVR, which has an isentropic efficiency typically of 80% and compressed, which increases the temperature of vapour (plus the addition of superheat) and sent to shell-side of evaporator for condensation (Jebson & Chen, 1997).

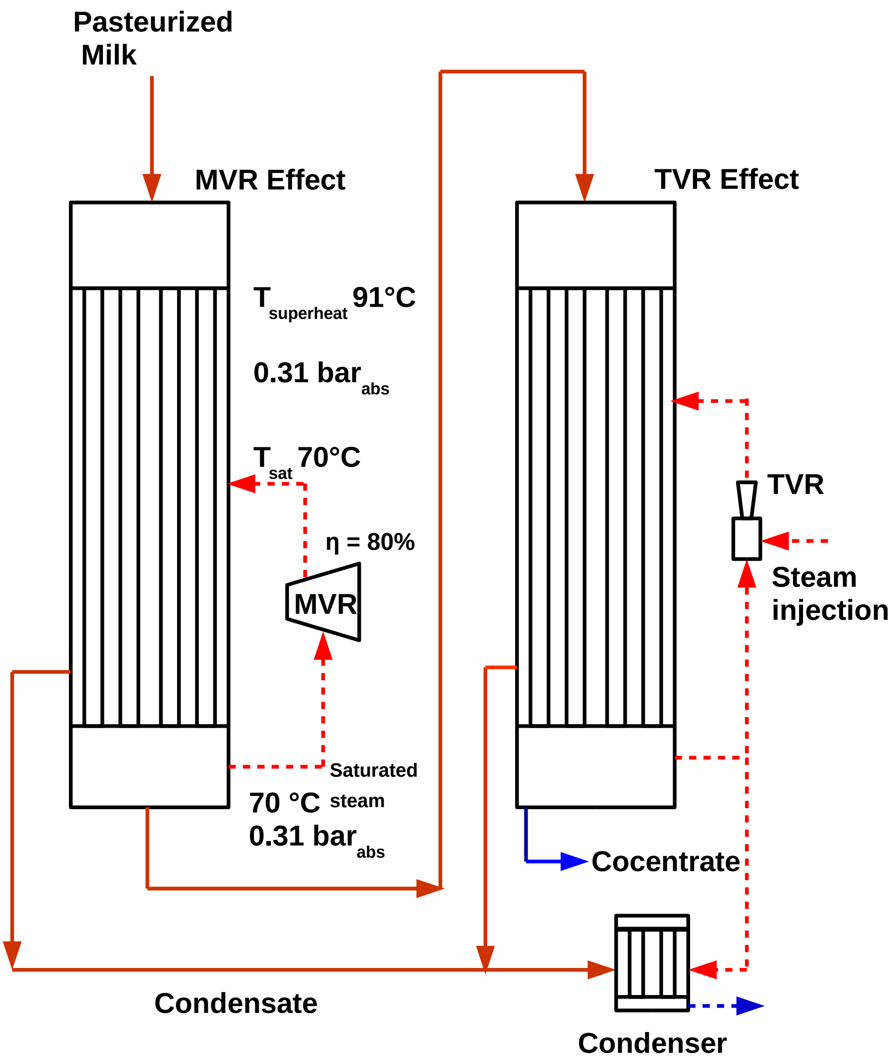

Figure 5.1: Mechanical Vapour Recompression (MVR) in dairy industry (Walmsley *et al.*, 2015).

In the evaporator, pasteurized milk at boiling temperature of 65˚C flows in tube bundles at 20 kg/s at 13% solid contents. The rate of evaporation of vapour from the tube bundle is approximately equal to the latent heat of steam condensing on the shell-side of evaporator. Saturated steam at 70˚C flows at shell-side of evaporator at 13.5 kg/s. Therefore, at the end of evaporation effect, 40% of the solids concentrated at the tube exit respectively reducing milk flow rate to about 6.5 kg/s. High heat transfer coefficients of milk-side 2000 $W/m^{2\circ}C$ and condensation side 5000 $W/m^{2\circ}C$ achieved by overall heat transfer rate of about 31,497 kW across evaporator area of 4500 m^2.

After introducing saturated steam to the MVR unit, the temperature of vapour recirculating for condensation in shell-side raised above steam saturation temperature, i.e. vapor is superheated. Presently, industries opt to use water spray to reduce the superheat associated with required pressure to maintain evaporator efficiency. If superheated steam is sent for condensation then heat transfer duty could be decreased, consequentially affecting evaporation rate. Present analysis of vacuum steam desuperheating and condensation gives amounts of superheat and different heat transfer coefficients for desuperheating section. By applying the present value of desuperheating section heat transfer coefficient, which has been found experimentally in chapter 4 (175.2 $W/m^{2\circ}C$), the percentage reduction in the evaporation rate can be estimated. Figure 5.2 presents temperature plot of shell-side condensation and milk evaporation inside tube bundle. Superheated temperature causes influence on maximum temperature potential of evaporator, which reduced overall heat transfer duty of the evaporator.

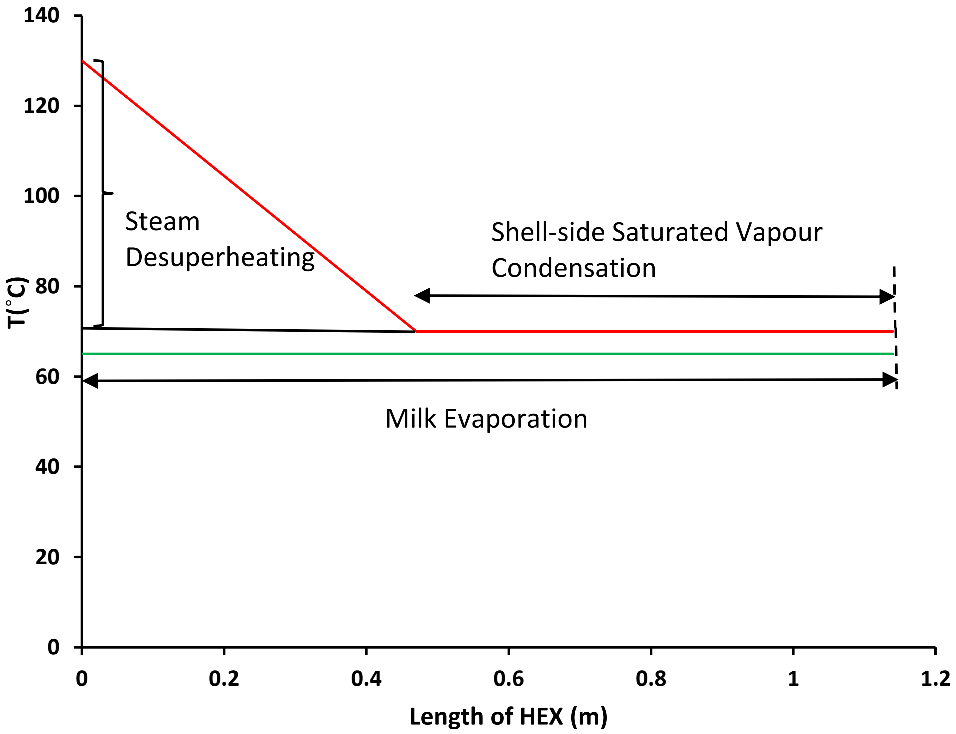

Figure 5.2: Temperature profile of milk evaporation.

Table 5.1 presents the reduction in the milk flowrates and equivalent steam flowrates on the shell-side of evaporator, and overall heat transfer duty of milk evaporator. An increase in superheat of steam decrease the milk flowrate running through tube bundle. Figure 5.3 presents percentage reduction in milk flowrate by varying the vapour superheat.

Table 5.1: Effect of superheat on the rating of milk evaporator.

Shell-side saturated steam condensation in milk evaporator						
$\mathbf{m_{milk}}$ (kg/s)				20		
$\mathbf{m_{steam}}$ (kg/s)				13.5		
$\mathbf{A_{evaporation}}$ (m^2)				4410		
$\mathbf{Q_{evaporation}}$ (kW)				31,497		
Shell-side superheated steam condensation in milk evaporator $\mathbf{U_{desuperheat}}$ = 175.2 W/m^2°C						
$\mathbf{\Delta T_{superheat}}$	$\mathbf{m_{milk}}$	$\mathbf{m_{steam}}$	**milk flowrate reduction**	$\mathbf{Q_{evaporation}}$	$\mathbf{A_{desuperheat}}$	$\mathbf{A_{cond}}$
(˚C)	kg/s	kg/s	%	kW	m^2	m^2
60	18.45	12.45	7.7	30508.65	353.78	4055.73
50	18.49	12.48	7.5	30334.89	332.87	4076.65
40	18.60	12.55	6.9	30281.04	307.44	4102.07
30	18.75	12.65	6.2	30274.77	275.06	4134.46
20	18.95	12.79	5.2	30351.1	230.67	4178.85
10	19.27	13.00	3.6	30604.22	160.84	4248.68
5	19.53	13.18	2.3	30889.88	103.20	4306.32

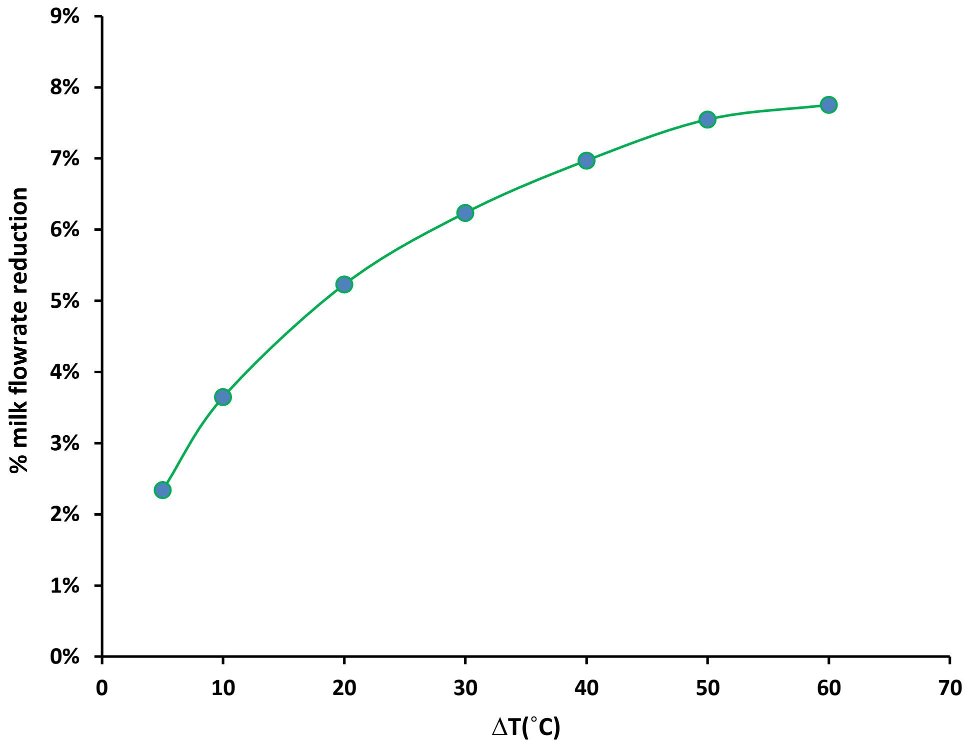

Figure 5.3: Effect of superheat on the milk flowrate in milk evaporator.

B) Effect of Superheated Vacuum Steam Condensation on Area of Evaporation (Fixed Duty of Evaporation)

Another possible approach to confront involved superheat is to size the evaporator for desired evaporation rate accordingly. In this example, the milk flowrate going in to the tube bundle is kept the same, the steam flow also constant. Therefore, the area requirement of evaporator changes as the amount of superheat varies to achieve desired duty. Different amount of superheat associated with respective additional desuperheating areas while condensation area remains same. Table 5.2 shows percentage change in area of evaporator to maintain the desired rate of evaporation for different superheated vacuum steam temperatures, which is condensing on the shell-side of evaporator. Figure 5.4 shows percentage oversizing of milk evaporator with increase in superheated vacuum steam temperature.

Table 5.2: Effect of superheated steam condensation on sizing of evaporator

m_{milk} (kg/s)	20	
m_{steam} (kg/s)	13.5	
$A_{condensation}$ (m^2)	4410	
$Q_{evaporation}$ (kW)	31,497	
$\Delta T_{superheat}$	$A_{desuperheat}$	**area of Oversize**
(˚C)	(m^2)	%
60	384.6	8.7
50	360.1	8.2
40	330.5	7.5
30	293.3	6.7
20	243.4	5.5
10	167	3.8
5	105.7	2.4

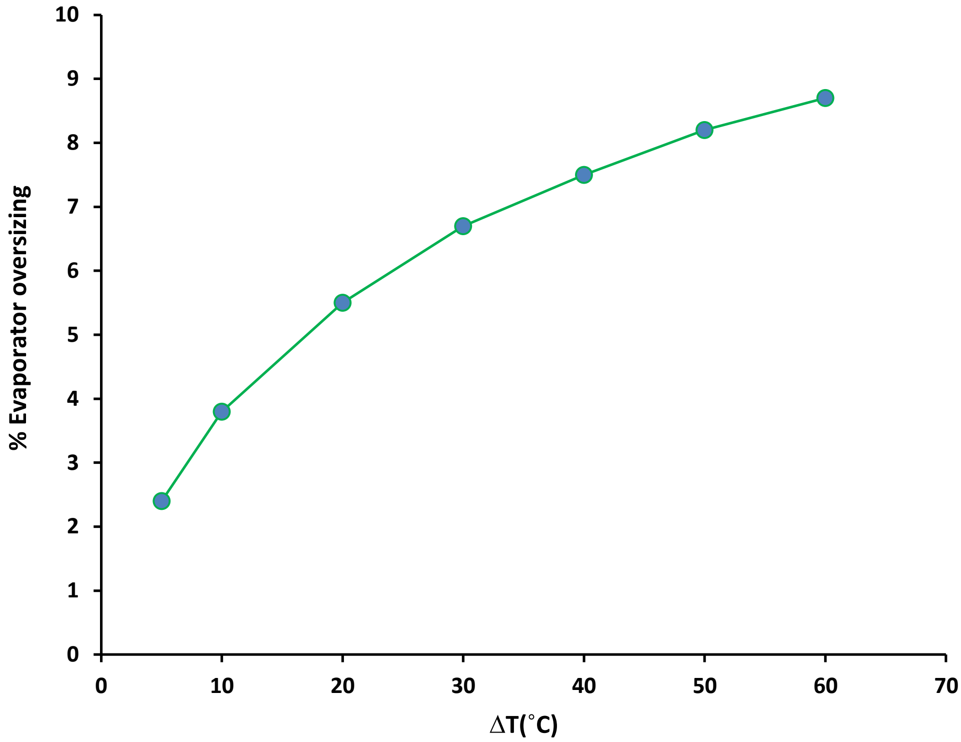

Figure 5.4: Influence of superheat on the area of milk evaporator.

5.3 Conclusion

Influence of present vacuum steam desuperheating and condensation heat transfer analysis on the industrial milk evaporation has been described in this industrial application section. Milk evaporators in dairy industries are equipped with mechanical vapour recompression (MVR) and Thermal vapour recompression (TVR) for effective utilisation of energy (steam utility system). These systems generate superheated steam, which is inefficient for milk evaporation. Thus, after superheated steam generation, desuperheating sprays are used to desuperheat the steam and then saturated steam sends to the evaporator. However, desuperheating spray increases mass flowrate of saturated vapour due to extra mass of sprayed water added in it, which can affect condensation significantly. This chapter estimated reduction in the milk and vapour flowrates if superheated steam uses for evaporation. Superheated steam therefore is not useful in the milk evaporation.

Chapter Six

Conclusion and Future Work

6.1 Conclusion

About 60% of the shell-side area of total vertical shell and tube condenser (VSTC) involved desuperheating of steam and the remaining area was steam condensation. Degree of superheat varies with vacuum steam pressure; it is more for high vacuum steam pressure (e.g. 0.3 bar_{abs}) and shows approximately linear decrease towards low vacuum steam pressure (e.g. 0.8 bar_{abs}), therefore the area required for desuperheating reduced as vacuum pressure lowers. The probability of steam flowrate influencing the averaged heat transfer coefficient is significant. Averaged heat transfer coefficients varied between 140 W/m^2 °C (at vacuum steam pressure about 0.8 bar_{abs}) and 287 W/m^2 °C (at vacuum steam pressure about 0.32 bar_{abs}) in the desuperheating section. Out of total heat transfer, approx. 0.70 kW average sensible heat transfer was attained across the desuperheating section. Nearly 45% of the vacuum steam condensed in the shell-side VSTC, and two-phase flow of saturated vapour and condensate was observed at the shell outlet of VSTC.

A dry tube wall facing shell-side steam promotes smooth increase in sensible heat transfer without change in steam phase in the desuperheating section. Temperature fluctuations along the length of VSTC during desuperheating section is due to low tube wall temperature that are below saturation temperature of steam, which promotes localised condensing and evaporating vacuum steam. Reduction in steam flowrate by 20% to 40% entering shell-side of VSTC reduces desuperheating section by 10%. About 20% to 50% reduction in Reynolds number observed after steam flowrate reduction due to decrease in steam mass velocity.

On an average 10 kW heat transfer achieve in the remaining condensation section of VSTC, and the averaged condensation heat transfer ranges from 4000-7000 W/m^2 °C. No significant change in Reynolds number of condensation section observed after desuperheating section. Decrease in the steam flowrate increases the condensation section by approximately 30% of VSTC, therefore increases the duty of VSTC by 10%. Increasing tube-wall temperature reduces condensation section.

Use of superheated steam in the milk evaporator for milk powder production:

a) for fixed area of evaporation- reduces the overall evaporation duty by dropping milk flowrates inevitably lowering percentage milk powder at evaporator exit; and

b) for fixed evaporation duty (constant milk and steam flowrates) - increases area of evaporator to achieve steam desuperheating and then condensation on shell-side of milk evaporator.

6.2 Recommendations for Future Work

A number of areas for future research have been identified based on the experimental work presented in this thesis.

6.2.1 Advancement in Test Facility and Experimentation

The present investigation of vacuum steam desuperheating and condensation was limited to vertical tube geometry. The orientation and geometry can greatly affect the performance of the condenser. For example, condensate flow patterns on horizontal tube bundles are different for vertical tubes. Similar vacuum steam desuperheating and condensation investigations can performed by changing geometries of condenser such as horizontal and inclined condensers, and flow arrangements. Different fluids can be used as a coolant instead of cold water to see consecutive effect on rate of vacuum steam condensation. The constant parameters in the current experiments such as flowrate of cooling water through tubes, condensate flowrate can be changed to see their effect on desuperheating.

6.2.2 Combination of Different Parameters

The influence of non-condensable gas (NCG) for low vacuum steam desuperheating and condensation could be investigated. Minkowycz and Sparrow (1969) investigated involvement of NCG with superheated steam condensation, however at sub-ambient pressures and on flat vertical plate. Therefore, influence of NCG on desuperheating at tested vacuum steam pressures can affect the performance and condensation mechanism. Temperature profile of desuperheating and condensation section can be analysed with different models.

References

Al-Shammari, S. B., Webb, D. R., & Heggs, P. (2004). Condensation of steam with and without the presence of non-condensable gases in a vertical tube. *Desalination, 169*, 151-160.

Berrichon, J. D., Louahlia-Gualous, H., Bandelier, P., & Bariteau, N. (2014). Experimental and theoretical investigations on condensation heat transfer at very low pressure to improve power plant efficiency. *Energy Conversion and Management, 87*, 539-551.

Blangetti, F., & Schlunder, E. U. (1978). *Local heat transfer coefficients in condensation in vertical tubes*. Presented at the Sixth International Heat Transfer Conference, Toronto, Canada.

Buglaev, V. T., Andreev, M. M., & Kleshchevnikov, V. P. (1971). Investigation of steam condensation in the presence of air on a horizontal tube bank under vacuum conditions. *Thermal Engineering 18*(2), 19-22.

Cengel, Y. (2007). *Heat and mass transfer : A practical approach* Boston, MA: McGraw-Hill.

Chen, S. L., Gerner, F. M., & Tien, C. L. (1987). General film condensation correlations. *Experimenlal Heal Transfer: A Journal of Thermal Energy Generation, Transport, Storage, and Conversion, 1*, 93-107.

Cheng, S., Sun, F., & Shi, Y. (2012). Experimental study of condensation heat transfer characteristics of horizontal tube bundles in vacuum states. *Journal of Hydrodynamics, 24*(4), 628-634.

Chun, K. R., & Seban, R. A. (1971). Heat transfer to evaporating liquid film. *Journal of Heat Transfer, 93*, 391-396.

Chun, M., & Kim, K. (1991). Assessment of the new and existing correlations for laminar and turbulent flow film condensations on a vertical surface. *Journal of Korean Nuclear Society, 23*, 200-210.

Corradini, M. (1984). Turbulent condensation on a cold wall in the presence of a noncondensable gas. *Heat Transfer and Fluid Flow, 64*, 186-195.

Dehbi, A., & Guentay, S. (1997). A model for the performance of a vertical tube condenser in the presence of noncondensable gases. *Nuclear Engineering and Design, 177*, 41–52.

Dharma Rao, V., Murali Krishna, V., Sharma, K. V., & Rao, P. V. J. M. (2008). Convective condensation of vapor in the presence of a non-condensable gas of high concentration in laminar flow in a vertical pipe. *International Journal of Heat and Mass Transfer, 51*(25-26), 6090-6101.

Jebson, R. S., & Chen, H. (1997). Performances of falling film evaporators on whole milk and a comparison with performance on skim milk. *Journal of Dairy Research, 64*(1), 57-67.

Kakac, S., Liu, H., & Pramuanjaroenkij, A. (2002). *Heat exchangers: Selection, rating, and thermal design*. Boca Raton, FL: CRC Press.

Kays, W. M., & London, A. L. (1984). *Compact heat exchangers*. Malabar, FL: Krieger.

Kern, & Quentin, D. (1950). *Process heat transfer*. New York: Tata McGraw-Hill Education.

Mackereth, A. R. (1995). *Thermal and hydraulic aspects of falling film evaporation.* PhD thesis, University of Canterbury, Christchurch, New Zealand.

Maheshwari, N. K., Saha, D., Sinha, R. K., & Aritomi, M. (2004). Investigation on condensation in presence of a noncondensable gas for a wide range of reynolds number. *Nuclear Engineering and Design, 227*(2), 219-238.

Minkowycz, W. J., & Sparrow, E. M. (1966). Condensation heat transfer in the presence of noncondensables, interfacial resistance, superheating, variable properties, and diffusion. *An international Journal of Heat Mass Transfer, 9*, 1125-1144.

Minkowycz, W. J., & Sparrow, E. M. (1969). The effect of superheating on condensation heat transfer in a forced convection boundary layer flow. *An International Journal of Heat Mass Transfer, 12*, 147-154.

Miropolskiy, Z. L., Shneerova, R. I., & Ternakova, L. M. (1974). Heat transfer at superheated steam condensation inside tubes. In *Proceedings - 5th International Heat Transfer Conference* (pp. 246-249).

Shang, D. Y. (1997). An extended study on steady-state laminar film condensation of a superheated vapour on an isothermal vertical plate. *An international Journal of Heat Mass Transfer, 40*(4), 10.

Sinnott, R. K. (2005). *Coulson & Richardson's chemical engineering, Vol. 6: Chemical engineering design* Chemical Engineering Design. Oxford, U.K.: Elsevier Butterworth-Heinemann.

Sparrow, E. M., Minkowycz, W. J., & Saddy, M. (1967). Forced convection condensation in the presence of noncondensables and interfacial resistance. *An international Journal of Heat and Mass Transfer, 10*, 1829-1845.

Spirax-Sarco. (2007). *The steam and condensate loop book*. Cheltenham, U.K.: Author.

Statistics New Zealand. (2014). *New Zealand in Profile 2014: Economy*. Retrieved May, 2015, from http://www.stats.govt.nz/browse_for_stats/snapshots-of-nz/nz-in-profile-2014/economy.aspx.

Tanner, D. W., Pope, D., Potter, C. J., & West, D. (1968). Heat transfer in dropwise condensation at alow steam pressures in the absence and presence of non-condensable gas. *An International Journal of Heat Mass Transfer, 11*, 181-191.

Walmsley, T. G., Walmsley, M. R. W., Neale, J. R., & Atkins, M. J. (2015). Pinch analysis of an industrial milk evaporator with vapour recompression technologies. *Chemical Engineering Transactions, 45,* In press.

Wang, C. Y., & Chuan, J. T. (1988). Effects of non-condensable gas on laminar film condensation in a vertical tube. *International Journal of Heat and Mass Transfer*, *31*(11), 2339-2345.

Yang, S. (1997). Superheated laminar film condensation on a nonisothermal horizontal tube. *Journal of Thermophysics and Heat Transfer, 11*(4), 526-531.

Appendix A: Heat Transfer Correlations

Following formulae used to calculate the averaged heat transfer coefficient of shell-side vertical shell and tube condenser (VSTC).

Heat Transfer areas,

Area of tube VSTC,

$$A_{c_t} = \left(\left({}^{\pi}/_{4} \right) \times {d_i}^2 \times N_t \right) \tag{6-1}$$

Area of Shell VSTC,

$$A_{c_s} = \left\{ \left[\left({}^{\pi}/_{4} \right) \times {d_{is}}^2 \right] - \left[\left({}^{\pi}/_{4} \right) \times {d_i}^2 \times N_t \right] \right\} \tag{6-2}$$

Hydraulic diameter of shell VSTC,

$$D_h = \frac{4 \times A_{c_s}}{\left(\left({}^{\pi}/_{4} \right) \times d_i \times N_t \right)} \tag{6-3}$$

Velocity,

$$V_s = \left(\frac{{}^{m_{steam}}/_{\rho_s}}{A_{c_t}} \right) \tag{6-4}$$

Reynold number,

$$Re_s = \left(\frac{\rho_s \times V_s \times d_i}{\mu_s} \right) \tag{6-5}$$

Prandtl number,

$$Pr = \frac{\mu_s \times c_p}{k_s} \tag{6-6}$$

Nusselt number of VSTC,

$$Nu = 0.023 \times Re^{0.8} \times Pr^{0.4} \tag{6-7}$$

Heat transfer coefficient for VSTC,

$$h_s = \frac{(Nu \times k_s)}{d_i} \tag{6-8}$$

Rate of Heat transfer in VSTC,

$$Q_s = m_{cond} \times \Delta h_s \tag{6-9}$$

$$Q_w = m_w \times \Delta h_w \tag{6-10}$$

Averaged heat transfer coefficient,

$$Q = U \times A \times \Delta T_{LMTD} \tag{6-11}$$

Mass of steam condensate at shell of VSTC,

$$m_{cond} = \frac{Q_w}{\Delta h_s} \tag{6-12}$$

Where,

$h = f(\,Temperature)$ At saturated vapour or liquid phase.

Percentage steam condensation in VSTC,

$$Condensation = \frac{m_s}{m_{cond}}\% \tag{6-13}$$

Amount of superheat in steam,

$$\Delta T_{superheat} = T_s - T_{sat} \tag{6-14}$$

Vapour fraction at shell exit of VSTC,

$$Vapour\ fraction = \left(1 - \frac{m_{cond}}{m_s}\right) \tag{6-15}$$

Nusselt number of desuperheating section,

$$Nu = \left(\frac{h \times L_c}{k}\right) \tag{6-16}$$

Appendix B: Temperature and Flow-rate of Test Pressures

Table 6.1: Temperature profile for different test pressures along the length of VSTC (Test: 2)

Length of VSTC (m)		**0**	**0.07**	**0.17**	**0.27**	**0.37**	**0.47**	**0.57**	**0.67**	**0.77**	**0.87**	**0.97**	**1.07**	**1.14**	**0**	**1.14**
Pressures		***Steam temperatures (˚C)***													***Water Temperatures (˚C)***	
bar_{abs}	***kPa_g***	T_1	T_5	T_6	T_7	T_8	T_9	T_{10}	T_{11}	T_{12}	T_{13}	T_{14}	T_{15}	T_3	T_2	T_4
0.3	**-68.0**	131.8	102.0	114.0	78.2	104.4	71.6	89.0	70.8	70.2	69.4	69.7	69.8	73.5	48.6	54.5
0.3	**-66.0**	132.3	101.5	115.1	80.5	107.0	73.3	92.6	73.0	71.3	70.7	71.0	71.1	72.0	49.1	55.3
0.3	**-64.0**	133.1	103.9	117.1	81.4	108.8	73.9	94.3	74.5	72.2	71.6	71.9	72.0	72.0	48.9	55.5
0.4	**-62.0**	129.4	102.4	115.3	82.3	108.4	74.9	94.6	75.9	73.3	72.9	73.1	73.3	73.2	48.8	55.8
0.4	**-60.0**	126.5	101.0	113.8	83.2	108.0	75.3	87.8	76.2	73.8	73.7	73.8	74.0	73.8	49.1	56.4
0.4	**-58.0**	127.1	101.4	114.1	83.8	108.1	75.8	85.7	76.8	74.3	74.1	74.2	74.4	74.2	48.8	56.3
0.4	**-56.0**	128.7	105.6	114.6	86.1	109.5	76.5	86.3	78.4	75.1	75.1	75.1	75.3	75.0	48.6	56.5
0.4	**-54.0**	129.4	102.7	110.6	85.4	110.2	77.7	84.5	78.5	76.2	76.2	75.8	76.3	76.2	49.2	57.7

Length of VSTC (m)		**0**	**0.07**	**0.17**	**0.27**	**0.37**	**0.47**	**0.57**	**0.67**	**0.77**	**0.87**	**0.97**	**1.07**	**1.14**	**0**	**1.14**
Pressures		***Steam temperatures (˚C)***													***Water Temperatures (˚C)***	
bar_{abs}	***kPa_g***	*T_1*	*T_5*	*T_6*	*T_7*	*T_8*	*T_9*	*T_{10}*	*T_{11}*	*T_{12}*	*T_{13}*	*T_{14}*	*T_{15}*	*T_3*	*T_2*	*T_4*
0.4	**-52.0**	130.2	106.0	118.6	106.6	113.6	78.3	83.8	79.3	76.6	76.7	76.7	76.8	76.5	48.6	57.1
0.4	**-50.0**	131.2	104.5	103.1	91.0	112.9	78.7	79.9	79.2	76.7	76.9	76.4	76.9	76.6	49.2	58.1
0.5	**-48.0**	130.0	102.3	119.0	89.4	114.2	81.8	88.1	81.9	80.7	80.7	80.5	80.8	80.8	48.0	57.5
0.5	**-46.0**	130.8	104.5	119.6	92.8	115.4	82.5	87.3	82.5	81.2	81.2	81.1	81.3	81.2	48.8	58.4
0.5	**-44.0**	131.2	105.4	120.3	93.9	116.2	83.3	86.8	83.3	82.0	82.1	81.8	82.1	82.0	49.0	58.8
0.5	**-42.0**	131.6	106.3	121.2	95.0	117.1	83.3	85.1	83.4	81.8	81.9	81.7	82.0	81.8	49.3	59.0
0.5	**-40.0**	133.7	107.3	118.8	96.8	119.0	83.0	83.4	83.2	80.5	80.8	80.3	81.0	80.4	49.2	59.4
0.5	**-38.0**	132.8	107.9	122.5	98.0	118.8	84.9	85.7	85.0	83.3	83.5	83.3	83.6	83.3	49.6	59.7
0.6	**-36.0**	133.2	107.3	122.9	98.9	119.4	85.8	86.4	85.9	84.2	84.4	84.1	84.5	84.2	49.0	59.5
0.6	**-34.0**	133.4	104.6	123.0	99.7	119.7	86.3	86.8	86.4	84.7	84.9	84.7	85.0	84.7	49.1	59.7
0.6	**-32.0**	133.8	105.3	123.4	100.3	120.4	87.4	87.9	87.5	85.7	85.9	85.7	86.1	85.7	49.7	60.5
0.6	**-30.0**	134.0	110.6	122.7	99.8	120.4	87.9	88.4	88.1	86.1	86.3	86.1	86.5	86.1	49.3	60.4

Length of VSTC (m)		**0**	**0.07**	**0.17**	**0.27**	**0.37**	**0.47**	**0.57**	**0.67**	**0.77**	**0.87**	**0.97**	**1.07**	**1.14**	**0**	**1.14**
Pressures		***Steam temperatures (˚C)***													***Water Temperatures (˚C)***	
$\textbf{bar}_{abs}$	$\textbf{kPa}_g$	T_1	T_5	T_6	T_7	T_8	T_9	T_{10}	T_{11}	T_{12}	T_{13}	T_{14}	T_{15}	T_3	T_2	T_4
0.6	**-28.0**	131.6	108.6	121.5	93.6	119.2	86.9	87.4	87.2	84.0	84.4	84.0	84.6	83.8	49.1	60.7
0.6	**-26.0**	131.3	108.6	121.5	94.4	119.1	87.6	88.1	87.9	84.6	85.1	84.7	85.3	84.5	49.2	61.0
0.6	**-24.0**	131.5	110.9	120.2	92.6	117.9	88.0	88.4	88.3	85.0	85.5	85.2	85.7	84.9	49.3	61.2
0.6	**-22.0**	131.6	113.8	121.1	92.6	117.2	88.0	88.5	88.3	85.1	85.5	85.2	85.8	84.9	48.9	60.3
0.6	**-20.0**	130.5	105.8	121.6	95.9	117.6	88.9	89.3	89.2	85.9	86.3	86.1	86.6	85.7	49.0	60.8
0.8	**-7.5**	132.2	115.8	123.2	98.3	117.1	94.7	95.0	94.8	92.9	93.2	92.3	93.4	92.9	49.4	62.4
0.8	**-5.0**	132.3	116.6	124.1	98.9	117.8	95.2	95.6	95.4	93.5	93.7	92.8	93.9	93.4	48.9	62.2
0.9	**0.0**	132.4	113.0	123.0	100.8	120.5	96.8	97.2	96.8	95.4	95.5	94.4	95.7	95.4	49.5	63.3
1.3	**25.0**	133.3	119.0	126.3	108.8	122.2	107.0	107.4	106.9	106.4	106.3	104.7	106.5	106.4	48.5	65.3
1.4	**50.0**	133.6	121.3	128.8	113.2	121.8	109.6	109.9	109.8	107.9	108.2	107.9	108.5	107.8	49.0	66.8
1.6	**75.0**	134.7	123.8	130.0	117.6	120.0	114.3	114.7	114.6	112.3	112.7	112.6	112.9	112.1	49.7	69.0
1.9	**100.0**	135.9	129.4	131.1	121.7	122.5	119.2	119.5	119.4	117.3	117.6	117.1	117.9	117.3	48.7	70.8

Appendix C: Steam Flowrate and Condensation in VSTC

Steam flow rate for each run of experiment.

Table 6.2: Steam flow-rate and condensation inside shell-side VSTC

Pressures		**m_{steam}**	**Percentage condensation in VSTC**
kPa_g	**P_{sat}**	***kg/s***	***%***
Experiment 1: Vacuum steam condensation at different steam pressures (Test 2)			
-68	0.33	0.007229	8
-66	0.34	0.006394	8
-64	0.36	0.006373	8
-62	0.37	0.009054	10
-60	0.37	0.008877	10
-58	0.39	0.007743	12
-56	0.40	0.006736	12
-54	0.41	0.007882	13
-52	0.41	0.009218	15
-50	0.49	0.009916	15
-48	0.50	0.009589	17
-46	0.51	0.009444	16
-44	0.52	0.008463	17
-42	0.50	0.008992	18
-40	0.55	0.009160	20
-38	0.57	0.009590	22
-36	0.59	0.010061	21
-34	0.61	0.010779	22
-32	0.61	0.010677	22
-30	0.56	0.009976	21
-28	0.59	0.008528	25
-26	0.59	0.009591	29
-24	0.60	0.010094	33
-22	0.77	0.014518	20
-20	0.79	0.012423	31
-7.5	0.80	0.015276	25
-5	0.82	0.014890	23
0	0.87	0.014756	24
25	1.27	0.017587	26
50	1.37	0.021407	32
75	1.60	0.021661	38
100	1.87	0.026795	40
Experiment 2: Reduced steam flowrate			
-66	0.33	0.003273	51
-64	0.34	0.005564	89
-62	0.36	0.005564	57
-52	0.41	0.005522	60

Appendix D: Generated Condensation Models for Test Pressures

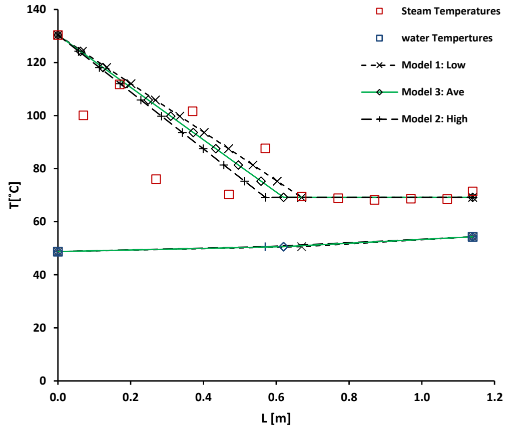

Figure 6.1: -70 kPa$_g$

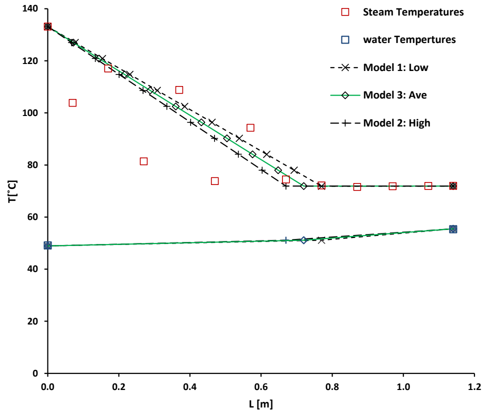

Figure 6.4: -64 kPa$_g$

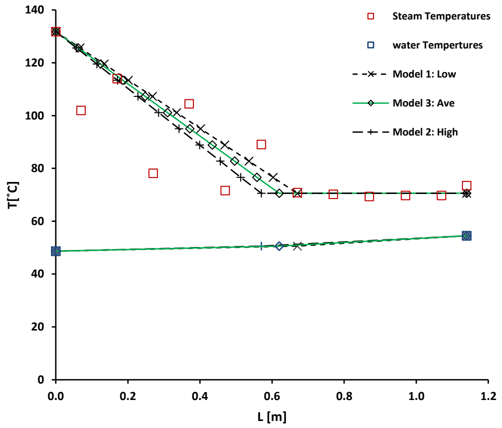

Figure 6.2: -68 kPa$_g$

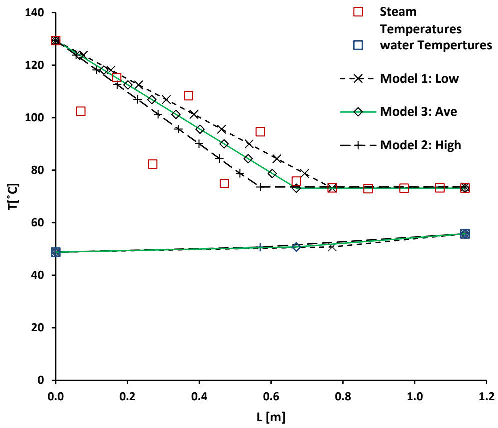

Figure 6.5: -62 kPa$_g$

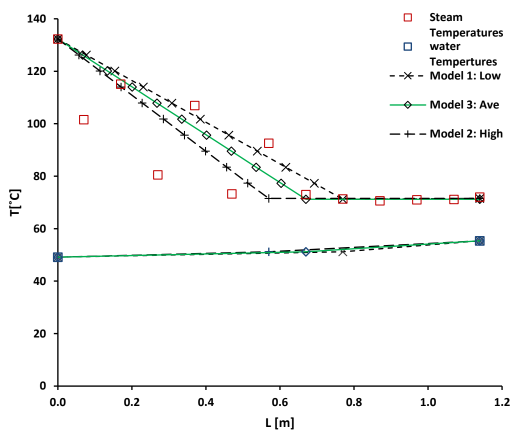

Figure 6.3: -66 kPa$_g$

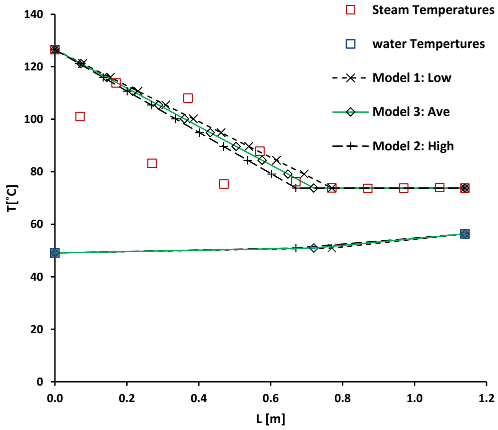

Figure 6.6: -60 kPa$_g$

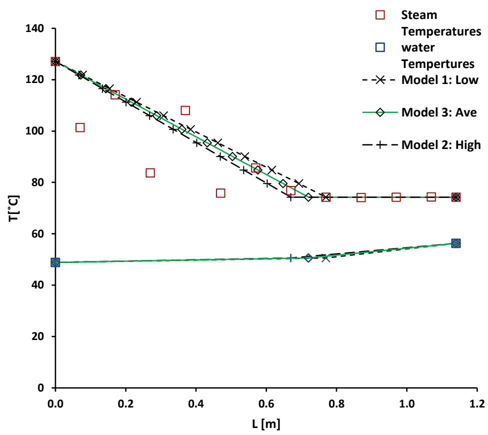

Figure 6.7: -58 kPa$_g$

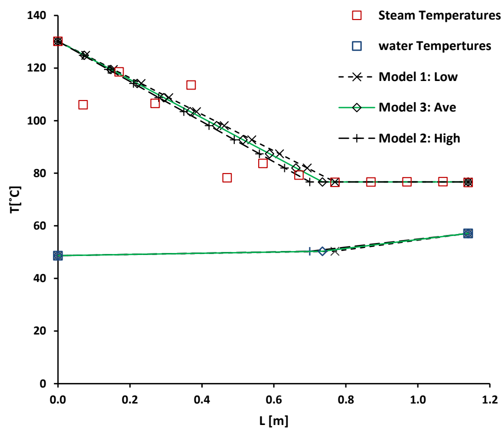

Figure 6.10: -52 kPa$_g$

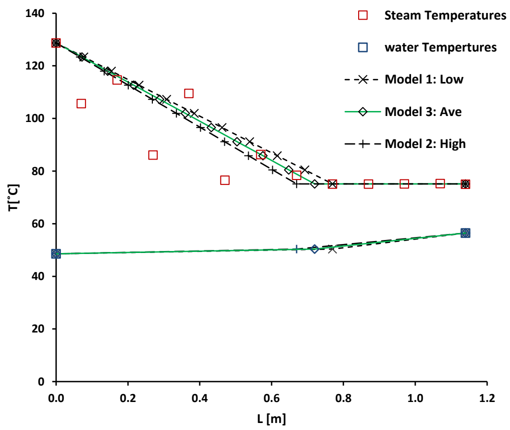

Figure 6.8: -56 kPa$_g$

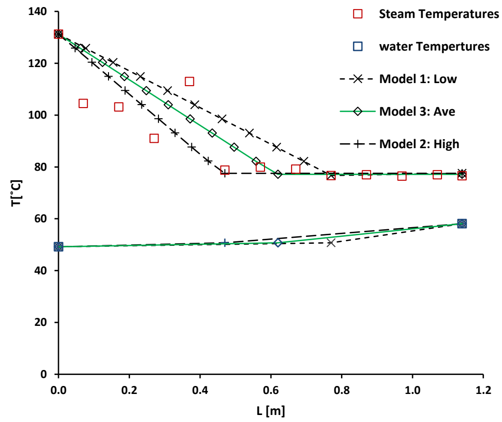

Figure 6.11: -50 kPa$_g$

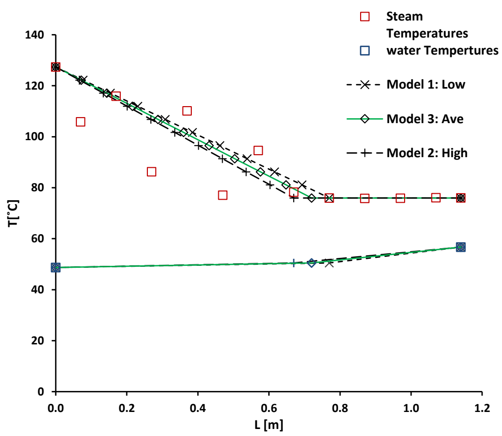

Figure 6.9: -54 kPa$_g$

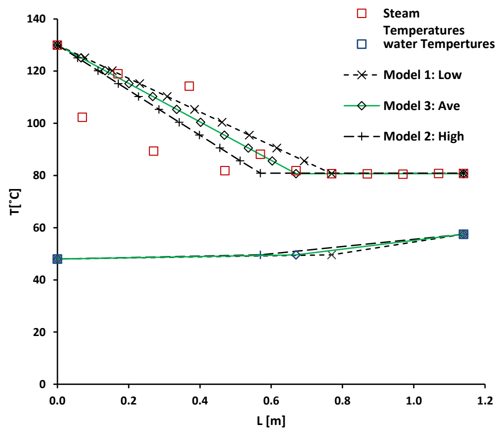

Figure 6.12: -48 kPa$_g$

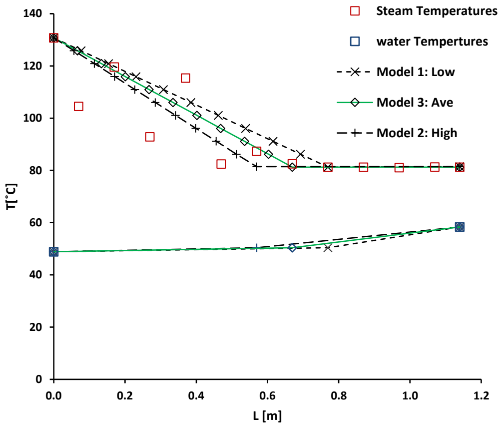

Figure 6.13: -46 kPa$_g$

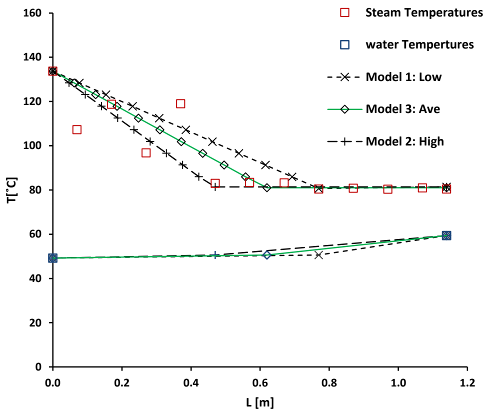

Figure 6.16: -40 kPa$_g$

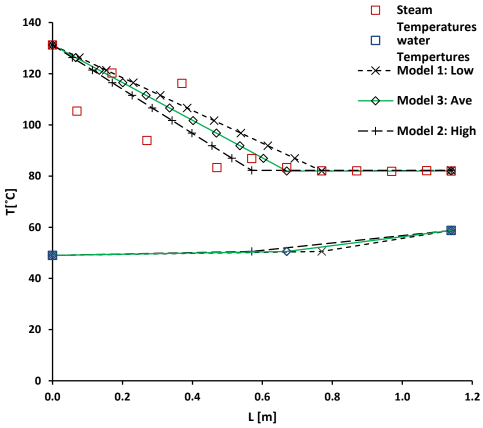

Figure 6.14: -44 kPa$_g$

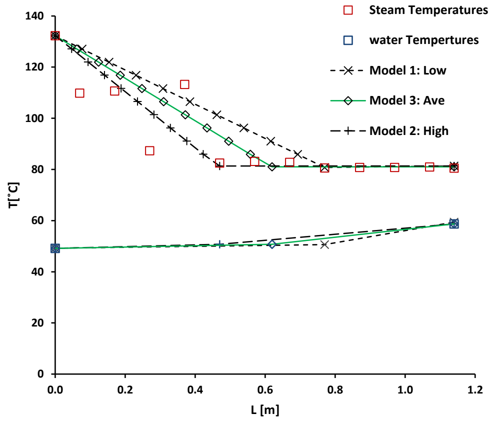

Figure 6.17: -38 kPa$_g$

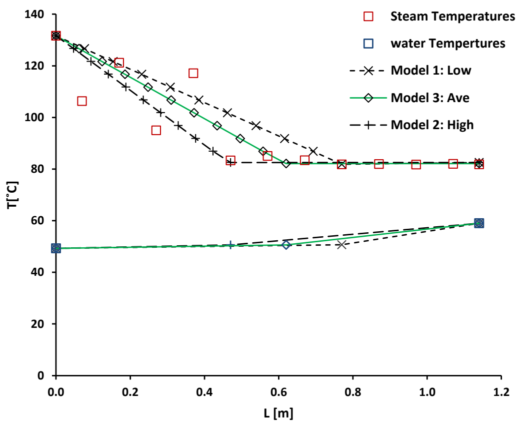

Figure 6.15: -42 kPa$_g$

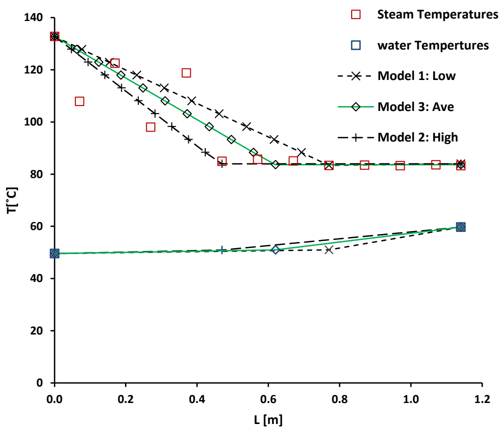

Figure 6.18: -36 kPa$_g$

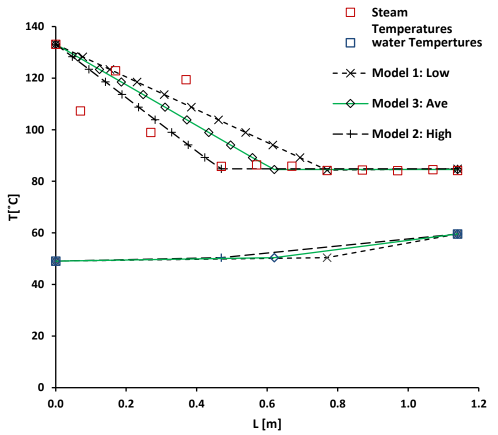

Figure 6.19: -34 kPa_g

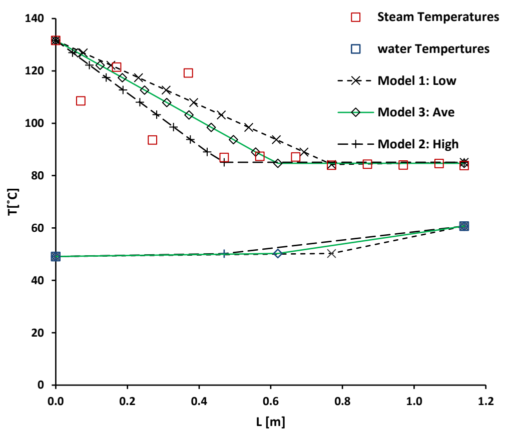

Figure 6.22: -28 kPa_g

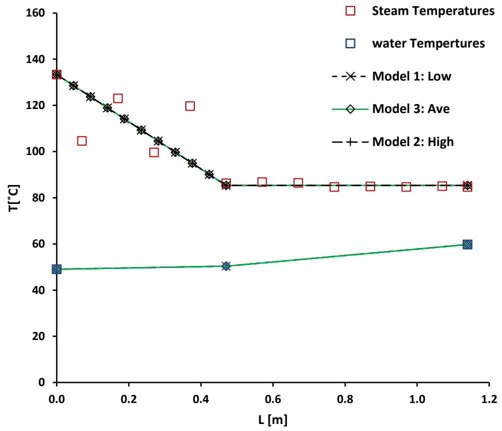

Figure 6.20: -32 kPa_g

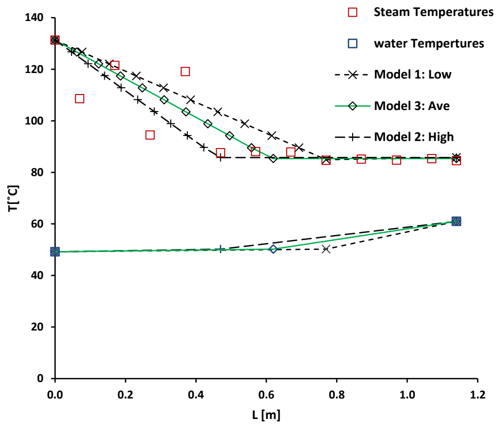

Figure 6.23: -26 kPa_g

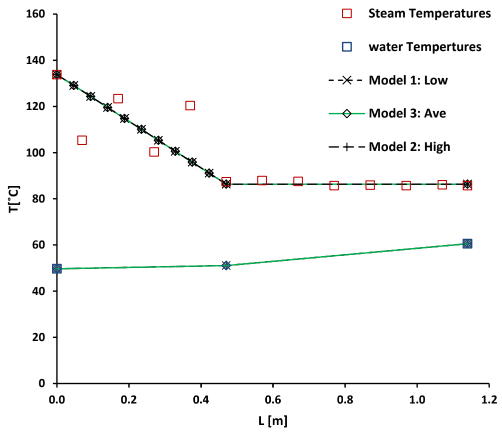

Figure 6.21: -30 kPa_g

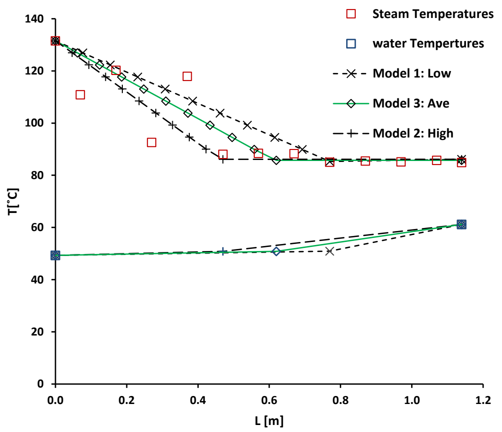

Figure 6.24: -24 kPa_g

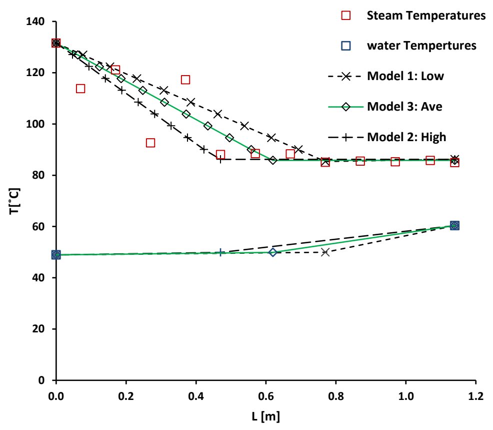

Figure 6.25: -22 kPa$_g$

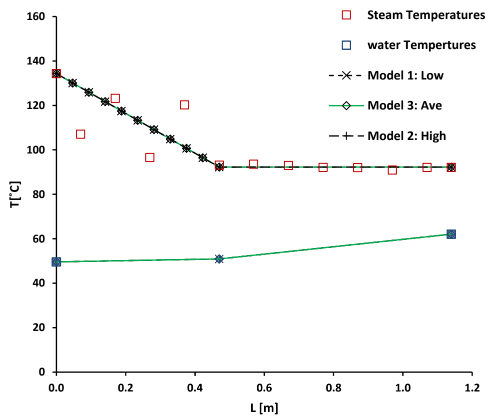

Figure 6.28: -16 kPa$_g$

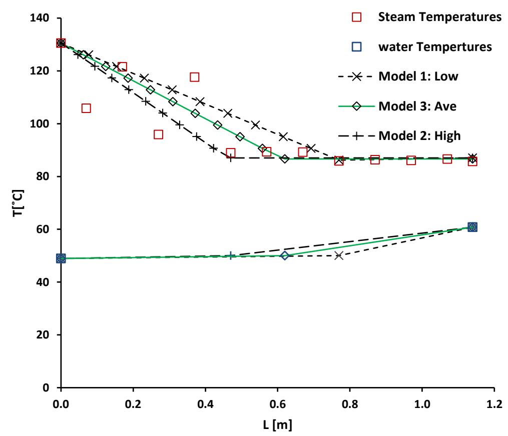

Figure 6.26: -20 kPa$_g$

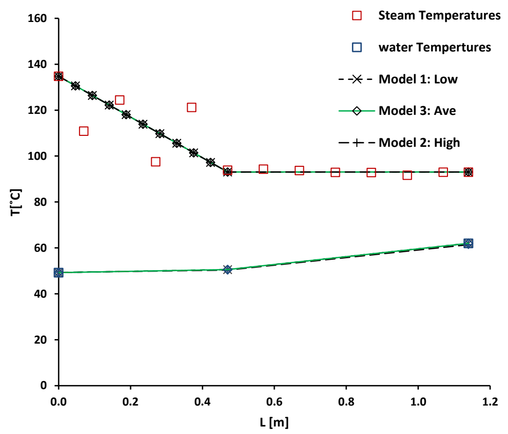

Figure 6.29: -14 kPa$_g$

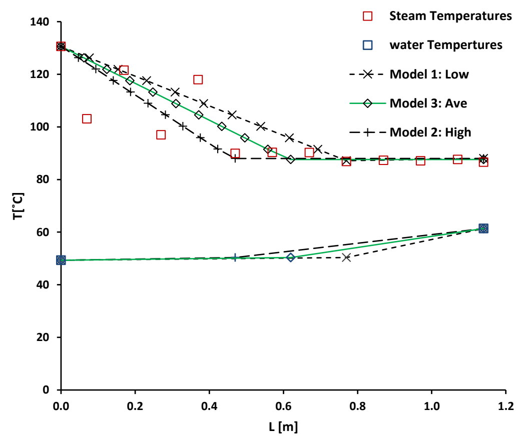

Figure 6.27: -18 kPa$_g$

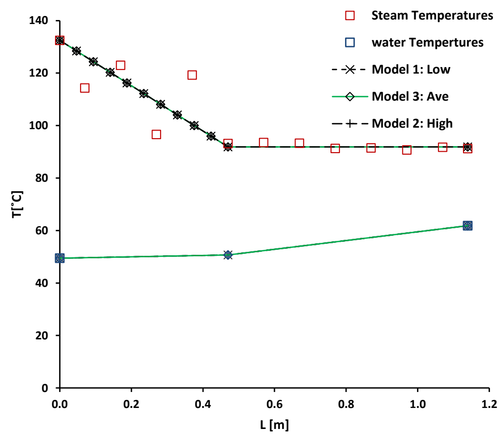

Figure 6.30: -12 kPa$_g$

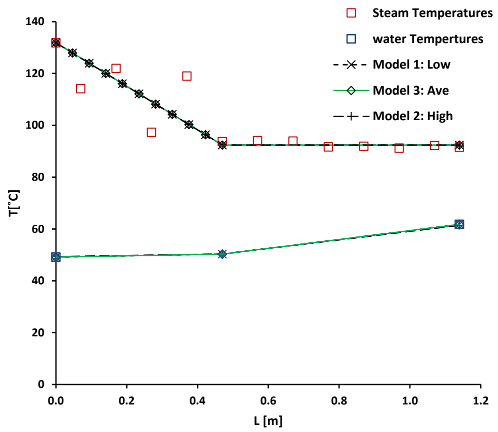

Figure 6.31: -10 kPa$_g$

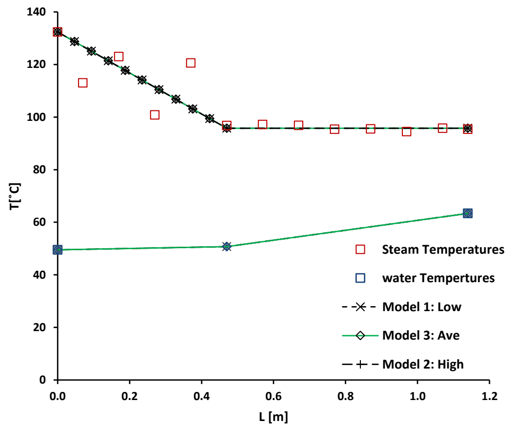

Figure 6.34: 0 kPa$_g$

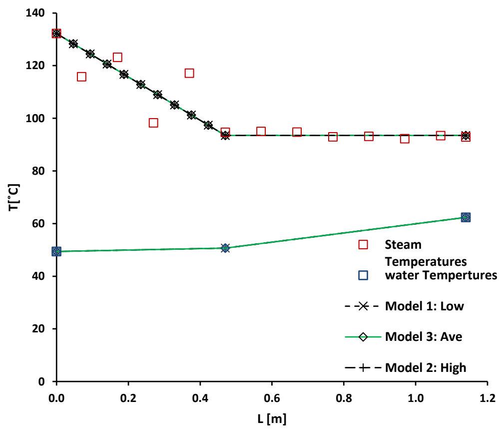

Figure 6.32: -7.5 kPa$_g$

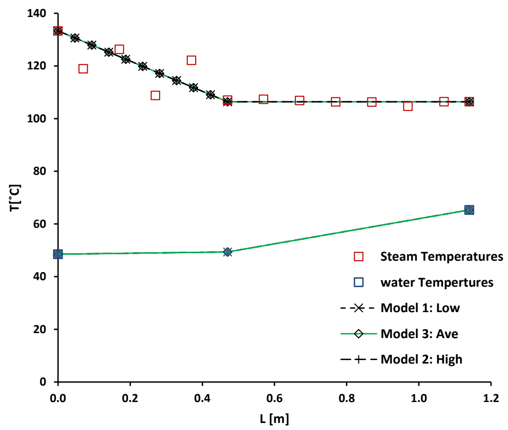

Figure 6.35: 25 kPa$_g$

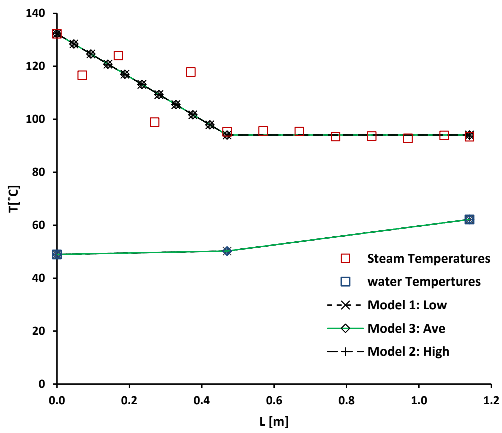

Figure 6.33: -5 kPa$_g$

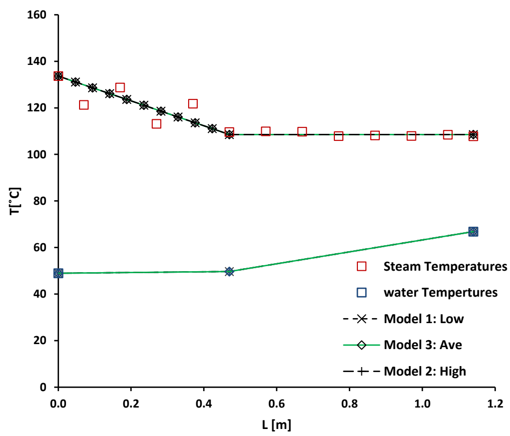

Figure 6.36: 50 kPa$_g$

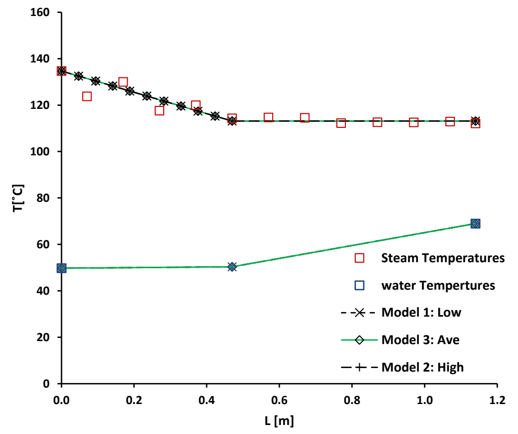

Figure 6.37: 75 kPa$_g$

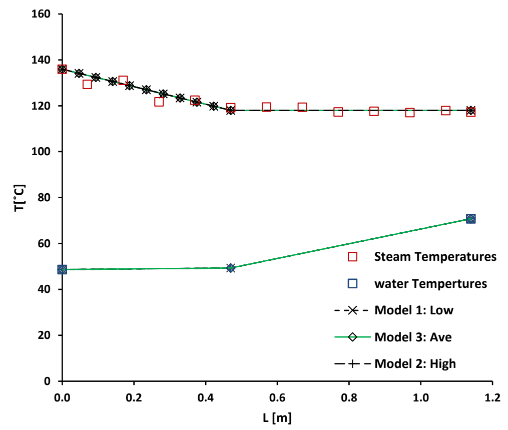

Figure 6.38: 100 kPa$_g$

Appendix E: Calculated Factors from Heat Transfer Analysis of Model 3 – Low Desuperheating and Condensation Sections of VSTC

P_g	P_{sat}	$\Delta T_{superheat}$	T_{sat}	m_{cond}	Vapour fraction	LMTD desup	LMTD cond	A desup	A_{cond}	Q desup	Q cond	U desup	U_{cond}	Re desup	Re cond	Pr desup	Pr cond	Nu desup
Experiment 1: Different vacuum steam pressures																		
-68	0.33	61	71	0.0023	0.68	45	19	0.08	0.07	0.7	5.4	205	4717	19531	21418	0.98	1.02	397
-66	0.34	61	72	0.0027	0.58	47	19	0.09	0.05	0.6	6.3	151	6463	17207	18869	0.98	1.02	289
-64	0.36	56	73	0.0029	0.54	47	20	0.09	0.05	0.6	6.8	139	6611	17218	18740	0.98	1.02	266
-62	0.36	53	74	0.0029	0.67	46	21	0.09	0.05	0.7	6.9	190	6626	24543	26573	0.99	1.02	368
-60	0.37	53	74	0.0030	0.66	46	21	0.09	0.05	0.7	7.1	183	6657	24026	26019	0.99	1.02	354
-58	0.39	54	75	0.0032	0.58	48	22	0.09	0.05	0.6	7.6	156	6866	20883	22640	0.99	1.02	300
-56	0.40	51	76	0.0034	0.50	48	23	0.09	0.06	0.5	7.9	140	6126	18181	19646	0.99	1.02	268
-54	0.41	54	77	0.0036	0.55	50	23	0.09	0.06	0.7	8.2	164	6257	21167	22943	0.99	1.02	316
-52	0.41	54	77	0.0037	0.60	49	22	0.09	0.06	0.8	8.6	196	6773	24714	26826	0.99	1.02	379
-50	0.48	49	81	0.0040	0.60	53	27	0.09	0.06	0.8	9.2	177	5959	26489	28528	0.99	1.02	341
-48	0.49	50	81	0.0040	0.58	53	27	0.09	0.06	0.8	9.2	172	6077	25568	27545	0.99	1.02	331
-46	0.51	49	82	0.0041	0.56	53	28	0.09	0.06	0.7	9.4	166	6125	25140	27069	0.99	1.02	320

P_g	P_{sat}	$\Delta T_{superheat}$	T_{sat}	m_{cond}	Vapour fraction	LMTD desup	LMTD cond	A desup	A_{con} d	Q desup	Q cond	U desup	U_{cond}	Re desup	Re cond	Pr desup	Pr cond	Nu desup
-44	0.51	49	82	0.0041	0.51	53	27	0.08	0.06	0.6	9.5	162	5566	22512	24249	0.99	1.02	311
-42	0.49	51	81	0.0040	0.55	53	27	0.08	0.07	0.7	9.2	179	5622	23929	25843	0.99	1.02	346
-40	0.54	49	83	0.0043	0.53	55	28	0.08	0.07	0.7	10	169	5608	24273	26131	0.99	1.02	325
-38	0.56	50	84	0.0045	0.53	56	30	0.08	0.06	0.7	10	171	5580	25367	27286	0.99	1.02	328
-36	0.58	48	85	0.0046	0.55	57	30	0.05	0.09	0.7	10	257	3984	26573	28553	0.99	1.02	503
-34	0.61	47	86	0.0046	0.57	57	31	0.05	0.09	0.8	11	270	4009	28413	30502	0.99	1.02	530
-32	0.61	47	86	0.0048	0.55	57	31	0.08	0.06	0.8	11	180	5654	28132	30206	0.99	1.02	347
-30	0.56	47	84	0.005	0.50	55	29	0.08	0.06	0.7	11	164	7092	26461	28415	0.99	1.02	315
-28	0.58	46	85	0.0051	0.40	56	30	0.08	0.06	0.6	12	145	6360	22596	24210	0.99	1.02	277
-26	0.58	46	85	0.005	0.49	56	30	0.09	0.05	0.7	11	140	7482	25405	27233	0.99	1.02	268
-24	0.60	44	86	0.0051	0.49	56	31	0.09	0.05	0.7	12	141	7628	26746	28591	0.99	1.02	271
-22	0.76	42	92	0.005	0.63	61	36	0.05	0.09	0.97	12	297	3942	37941	40398	1	1.02	587
-20	0.79	42	93	0.005	0.56	62	37	0.05	0.09	0.8	13	247	3960	32411	34492	1	1.02	482
-7.5	0.80	39	94	0.0056	0.63	61	37	0.05	0.09	0.9	13	287	3966	39979	42354	1	1.02	566
-5	0.82	38	94	0.0057	0.61	62	38	0.05	0.09	0.8	13	272	3988	38938	41220	1	1.02	535
0	0.87	37	96	0.0060	0.59	62	39	0.05	0.09	0.8	13	256	4090	38494	40654	1	1.02	500

P_g	P_{sat}	$\Delta T_{superheat}$	T_{sat}	m_{cond}	Vapour fraction	LMTD desup	LMTD cond	A desup	A_{con} d	Q desup	Q cond	U desup	U_{cond}	Re desup	Re cond	Pr desup	Pr cond	Nu desup
25	1.27	27	106	0.0074	0.57	70	49	0.05	0.09	0.7	17	194	4017	45209	47055	1	1.03	376
50	1.37	25	109	0.0080	0.62	71	50	0.06	0.08	0.7	18	215	4170	54848	56923	1	1.03	419
75	1.59	22	113	0.0088	0.60	73	53	0.05	0.09	0.7	19	179	4255	55106	56889	1	1.04	345
100	1.87	18	118	0.0101	0.62	78	57	0.05	0.09	0.7	22	171	4536	67645	69455	1	1.02	329
Experiment 2: Reduced steam flowrate																		
-66	0.34	59	72	0.0029	0.11	47	20	0.08	0.06	0.3	6.8	87	4721	8833	9661	0.98	1.01	164
-64	0.33	58	71	0.0029	0.49	45	19	0.08	0.06	0.5	6.6	151	4916	15086	16453	0.98	1.01	289
-62	0.36	54	73	0.0031	0.43	45	20	0.08	0.06	0.5	7.3	138	5331	14974	16242	0.99	1.02	265
-52	0.41	50	76	0.0037	0.32	49	23	0.08	0.06	0.5	8.6	1331	5444	16692	17996	0.99	1.02	255
Experiment 3: Shell-side tube wall temperatures greater than steam saturation temperatures																		
-60	0.37	53	74	0.0004	0.59	18	2	0.09	0.05	0.08	1.0	56	8673	2754	2985	0.99	1.02	105
-50	0.43	52	78	0.0004	0.81	20	3	0.09	0.05	0.20	1.1	120	6117	6792	7344	0.99	1.02	228
-42	0.52	44	82	0.0006	0.78	15	2	0.09	0.05	0.2	1.4	141	13995	7364	7868	0.99	1.02	270
-36	0.56	45	84	0.0006	0.84	15	2	0.09	0.05	0.2	1.3	186	14982	9356	10004	0.99	1.02	359

Appendix F: Re-testing of Test Pressures

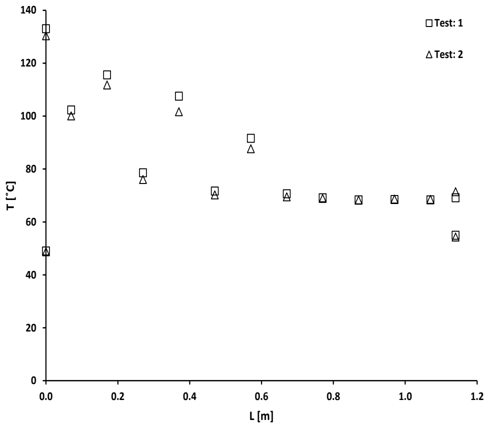

Figure 6.39: -70 kPa_g reinspection

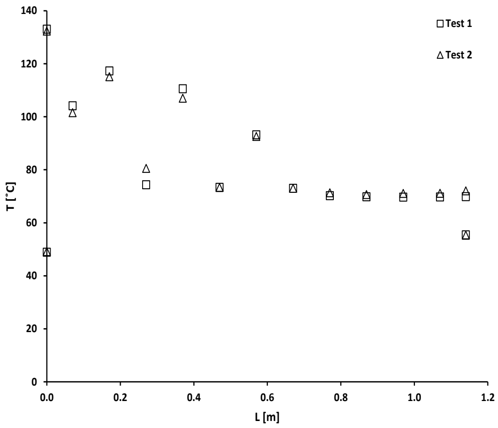

Figure 6.42: -64 kPa_g reinspection

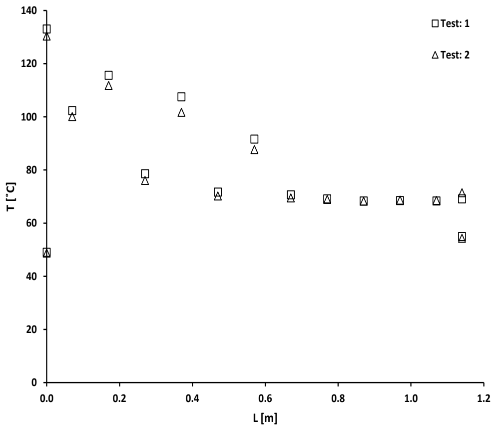

Figure 6.40: -68 kPa_g reinspection

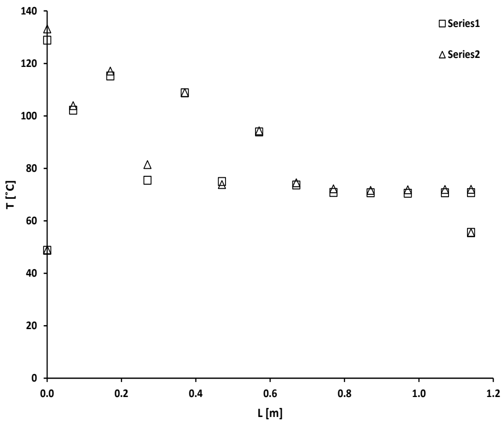

Figure 6.43: -62 kPa_g reinspection

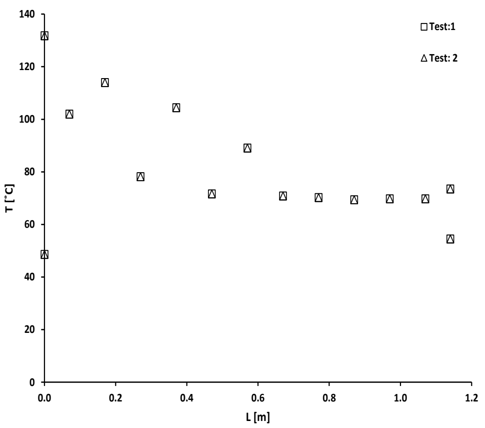

Figure 6.41: -66 kPa_g reinspection

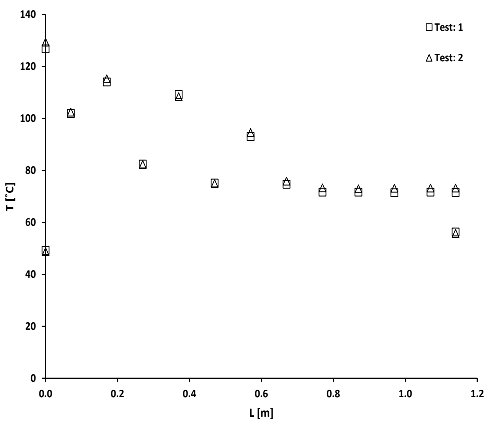

Figure 6.44: -60 kPa_g reinspection

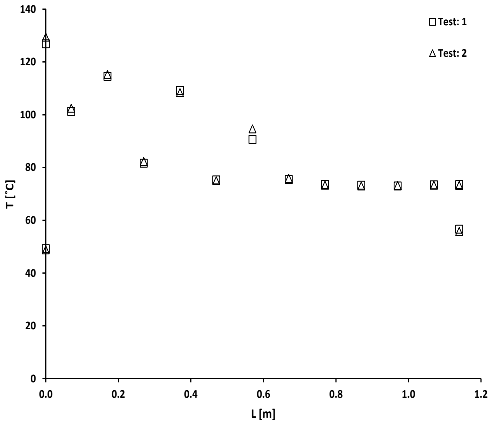

Figure 6.45: -58 kPa$_g$ reinspection

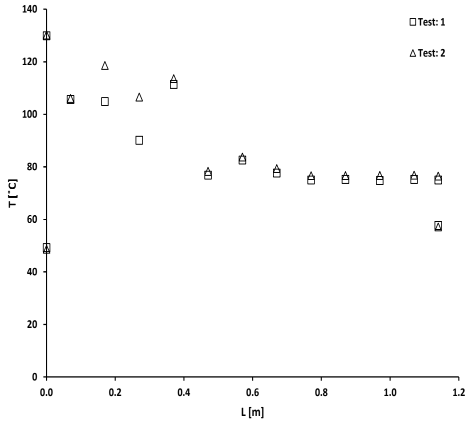

Figure 6.48: -52 kPa$_g$ reinspection

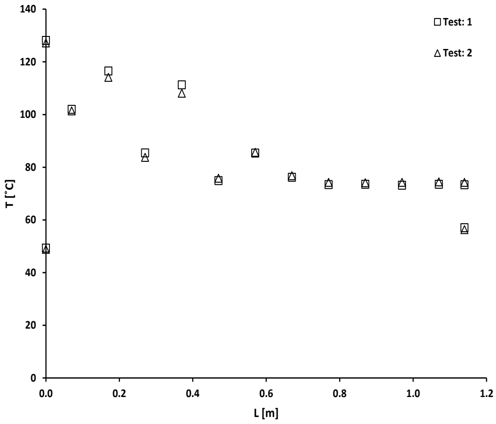

Figure 6.46: -56 kPa$_g$ reinspection

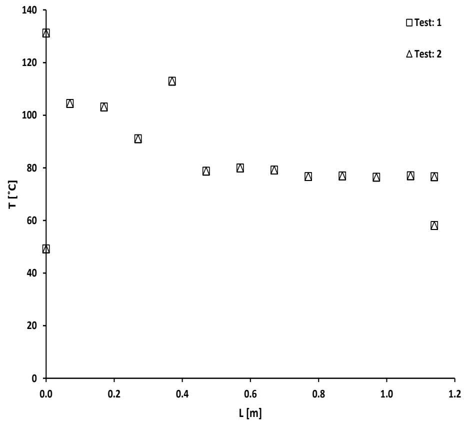

Figure 6.49: -50 kPa$_g$ reinspection

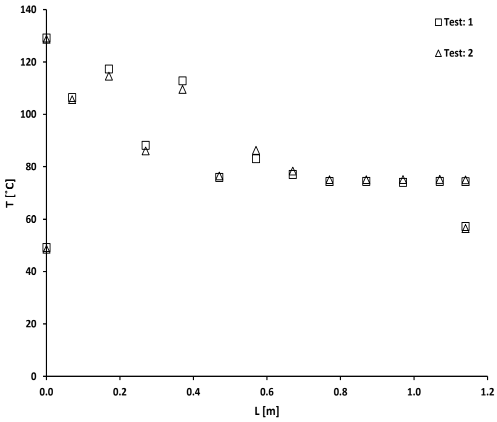

Figure 6.47: -54 kPa$_g$ reinspection

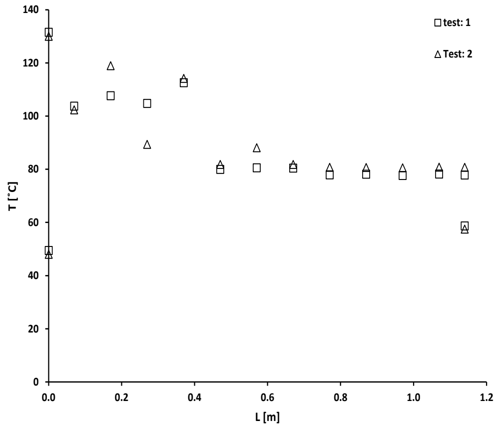

Figure 6.50: -48 kPa$_g$ reinspection

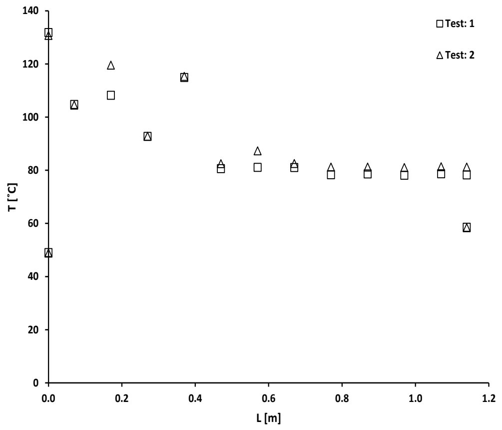

Figure 6.51: -46 kPa$_g$ reinspection

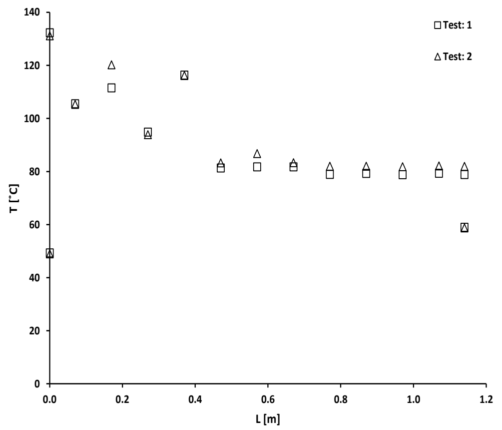

Figure 6.52: -44 kPa$_g$ reinspection

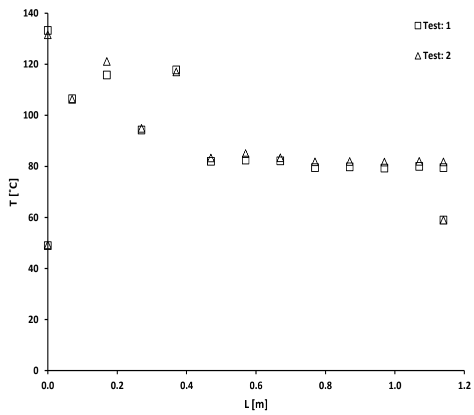

Figure 6.53: -42 kPa$_g$ reinspection

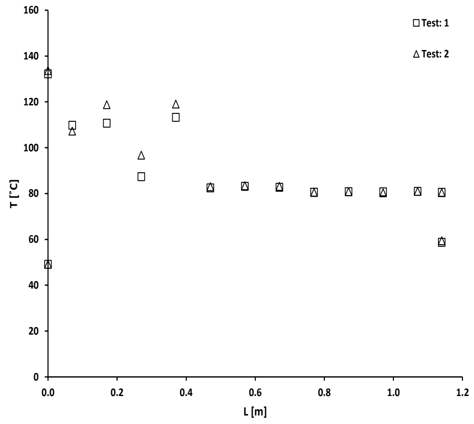

Figure 6.54: -40 kPa$_g$ reinspection

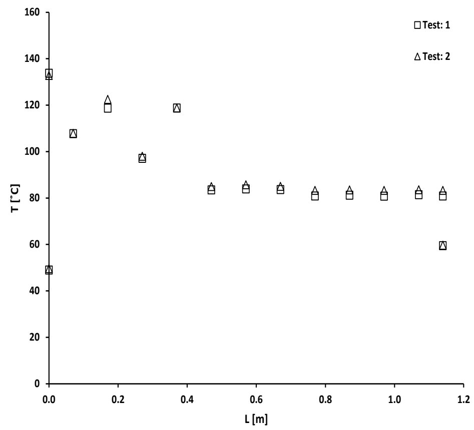

Figure 6.55: -38 kPa$_g$ reinspection

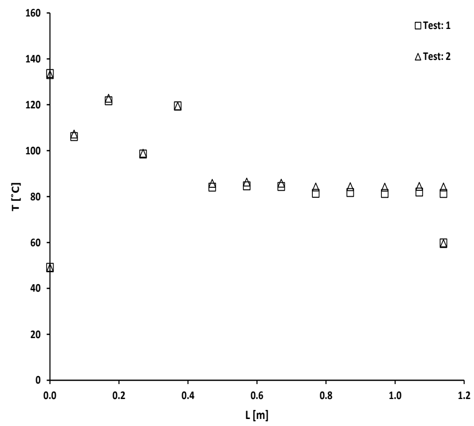

Figure 6.56: -36 kPa$_g$ reinspection

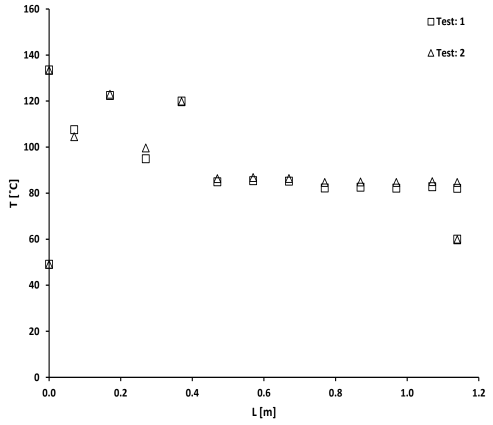

Figure 6.57: -34 kPa$_g$ reinspection

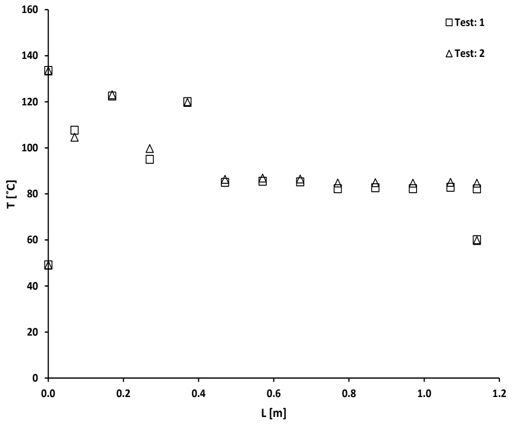

Figure 6.58: -30 kPa$_g$ reinspection

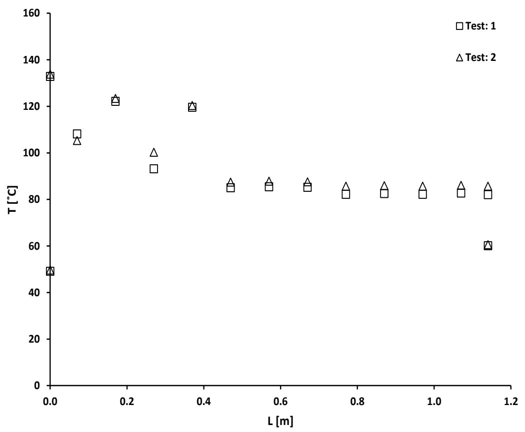

Figure 6.59: -32 kPa$_g$ reinspection